



UNIVERSITÀ
DEGLI STUDI
DI PADOVA

Università degli Studi di Padova

Dipartimento di Tecnica e Gestione dei Sistemi Industriali

SCUOLA DI DOTTORATO DI RICERCA IN INGEGNERIA MECCATRONICA
E DELL'INNOVAZIONE MECCANICA DEL PRODOTTO

XXVI° CICLO

**INFLUENCE OF TRACE ELEMENTS ON SECONDARY DIE-CAST
ALUMINIUM ALLOYS**

Direttore della Scuola : Ch.mo Prof. Alessandro Persona

Supervisore :Ch.mo Prof. Giulio Timelli

Dottorando: Stefano Ferraro

*"...It matters not how strait the gate,
How charged with punishments the scroll,
I am the master of my fate:
I am the captain of my soul."*

*"...Non importa quanto stretto sia il passaggio,
Quanto piena di castighi la vita,
Io sono il padrone del mio destino:
Io sono il capitano della mia anima."*

William Ernest Henley, "Invictus", 1875

Preface

This thesis is submitted in fulfilment of the requirements for the degree of Doctor of Philosophy at the University of Padova. The work is the result of three years full-time studies, including courses and research, from January 2011 to December 2013. The research was done at the Department of Management and Engineering (DTG), Vicenza (Italy), and at the Swerea Swecast AB, Jönköping (Sweden), in cooperation with the School of Engineering at Jönköping University, during a six months visit from April to September 2013.

Doctor Giulio Timelli has been the principal supervisor and Doctor Salem Seifeddine has been co-supervisor during the research period at the Swerea Swecast.

The results have mainly been reported and published throughout the three years period. The articles included in the thesis are presented in the form they were submitted for publication or printed. Deviations from the original text, such as typing errors etc, are marked with a footnote. The thesis is composed of two parts:

PART 1 is intended to give the reader sufficient background on the influence of alloying elements on properties of secondary aluminium alloy castings, physical fundamentals and literature review as well as industrial challenges, motivations and goals.

PART 2 is a collection of four articles dealing with different aspects of trace elements in secondary aluminium foundry alloys. The manuscripts included in this section are:

Article 1

Effects of Bismuth on the microstructure and mechanical properties of AlSi9Cu3(Fe) diecasting alloys

S. Ferraro, G. Timelli and A. Fabrizi, Presented at Sixth International Light Metals Technology Conference (LMT 2013), July 24-26, 2013, Old Windsor, United Kingdom. Also published in Materials Science Forum, vol.765, 59-63, 2013.

Article 2

On the formation of sludge intermetallic particles in Secondary Aluminum Alloys

S. Ferraro, A. Bjurenstedt and S. Seifeddine, Submitted for publication in Metallurgical and Materials Transactions A, 2013.

Article 3

Evolution of Sludge particles in Secondary Die-cast Aluminum Alloys as function of Fe, Mn and Cr contents

S. Ferraro, A. Fabrizi and G. Timelli, Submitted for publication in Metallurgical and Materials Transactions A, 2013.

Article 4

Influence of Sludge Particles on the Tensile Properties of Die-cast Secondary Aluminium Alloys

S. Ferraro and G. Timelli, Submitted for publication in Materials Science and Engineering: A, 2013.

In addition to the articles included in the thesis, parts were presented in the following publications:

1. **The influence of Sr, Mg and Cu addition on the microstructural properties of a secondary AlSi9Cu3(Fe) die casting alloy**, A. Fabrizi, S. Ferraro, G. Timelli, Material Characterization, vol.85, 13-25, 2013.

2. **Effects of chromium and bismuth on secondary aluminium foundry alloys**, G. Timelli, S. Ferraro, A. Fabrizi, International Journal of Cast Metal Research, vol.26(4), 239-246, 2013.
3. **The influence of Fe, Mn and Cr additions on the formation of Iron-rich intermetallic phases in an Al-Si die-casting alloy**, A. Fabrizi, S. Ferraro, G. Timelli, Shape Casting 5: International Symposium, Ed. by M. Tiryakioglu, J. Campbell and G. Byszynski, TMS, 2014.
4. **Microstructure and mechanical properties of automotive components die cast with secondary aluminum alloys by SEED semi-solid process**, G. Timelli, S. Capuzzi, S. Ferraro, A. Fabrizi, L. Capra, Shape Casting 5: International Symposium, Ed. by M. Tiryakioglu, J. Campbell and G. Byszynski, TMS, 2014.
5. **Effect of Grain refinement and Cooling rate on the Microstructure and Mechanical properties of Secondary Al-Si-Cu alloys**, G. Timelli, G. Camicia, S. Ferraro, Journal of Materials Engineering and Performance, 2013.
6. **Effects of Grain refinement on the Microstructure, Mechanical properties and Reliability of AlSi7Cu3Mg Gravity Die cast Cylinder heads**, G. Timelli, G. Camicia, S. Ferraro, R. Molina, Submitted for publication in Metals and Materials International, 2013.
7. **Sviluppo di sospensioni in Al Thixotropico**, S. Capuzzi, L. Capra, S. Ferraro, G. Timelli, F. Bonollo: A&L - Alluminio e leghe, 2013
8. **Multiscale characterisation of AlSi9Cu3(Fe) die casting alloys after Cu, Mg, Zn and Sr addition**, F. Sanna, A. Fabrizi, S. Ferraro, G. Timelli, P. Ferro, F. Bonollo, La Metallurgia Italiana vol.105(4), 13-24, 2013.

9. **Caratterizzazione multiscala di leghe AlSi9Cu3(Fe) pressocolate dopo alligazione con Cu, Mg, Zn e Sr**, F. Sanna, A. Fabrizi, S. Ferraro, G. Timelli, P. Ferro, F. Bonollo, Proc. XXXIV Convegno nazionale AIM. 7-9 October 2012, Trento (Italy).
10. **Caratterizzazione meccanica e microstrutturale di leghe di alluminio pressocolate**, G. Timelli, S. Ferraro, F. Grosselle, F. Bonollo, F. Voltazza, L. Capra, La Metallurgia Italiana, vol.103(1), 5-17, 2011.
11. **The Multidisciplinary Virtual Product Development Integrates the Influence of Die Casting Defects in the Mechanical Response**, N. Gramegna, I. Loizaga, S. Berrocal, F. Bonollo, G. Timelli, S. Ferraro, Proc. APMS 2012 Conference - Advances in Production Management Systems, 24-26 September 2012, Rhodes (Greece). Also published in Competitive Manufacturing for Innovative Products and Services, 502-509, 2013.
12. **The Influence of Cr content on the Fe-rich phase Formation and Impact toughness of a Die-cast AlSi9Cu3(Fe) alloy**, G. Timelli, S. Ferraro, A. Fabrizi, S. Capuzzi, F. Bonollo, L. Capra, G. Capra, Proc. 71st World Foundry Congress, Bilbao (Spain), 19-21 May 2014.
13. **Development of Heat Treatments for Automotive Components diecast with Secondary Aluminium Alloy at Semi-Solid state**, S. Capuzzi, S. Ferraro, G. Timelli, L. Capra, G. Capra, I. Loizaga, Proc. 71st World Foundry Congress, Bilbao (Spain), 19-21 May 2014.
14. **The role of Cr additions and Fe-rich compounds on microstructural features and impact toughness of AlSi9Cu3(Fe) diecasting alloys**, G. Timelli, A. Fabrizi, S. Capuzzi, F. Bonollo, S. Ferraro, Submitted for publication in Materials Science and Engineering: A, 2014.
15. **Investigation on grain refinement by carbon addiction on AZ91D magnesium alloy**, M. Dabalà, S. Ferraro, K. Brunelli, Proc. Euromat 2011, 12-15 September 2011, Montpellier (France).

In addition, the following M.S. thesis have been supervised:

1. S. Farronato, **Influence of Bi amount on the microstructure and the dynamic mechanical proprieties of secondary aluminium alloys EN AC-46000**, Supervisors: G. Timelli, S. Ferraro, L. Capra, G. Capra, AA. 2010-2011.
2. F. Fontana, **Analysis of the effects of Bismuth content on microstructure and mechanical properties of EN AC-46000 diecasting alloys**, Supervisors: G. Timelli, S. Ferraro, L. Capra, AA. 2010-2011.
3. D.M. Fabio, **Nuovi processi nella fonderia d'alluminio: applicazione della tecnologia SEED a leghe di alluminio secondario**, Supervisors: G. Timelli, S. Ferraro, L. Capra, G. Capra, I. Loizaga, AA. 2011-2012.
4. G. Camicia, **Trattamenti di affinazione e modifica di leghe AISi7Cu3Mg per componenti automotive colati in conchiglia a gravità**, Supervisors: G. Timelli, S. Ferraro, R. Molina, AA. 2011-2012.
5. L. Camparmò, **Comportamento tribologico di leghe di alluminio EN AC-46000 pressocolate al variare del contenuto di Fe, Mn e Cr**, Supervisors: G. Timelli, S. Ferraro, AA. 2012-2013.
6. S. Capuzzi, **Sviluppo di trattamenti termici per componenti automotive colati in lega di alluminio secondario allo stato semi-solido**, Supervisors: G. Timelli, S. Ferraro, L. Capra, G. Capra, I. Loizaga, AA. 2012-2013.

Summary

Recycling play a key role on saving of natural resources and on reducing pollution. The recycling of aluminium alloys is also cost-effective, since it reduce the material cost and creates a considerable energy-saving. The use of recycled Al alloys (usually called secondary) has improved in recent years also because of their comparable mechanical properties with primary aluminium alloys.

During the production of secondary aluminium alloys, the scrap are mixed regardless of their specific chemical composition, and then master alloys or pure elements are added to the molten metal. Furthermore, certain impurity elements are either difficult or expensive to remove, and their role in mechanical properties can be important. Due to the presence of these additional trace elements, a number of complex intermetallic phases can therefore form in multi-component Al-Si alloys. Mechanical and physical properties of alloys and castings are strongly related to sizes, morphologies and distribution of these intermetallic phases, which are in turn a function of alloy composition and cooling rate.

The Al-Si based alloys are transversally used in different foundry processes. Among all the technologies, high-pressure die-casting (HPDC) represents the most common process to produce automotive components by secondary Al-Si alloys because it allows one to increase the production by lowering the cycle time and to obtain economically components with complex geometries and high quality surface.

The effects of trace elements and intermetallics phases on features of aluminium castings are still not fully understood, especially when components are made by means of HPDC process. The motivation of the research presented in this doctoral thesis was, therefore, to fill this gap in knowledge. The study has

aimed at understanding the influence of various trace elements on the microstructure and mechanical properties of secondary die-cast aluminium alloys and, in particular, on secondary AlSi9Cu3(Fe) die-cast alloys.

A literature review and a sufficient background of previously reported results on the influence of trace elements on the features of aluminium alloys as well as the formation of intermetallic phases were carried out. It was found that the mechanical and microstructural analysis generally referred to primary cast Al alloys with low concentration of trace elements outside of those studied. Furthermore the samples were usually produced on gravity die-cast, while some intermetallics phases were frequently observed in high-pressure die-casting, where higher cooling rates and different feeding conditions exist.

Special attention has been given to:

The effects of Bismuth addition on secondary die-cast aluminium alloys: Bismuth substitute the lead in free-cutting wrought Al alloys, and this is leading to a steady increase of Bi content in secondary Al alloys due to the recycling process.

The nucleation temperature of primary Fe-rich intermetallic compounds, as function of Fe, Mn and Cr content and cooling rate: Fe-rich phases have a high specific gravity and tend to segregate to the bottom of aluminium melts and holding furnaces. These phases form primary solid particles, generally called sludge, thus reduce the effective capacity of the furnace.

The influence of Fe, Mn and Cr addition, separately or in combination, on the microstructural and mechanical characteristics of secondary die-cast aluminium alloys: sludge crystals are hard and brittle compact inclusions which can compromise the machining operations, with a considerable effects on the cutting tool life, and even more degrade the mechanical and physical properties of the component. As recycling of aluminium alloys becomes more common, sludge will be a problem of increasing importance due to the concentration of Fe, Mn and Cr in the scrap cycle.

Sommario

Il riciclaggio gioca un ruolo chiave sul risparmio delle risorse naturali e sulla riduzione dell'inquinamento. Il riciclo dell'alluminio è oltretutto economicamente conveniente, in quanto riduce il costo del materiale a fronte di un considerevole risparmio energetico. L'utilizzo di leghe di alluminio riciclate (comunemente chiamate leghe secondarie) è aumentato negli ultimi anni anche grazie alle loro proprietà meccaniche, le quali sono in alcuni casi comparabili con le leghe di alluminio primarie.

Durante il processo di produzione dell'alluminio secondario i rottami vengono mescolati assieme indipendentemente dalla loro composizione chimica specifica. Al termine del processo fusorio la composizione viene regolata tramite l'aggiunta di leghe madri o di metalli puri. Tuttavia alcune impurezze presenti nel rottame rimangono all'interno della lega in quanto il loro processo di rimozione è complicato o non economicamente conveniente. A causa della presenza di questi elementi in traccia, un certo numero di fasi intermetalliche complesse si può formare nei getti. Di conseguenza le proprietà meccaniche e fisiche dei componenti in lega di alluminio sono fortemente correlate alla dimensione, alla morfologia e alla distribuzione di tali fasi intermetalliche, le quali sono a loro volta funzione della composizione della lega e della velocità di raffreddamento del metallo.

Grazie alle loro elevata colabilità, le leghe Al-Si sono molto utilizzate in tutti i processi di fonderia. Tra le diverse tecnologie, la pressocolata (HPDC - *high-pressure die-casting*) rappresenta il processo più comune per la produzione di getti di alluminio nel settore automotive. Questa tecnologia permette di ottenere componenti con geometrie complesse e un'ottima finitura superficiale con una riduzione dei costi grazie alla elevata produttività e al basso tempo ciclo.

Gli effetti degli elementi in traccia e delle fasi intermetalliche sulle proprietà dei getti in alluminio non sono ancora del tutto noti, soprattutto quando i componenti sono prodotti tramite pressocolata. Obiettivo di questo lavoro di dottorato di ricerca era perciò quello di supplire a queste lacune. Lo scopo del presente lavoro è studiare l'influenza di diversi elementi in traccia sulla microstruttura e sulle proprietà meccaniche di getti in lega secondaria di alluminio prodotti mediante pressocolata, ed in particolare nella lega $AlSi9Cu3(Fe)$.

In prima analisi, è stata condotta una recensione della letteratura sull'influenza degli elementi in traccia sulle proprietà delle leghe di alluminio e sulla formazione delle fasi intermetalliche. Questo ha permesso di constatare che le caratteristiche meccaniche e microstrutturali legate alla presenza di fasi indesiderate sono normalmente valutate in getti prodotti con leghe primarie di alluminio, in cui è presente una bassa concentrazione di impurezze al di fuori di quelle studiate. Inoltre i campioni studiati sono generalmente prodotti mediante colata in gravità, mentre alcune fasi intermetalliche sono tipiche della pressocolata, in cui la velocità di raffreddamento è molto più elevata e sono presenti diverse condizioni di alimentazione e di riempimento dello stampo.

Nel presente lavoro è stata posta particolare attenzione a:

Gli effetti dell'aggiunta di Bismuto nelle leghe di alluminio secondarie pressocolate: il Bismuto ha sostituito il Piombo nelle leghe di alluminio da deformazione plastica ad alta lavorabilità alle macchine utensile. Questo ha comportato un aumento del contenuto di Bismuto nelle leghe secondarie di alluminio a causa del processo di riciclaggio degli sfridi di lavorazione.

La temperatura di nucleazione dei precipitati intermetallici ricchi in Ferro in funzione della velocità di raffreddamento e della concentrazione in lega di Ferro, Cromo e Manganese: le fasi ricche in ferro hanno un'elevata densità e tendono a segregare sul fondo del fondo del forno di mantenimento. L'insieme di queste fasi primarie forma una fanghiglia, chiamata *sludge*, che riduce l'effettiva capacità del forno.

L'effetto dell'aggiunta di Ferro, Cromo e Manganese, singolarmente o in combinazione tra di loro, sulle caratteristiche microstrutturali e meccaniche delle leghe di alluminio secondarie pressocolate: le particelle di *sludge* sono inclusioni compatte dure e fragili, le quali possono compromettere le operazioni di lavorazione meccanica, con una conseguente riduzione della durata degli utensili, ed una marcata riduzione delle proprietà meccaniche e fisiche del componente. Il problema delle particelle di *sludge* nelle leghe secondarie di alluminio assume un'importanza sempre maggiore a causa dell'aumento del riciclo dell'alluminio e della presenza di Fe, Mn e Cr nel ciclo del rottame.

Table of Contents

PREFACE	v
SUMMARY	xi
SOMMARIO	xiii
TABLE OF CONTENTS	xvii
PART 1: RESEARCH BACKGROUND	1
CHAPTER 1: INTRODUCTION.....	3
CHAPTER 2: BASIC CONCEPTS	5
2.1. Introduction	5
2.2. Aluminium foundry alloys	6
2.3. Effect of alloying elements	11
2.3.1. Silicon.....	11
2.3.2. Copper.....	12
2.3.3. Magnesium	12
2.3.4. Iron	12
2.3.5. Manganese and Chromium	13
2.3.6. Nickel.....	13
2.3.7. Zinc.....	13
2.3.8. Lead and Bismuth.....	13
2.3.9. Titanium and Boron	13
2.3.10. Phosphorus	14
2.3.11. Sodium, Strontium, Calcium and Antimony.....	14
2.4. High-pressure die-casting	15

CHAPTER 3: EFFECTS OF TRACE ELEMENTS	21
3.1. Introduction	21
3.2. Bismuth.....	21
3.2.1. Bismuth source in Al casting alloys.....	21
3.2.2. Bismuth phase diagrams	22
3.2.3. Al-Bi phase diagram	22
3.2.4. Mg-Bi phase diagram.....	23
3.2.5. Bi-Pb phase diagram	24
3.2.6. Effect of Bismuth in Al-Si casting alloys	24
3.3. Iron, Manganese and Chromium.....	26
3.3.1. Fe-rich phases in commercial Al-Si alloys	26
3.3.2. The Al-Fe-Si system	27
3.3.3. Segregation of primary Fe-rich particles	29
3.3.4. Critical aspects	33
 CHAPTER 4: OBJECTIVES AND SURVEY OF THE ARTICLES	 35
 CHAPTER 5: CONCLUSIONS.....	 37
 REFERENCES	 39

PART 2: ARTICLES.....	47
ARTICLE 1.....	49
Effects of Bismuth on the microstructure and mechanical properties of AlSi9Cu3(Fe) diecasting alloys	
ARTICLE 2.....	61
On the formation of sludge intermetallic particles in Secondary Aluminum Alloys	
ARTICLE 3.....	85
Evolution of Sludge particles in Secondary Die-cast Aluminum Alloys as function of Fe, Mn and Cr contents	
ARTICLE 4.....	115
Influence of Sludge Particles on the Tensile Properties of Die-cast Secondary Aluminium Alloys	

PART 1

RESEARCH BACKGROUND

Chapter 1

INTRODUCTION

Aluminium–Silicon foundry alloys are the most commonly diffused alloys in the automotive industries because of their high strength to weight ratio, excellent castability and good corrosion resistance. Aluminium castings can be and indeed are produced with very substantial amounts of recycled aluminium scrap. The treatment of this scrap to produce new aluminium metal and alloys is known as *recycling*, and metal produced this way is frequently termed *secondary*. About one-third of the aluminium produced in the world is now obtained from secondary sources¹. The production of secondary Al alloys shows significant advantages such as an important saving of natural resources with a consequent material cost reduction and a considerable energy-saving associated to reduction in pollution and CO₂ emissions. It is worth mentioning that almost 95% of the energy-saving is achieved from remelting recycled metal than producing primary Al from ore².

During recycling, the scrap are mixed regardless of their specific chemical composition, as sorting of the parts may not be commercially viable. Efforts are then made to correct the composition of the resulting alloy online. This practice has economic limitations too. Furthermore, certain impurity elements are either difficult or expensive to remove, and their role in mechanical properties can be important. Due to the presence of these additional trace elements, a number of complex intermetallic phases can therefore form in multi-component Al-Si alloys. Mechanical and physical properties of alloys and castings are strongly related to sizes, morphologies and distribution of these intermetallic phases, which are in turn a function of alloy composition and cooling rate.

A great contribution to the use of aluminium alloys comes from improvements in castings processes which allow to increase production, lower

the cycle time, and realised complex-shaped castings with thin wall thickness. As high-pressure die-casting (HPDC) reflects these advantages, several automotive components are made with this technique. Generally, the physical properties and mechanical performance of Al cast alloys are strongly related to the casting process and alloy composition, besides the melt treatment conditions and the post-casting operations, such as heat treatments.

The aim of the present research is to develop a new knowledge on the influence of trace elements on the features of a secondary AlSi9Cu3(Fe) die-cast alloys. A statistical approach was implemented in order to develop some functional equations useful to estimate some castings properties in HPDC as function of the initial chemical composition of the alloy.

The main study was to investigate:

- The effect of Bismuth addition on eutectic silicon refinement in high-pressure die-casting conditions.
- The nucleation temperature of primary Fe-rich intermetallic compounds, especially *sludge* particles, as function of Fe, Mn and Cr content.
- The effect of cooling rate on the *sludge* particle nucleation and growth.
- The influence of Fe, Mn and Cr addition, separately or in combination, on the features of secondary aluminium alloys die-cast under industrial conditions.

To accomplish this, a theoretical and literature background of previous investigations have been briefly reported in order to establish a basis for the present studies.

Chapter 2

BASIC CONCEPTS

2.1. Introduction

Aluminium and its alloys are widely used in the transport industry due to their relative low density, which allows approximately 50% weight saving over competing ferrous materials³. Recently, it has been estimated that 20% of the total worldwide aluminium production is converted into cast components and about 70% of all aluminium castings are used in the transport industry, especially in the automotive sector⁴. Lightweighting is one of the most effective variables on fuel consumption and CO₂ emissions: a weight saving on the car's mass of 100 kg is equivalent to a reduction of about 9 grams of CO₂ per km⁵.

Among the various forming processes of aluminium alloys, metal casting offers an economical and simple route to the production of one or several parts of the same alloy with a wide range of weights and dimensions. Higher mechanical properties in castings can be achieved through strict control of factors such as impurity level, melting and pouring practices, grain size and the use of metal chills to increase solidification rates. The common casting processes used for aluminium alloys include sand casting, permanent mould (gravity die) casting and pressure die-casting, depending on the volume of production, size and the type of products. Costs are strongly influenced by process choice. Tooling costs associated with die and permanent mold casting are justified by higher levels of production and product reproducibility. Moreover the mechanical properties, surface quality, dimensional tolerance and uniformity of the casting are correlated to the specific casting process^{3,6}.

Aluminium-silicon castings constitute 85% to 90% of the total aluminium cast parts produced, primarily because of their excellent casting characteristics.

Additions of Si to pure aluminium impart high fluidity, good feeding characteristics, low shrinkage and good hot cracking resistance⁶. The Al-Si binary system (Fig. 2.1) exhibits a simple phase diagram with a single eutectic point at 577°C and 12.6 wt% Si⁷. Depending on the amount of silicon, the alloys can be divided into three groups: hypo-eutectic alloys with Si content between 5 and 9 wt.% Si, eutectic alloys with 10-13 wt.% Si, and hyper-eutectic alloys, commonly with a Si content between 14 and 20 wt.%⁸. The characteristic feature of these alloys is that they consist of a primary phase, aluminium or silicon, and a eutectic mixture of these two elements. Below the eutectic composition aluminium precipitates from the liquid as the primary phase in the form of dendrite, while the eutectic consists of plates or needles of silicon in a continuous aluminium matrix^{8,9}.

Figure 2.1: Part of the equilibrium Al-Si phase diagram showing composition ranges of various alloy types⁸.

2.2. Aluminium foundry alloys

Aluminium castings are the subject of numerous specifications and standards. The major industrialized countries have their own National Specifications, which however exhibit limited correspondence between them.

The European Standard for aluminium casting alloys is the EN 1706:2010¹⁰, which specifies the chemical composition limits. For each alloy, the mechanical properties of separately cast test piece are specified for the commonly used methods of casting and tempers¹⁰. Table 2.1 lists the numerical and chemical designation of the most used alloys in high-pressure die-casting, well as their mechanical properties, while the chemical compositions limits are reported in Table 2.2, according to EN 1706:2010. Since the mechanical properties in HPDC are very dependent on injection parameters, the features reported in Table 2.1 are for guidance only. These are not typical values, but are the minimum values that may be expected from separately HPDC test pieces of 20,0 mm² cross sectional area with a typical wall thickness of 2,0 mm¹⁰. Refer to EN 1706:2010 for full details.

At present the European Standard specifies the chemical composition of 43 aluminium alloys, without any distinction between alloys produced from ore (primary alloys) and recycled aluminium, produced by remelting scrap (secondary alloys). The difficulty in recycling cast alloys is one of tolerance, which is the ability of an alloy to absorb different grades of scrap during its manufacture, rather than requiring the use of primary metal. The tolerance limit of most foundry aluminium alloys is low, especially for the alloys commonly used in sand and gravity casting¹¹. Most alloys have too much Cu, Fe, Si, or Zn to be used to any extent as scrap for preparing casting alloys outside their original class. Exceptions to this are some alloys widely used in high-pressure die-casting, such as EN AC-46000, which had reasonably high levels of all the major alloying elements. As a result, these alloys are often the main product of secondary smelters trying to make use of all the available cast scrap¹. These alloy can be diluted by customers with pure aluminium with primary metal, to produce more desirable alloys, since the removal of most alloying elements from molten aluminium is impractical¹².

Table 2.1: EN 1706:2010, Alloy designation and mechanical properties of alloys commonly used in pressure die-cast¹⁰.

Alloy group	Alloy designation		Temper designation	Tensile strength [MPa]	Yield strength [MPa]	Elongation [%]	Brinell hardness [HBW]
	Numerical	Chemical symbols					
Al	-	Al 99.6E	F	75	-	10	17
	-	Al 99.7E	F	75	-	10	17
AlSi10Mg	EN AC-43400	EN AC- <chem>AlSi10Mg(Fe)</chem>	F	240	140	1	70
	EN AC-43500	EN AC- <chem>AlSi10MnMg</chem>	F	250	120	5	65
			T5	270	150	4	80
			T7	200	120	12	60
AlSi	EN AC-44300	EN AC- <chem>AlSi12(Fe)(a)</chem>	F	240	130	1	60
	EN AC-44400	EN AC- <chem>AlSi9</chem>	F	220	120	2	55
AlSi9Cu	EN AC-44500	EN AC- <chem>AlSi12(Fe)(b)</chem>	F	240	140	1	60
	EN AC-46000	EN AC- <chem>AlSi9Cu3(Fe)</chem>	F	240	140	<1	80
	EN AC-46100	EN AC- <chem>AlSi11Cu2(Fe)</chem>	F	240	140	<1	80
	EN AC-46200	EN AC- <chem>AlSi8Cu3</chem>	F	240	140	1	80
	EN AC-46500	EN AC- <chem>AlSi9Cu3(Fe)(Zn)</chem>	F	240	140	<1	80
AlSi(Cu)	EN AC-47100	EN AC- <chem>AlSi12Cu1(Fe)</chem>	F	240	140	1	70
AlSiCuNiMg	EN AC-48100	EN AC- <chem>AlSi17Cu4Mg</chem>	F	220	160	<1	90
AlMg	EN AC-51200	EN AC- <chem>AlMg9</chem>	F	200	130	1	70
	EN AC-51500 ^a	EN AC- <chem>AlMg5Si2Mn</chem>	F	250	140	5	70

^{a)} These mechanical properties are typical for wall thickness up to 4 mm.

NOTE: For F temper (as cast condition), the values specified in this table can be eventually obtained only after holding a few days at room temperature.

Table 2.2: EN 1706:2010, Chemical composition of alloys commonly used in pressure die-cast (wt.%)¹⁰. Aluminium content is the remainder.

Alloy designation	Si	Fe	Cu	Mn	Mg	Cr	Ni	Zn	Pb	Sn	Ti ^b	Others ^a	
												Each	Total
EN AC-43400	9,0 - 11,0	1,0	0,10	0,55	0,20 - 0,50	-	0,15	0,15	0,15	0,05	0,20	0,05	0,15
EN AC-43500	9,0 - 11,5	0,25	0,05	0,4 - 0,8	0,10 - 0,60	-	-	0,07	-	-	0,20	0,05	0,15
EN AC-44300	10,5 - 13,5	1,0	0,10	0,55	-	-	-	0,15	-	-	0,15	0,05	0,25
EN AC-44400	8,0 - 11,0	0,65	0,10	0,50	0,10	-	0,05	0,15	0,05	0,05	0,15	0,05	0,15
EN AC-44500	10,5 - 13,5	1,0	0,20	0,55	0,40	-	-	0,30	-	-	0,15	0,05	0,25
EN AC-46000	8,0 - 11	1,3	2,0 - 4,0	0,55	0,05 - 0,55	0,15	0,55	1,2	0,35	0,15	0,25	0,05	0,25
EN AC-46100	10,0 - 12,0	1,1	1,5 - 2,5	0,55	0,30	0,15	0,45	1,7	0,25	0,15	0,25	0,05	0,25
EN AC-46200	7,5 - 9,5	0,8	2,0 - 3,5	0,15 - 0,65	0,05 - 0,55	-	0,35	1,2	0,25	0,15	0,25	0,05	0,25
EN AC-46500	8,0 - 11,0	1,3	2,0 - 4,0	0,55	0,05 - 0,55	0,15	0,55	3,0	0,35	0,15	0,25	0,05	0,25
EN AC-47100	10,5 - 13,5	1,3	0,7 - 1,2	0,55	0,35	0,10	0,30	0,55	0,20	0,10	0,20	0,05	0,25
EN AC-48100	16,0 - 18,0	1,3	4,0 - 5,0	0,50	0,25 - 0,65	-	0,30	1,5	-	0,15	0,25	0,05	0,25
EN AC-51200 ^c	2,5	1,0	0,10	0,55	8,0 - 10,5	-	0,10	0,25	0,10	0,10	0,20	0,05	0,25
EN AC-51500 ^c	1,8 - 2,6	0,25	0,05	0,4 - 0,8	4,7 - 6,0	-	-	0,07	-	-	0,25	0,05	0,25

^{a)} "Others" includes all the elements which are not listed in this Table or without specific values, while it does not include modifying or refining elements such as Na, Sr, Sb and P.

^{b)} Refining agents such as Ti, B or master alloys containing nucleating particles such as TiB₂ shall not be considered as impurities.

^{c)} For alloys with Mg ≥ 3 %, the alloy may contain 0,005 % Be max.

Cast aluminium alloys components for automotive are mostly (60-65%) manufactured by high-pressure die-casting, thanks to the high production rate and to the complexity of shape which can be obtained. Europe HPDC production of aluminium alloys components can be on average estimate at 1.5 millions of tons per year, and it is carried out by about 1500 HPDC foundries, mainly place in Italy, Germany and Spain¹³. Recently, the Stacast EU Project (*New Quality and Design Standards for Aluminium Alloys Cast Products*, FP7-NMP-2012-CSA-6 - project n° 319188) highlighted the EU scenario of aluminium foundries¹⁴. The results, reported in Fig. 2.2, show that almost 70% of EU foundries performing the HPDC process, with a equal division between the SMEs and IND interviewed (SME: < 250 employees; turnover < 50 million Euro/year; IND: > 250 employees; turnover > 50 million Euro/year).

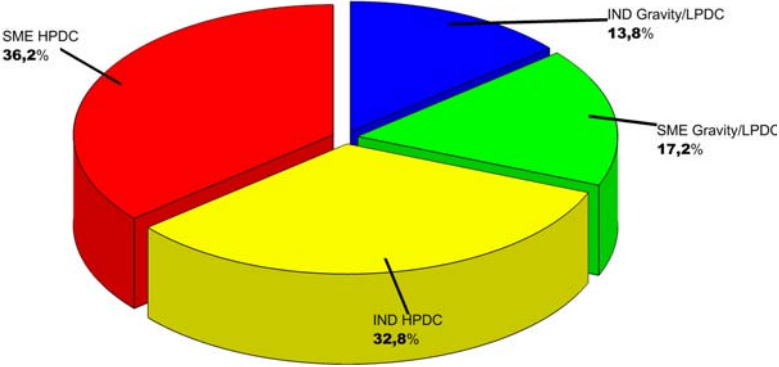


Figure 2.2: Partition of EU foundries: Gravity and LPDC (Low-Pressure Die-Casting) vs. HPDC (High-Pressure Die-Casting), taking into account SMEs and IND¹⁴.

The information concerning the alloys employed by the EU foundries interviewed within the project were reported in Fig. 2.3. These results highlight that the alloys which have the larger diffusions are typical high-pressure die-casting alloys¹⁴. Moreover, their wide chemical composition tolerance, reported in Table 2.2, allows secondary smelters to produce them with scrap material, i.e. as secondary aluminium alloys.

It is important to note that the most diffused and used foundry aluminium alloy in EU is the EN AB-46000, which corresponds to the alloy studied in the present work.

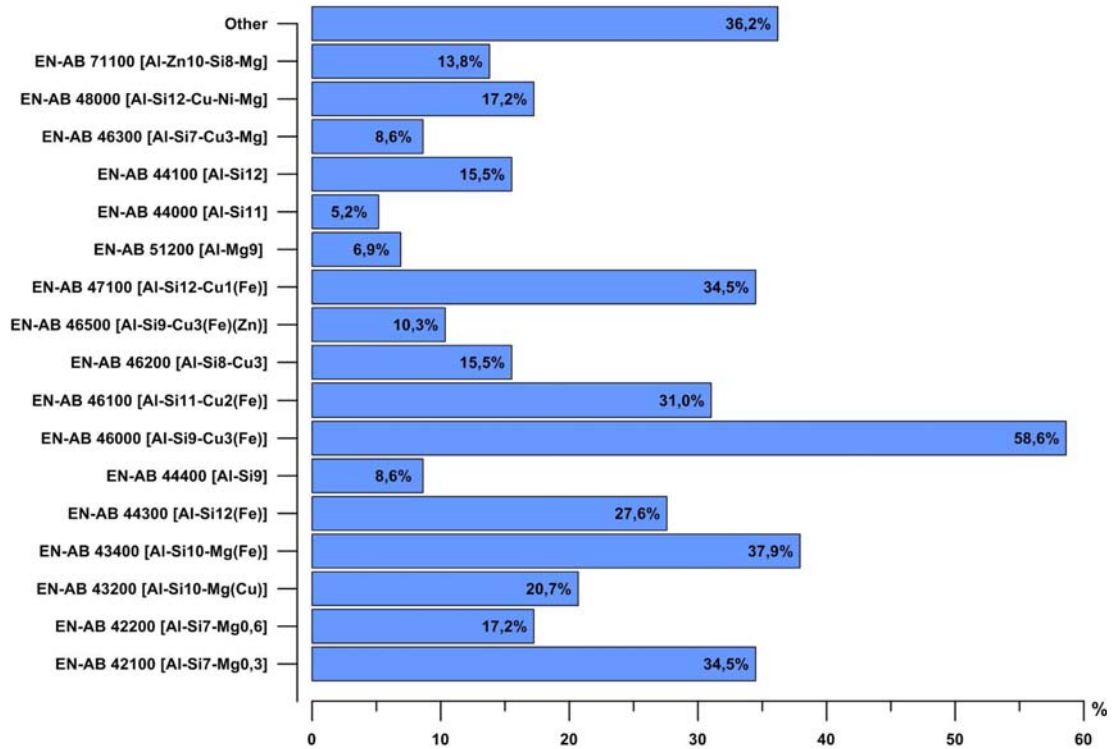


Figure 2.3: Alloys used by EU foundries interviewed during Stacast project¹⁴. The alloys designation refers to alloyed ingot for remelting, as specified in EN 1676:2010¹⁵.

2.3. Effect of alloying elements

As reported in Table 2.2, the Standard EN 1706:2010 list for each alloy 11 specific alloying elements, as well as the columns *others each* and *others total*, which mainly include the trace elements. Impurities and alloying elements, in general, partly go into solution in the matrix and partly form intermetallic particles during the solidification process.

2.3.1. Silicon

The outstanding effect of silicon in aluminium alloys is the improvement of casting characteristics. Silicon's high heat of fusion (~1810 J/g) contributes immensely to an alloy's fluidity, improving the feeding characteristics¹⁶. Increasing silicon content improves fluidity for filling thin walls and for reproducing more intricate designs and details³. Silicon also reduces specific gravity and thermal expansion coefficient, while it contributes significantly to an alloys wear resistance, especially in the hyper-eutectic, in which it is a primary

phase. Silicon alone contributes very little to the strength of aluminium casting alloys. However, when combined with magnesium to form Mg_2Si , Si provides a very effective strengthening mechanism in aluminium castings. Mg_2Si is soluble in the solid alloy to a limit of about 0.7% Mg, and provides the precipitation strengthening basis for an entire family of heat-treatable alloys¹⁷. Silicon can also be combined with Cu and produce finely dispersed $CuAl_2$ precipitates during artificial ageing.

2.3.2. Copper

Copper substantially improves strength and hardness in the as-cast and heat treated conditions. It also improves the machinability of alloys by increasing matrix hardness, making it easier to generate small cutting chips and fine machined finishes. Moreover, this element generally reduces the corrosion resistance of aluminium alloys and in specific compositions and material conditions increases stress-corrosion susceptibility¹⁸.

2.3.3. Magnesium

Small amount of Mg, that ranges from 0.25 to 0.5 wt.%, allowed strength and hardness development during heat treatment of aluminium-silicon alloys through the precipitation of Mg_2Si in a finely dispersed form. The hardening-phase Mg_2Si displays a useful solubility limit corresponding to approximately 0.70 wt.% Mg, beyond which either no further strengthening occurs or matrix softening takes place³. Mg is the basis for and is commonly used in more complex Al-Si alloys containing copper, nickel, and other elements for the same purpose. Mg is also used in hyper-eutectic piston alloys at content about 1 wt.%. Higher Mg contents, from 4 to 10 wt.%, are widely used in applications requiring a bright surface finish and excellent corrosion resistance. To avoid embrittlement, the Mg contents in HPDC alloys is kept low. Moreover the presence of Mg increases the oxidation losses of liquid aluminium and promote the formation of spinel ($MgO \cdot Al_2O_3$)¹⁹.

2.3.4. Iron

Fe is one of the most detrimental impurity element of Al-Si alloys, since it forms brittle intermetallic compounds that reduce mechanical properties and increase the amount of porosity^{12,20-25}. However, iron is a desirable and

necessary in aluminium die-casting alloys because it increase the high-temperature properties of Al alloys and it helps to prevent or alleviate the die soldering^{26,27}. Therefore, inexpensive secondary alloys with an already relatively high Fe content (in the range of 1 wt.%) are commonly used in HPDC^{12,16,28}. A detailed description of Fe-rich compounds and their effects is reported in the Chapter 3.

2.3.5. Manganese and Chromium

Normally considered an impurity in casting compositions, Mn can be added in small quantities in the alloy to neutralize or control the detrimental effect of iron^{8,12,16,25,28}. Cr has similar effect of Mn on Fe-rich phases^{16,29-31}. A more detailed description of these elements is provided in Chapter 3.

2.3.6. Nickel

In combination with Cu enhance strength and hardness at elevated temperature for use in the range for use in the range of 250°C to 375°C¹⁶. It also reduces the coefficient of thermal expansion³.

2.3.7. Zinc

Since Zn neither enhances nor detracts alloy's properties, it is present as an acceptable impurity element in many secondary die-casting alloys. However, combined with Cu and/or Mg, zinc improve the heat treatment and naturally ageing features and the fluidity, but shrinkage problems may occur.

2.3.8. Lead and Bismuth

Improve the machinability of the alloy at levels over 0.1 wt.%³². Low Bi addition, that ranges from 0.01 to 0.02 wt.%, can restore ductility in the Na-contaminated Al-Mg alloys³³.

2.3.9. Titanium and Boron

Titanium refine the grain structure of aluminium casting alloys, often in combination with smaller amounts of B, as show in Fig. 2.4³⁴. The operable phase is TiAl₃ with lattice spacing closely matched to that of aluminium^{35,36}. Titanium in excess of the stoichiometry of TiB₂ is necessary for effective grain refinement. Boron combines with other metals to form AlB₂ and TiB₂. The latter forms stable nucleation sites that interact with active grain-refining phases, such

as TiAl_3 , for grain refinement^{37,38}.

The addition of grain refiners, usually in the form of master alloys, promotes formation of a fine equiaxed macrostructure, that increase castability and mechanical properties compared to castings with columnar or larger grains. The finer grain size results in reduced total shrinkage porosity and the promotion of smaller and improved porosity dispersion⁶. Furthermore, a fine grain size creates a smaller and more uniform distribution of secondary-phase particles and pores from the evolution of dissolved gas in the melt³⁷. In addition, a fine grain size has better machinability and reduced susceptibility to hot tearing⁸.

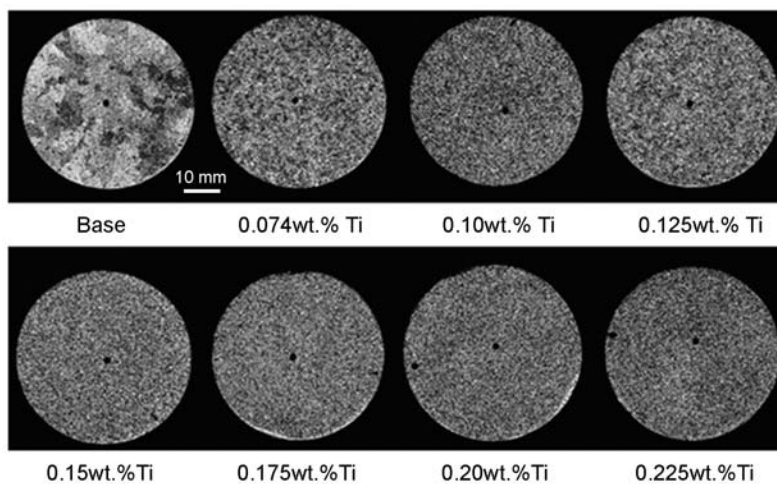


Figure 2.4: Effects of AlTi_5B_1 addition on the grain structure of secondary aluminium alloy. The amount of AlTi_5B_1 master alloy is expressed as Ti content³⁴.

2.3.10. Phosphorus

Nucleates and refines primary Si phase formation in hyper-eutectic alloys. Low level of phosphorus coarsens the eutectic structure in hypo-eutectic Al-Si alloys and reduce the effect of Na and Sr eutectic modifiers¹⁸.

2.3.11. Sodium, Strontium, Calcium and Antimony

These elements (one or another, and not in combination) are added to eutectic or hypoeutectic alloys to modify the morphology of the eutectic Si phase. In normal Al-Si casting alloys eutectic silicon solidifies in a relatively coarse continuous network of large platelets and needles, which provides high stress risers. Modification changes the eutectic silicon into a fine fibrous or lamellar structure, and thus improve ductility, fatigue life and tensile strength^{6,17}.

Moreover modification increase hot tear resistance and alloy feeding characteristics, decreasing shrinkage porosity³⁹. The range of chemical modified microstructures is divided into six classes to assess the modification level, as reported in Fig. 2.5.

The first hypo-eutectic modifiers were based on Na. Although this element provides optimal microstructural results, it has a high vapour pressure and high affinity to oxygen, it readily burns off and its modification efficiency is lost within a rather short time⁸. Strontium has a modifier has the advantage over sodium that is less reactive and fade only occurs over a period of several hours¹⁷.

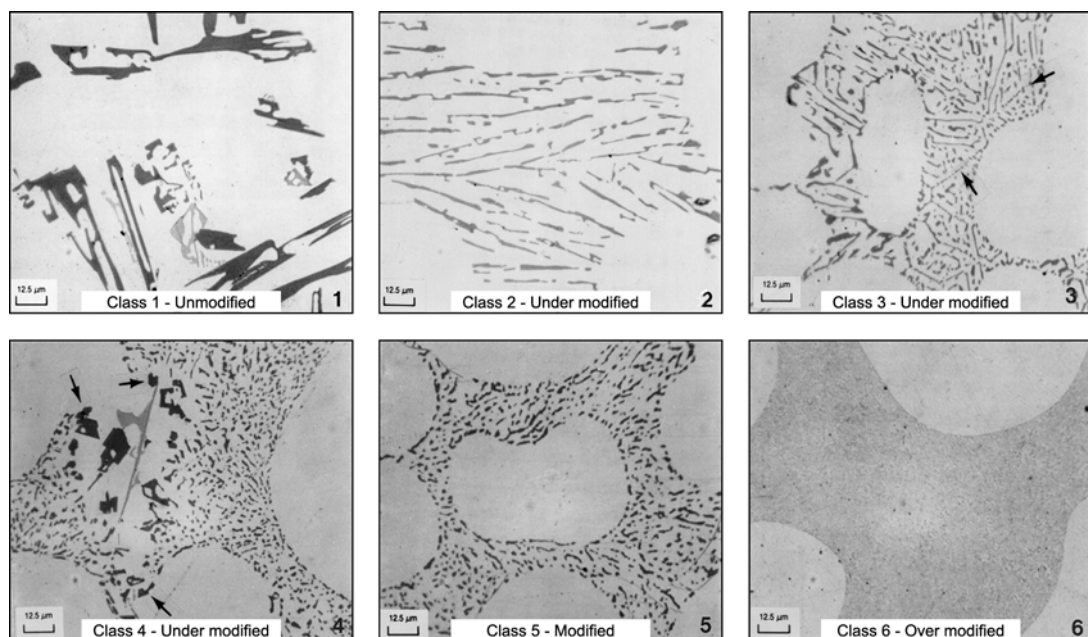


Figure 2.5: Classification of chemical modified microstructures to assess the modification level³⁹.

2.4. High-pressure die-casting

The production of Al alloy castings by the die-casting process exceeds that of all other foundry processes. High-pressure die-casting is a net-shape manufacturing process that provides dimensionally accurate parts with excellent surface finish, ideally suited for high production rate and volume production⁴⁰. A die-cast component may replace an assembly composed of a variety of parts produced by various manufacturing processes. Consequently, the consolidation

into a single casting can significantly reduce cost and labour. Little or no machining is needed on the cast, since holes, grooves and recesses can be finish cast. In recent years there has been an improvement of HPDC machine and technologies, that allowed to use high-speed and precision equipment to larger castings with heavier wall thicknesses, such as engine block⁴¹.

In conventional high-pressure die-casting, molten metal is injected under pressure into water-cooled dies and solidified under externally applied pressure of up to 100 MPa. The molten alloy rapidly fill the mold cavity by the action of a hydraulic piston in a containment chamber, generally called *shoot sleeve*. In order to facilitate the removal of the solidified casting from the die surface, to control the die temperature and to increase the die material life, a lubrication stage is necessary after each cycle.

The HPDC machine is composed of three main parts: the clamping unit, the die assembly and the injection unit. Depending on the design of the metal injection systems, two basic conventional HPDC exist: the hot- and the cold-chamber process, which were shown schematically in Fig. 2.6 and 2.7⁴¹.

In the hot-chamber process, a significant portion of the metal injection system is immersed in molten metal. A vertical plunger pushes the metal through the metal feed system, called *gooseneck*, into the die. This mechanism prevents oxidation of the melt and decrease the cycle time since molten metal needs to travel only a very short distance for each cycle. However, the machine size (i.e. its locking force) and the maximum shot weight are smaller than the cold-chamber process due to the injection system design. Hot-chamber die-casting is used for molten metal that is not aggressive with the materials of construction, such as magnesium and zinc.

Except in rare cases, aluminium alloys are cast in cold-chamber die-casting machine, in which the molten metal is introduced through a ladle (or metered by some other method, i.e. dosing furnace) into the shot sleeve with each cycle. The plunger moves horizontally inside the shoot sleeve and force the metal inside the die cavity. The shot sleeve is typically at 200-300°C. Unlike the hot-chamber machine, the metal injection system is only in intimate contact with the molten metal for a short period of time. Based on the design of the

metal injection system and the plunger movement, HPDC cold-chamber machine have a locking force that ranges from 100 up to 4500 tonnes. Die are expensive but can have life of more than 100000 shots⁴².

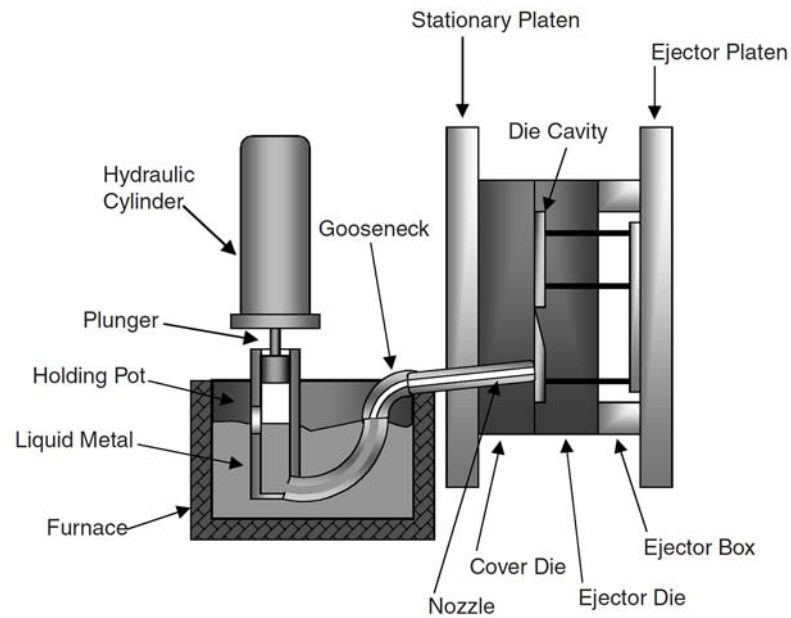


Figure 2.6: Graphical illustration of a hot-chamber high-pressure die-casting machine⁴¹.

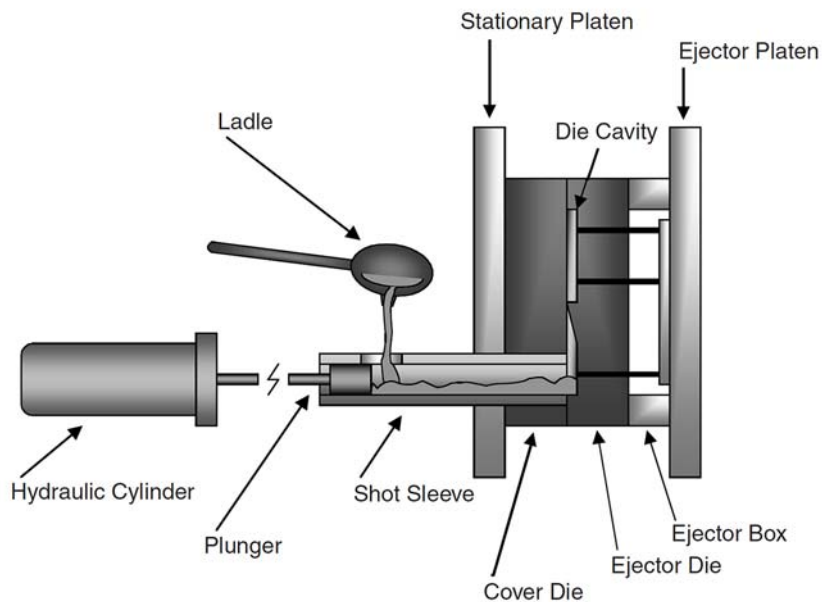


Figure 2.7: Graphical illustration of a cold-chamber high-pressure die-casting machine⁴¹.

All die casting processes follow a similar production cycle, reported in Fig. 2.8. It can be divided into 6 steps:

- a) liquid metal is poured or metered into an injection system;
- b) plunger slow movement (slow shot phase), with the metal that fills completely only the shoot sleeve;
- c) plunger fast movement, with a rapid filling of the die cavity. Castings with a wall thickness of 3-4 mm are filled in less than 0.1 seconds;
- d) plunger hydraulically pressurizes the metal during solidification stage to feed the shrinkage;
- e) die opens after complete solidification of the casting;
- f) component is ejected. The die is cleaned from any scrap remained from the previous shot and is lubricated to facilitate the ejection of the next casting.

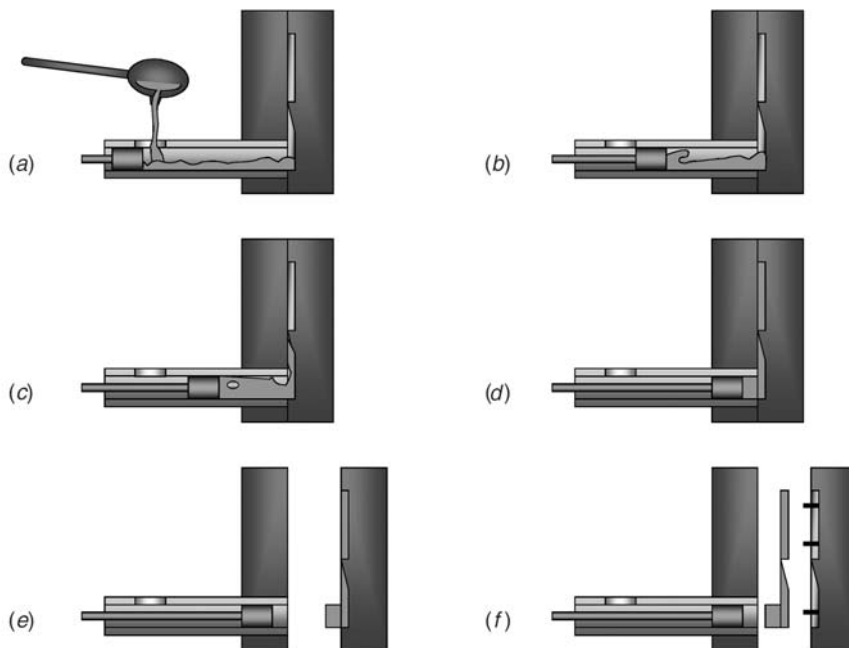


Figure 2.8: Casting cycle for cold-chamber high-pressure die-casting machine⁴¹.

The short filling time of die cavity and the typical thin wall thickness results in high cooling rates of the casting, which can exceed $1000^{\circ}\text{C}/\text{sec}$. This promotes a fine microstructure and theoretically increases the mechanical properties of the castings. However, the main disadvantage of the HPDC process is related to the presence of defects, such as air and gas porosity and inclusions of oxide films⁴³.

This is mainly due to the fast and turbulent die filling and fragmentation of the metal stream, with a metal flow speed that can reach around 60 m/sec at ingate⁴⁴. The presence of internal gas prevents subsequent solution heat treatment, since it expands and distorts the casting, reducing the surface quality and form blistering (Fig. 2.9). The use of conventional HPDC for structural parts is therefore restricted because not only are the castings limited in strength by internal defects, but also the presence of these defects in turn prevents any subsequent strength benefit from heat treatment⁴³.



Figure 2.9: Blistering of HPDC casting after solution heat treatment.

In order to reduce the gas entrapment and to obtain high quality die castings, an optimal movement of the plunger must be guaranteed. A controlled acceleration of the piston in the slow shot phase can cause a wave of liquid metal in the shot sleeve to expel the air ahead (Fig. 2.10a), while a rapid movement trap a bubble of air in the molten metal, which was then injected in the die cavity (Fig. 2.10b)⁴⁵. Moreover the application of maximum pressure is delayed until solidification has started in order to reduce the flash formation⁴⁶.

The shot sleeve filling time depends on the amount of metal being poured, (volume of shot sleeve), and is in the range of ~1-8 seconds, as a fill fraction of 0.5 is usually employed. Furthermore, a common foundry practice is to wait for a few second after pouring to let the metal settle and to allow the escape of any air bubbles from the melt.

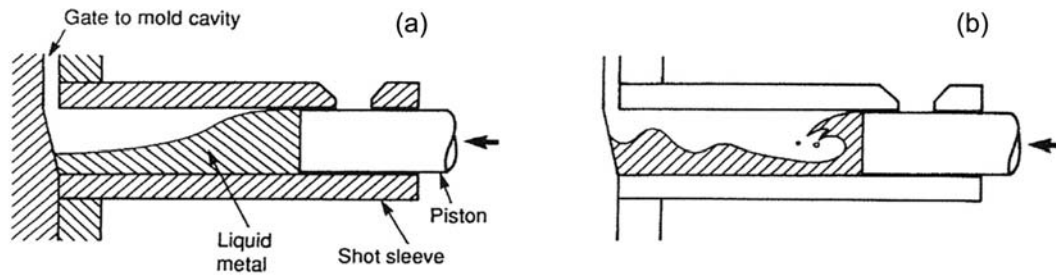


Figure 2.10: Injection of metal comparing (a) controlled and (b) uncontrolled slow shot phase of injection⁴³.

Besides several process parameters which can affect the properties of the castings, the alloy itself is similarly important. Die filling and solidification conditions in HPDC require alloys with high castability, i.e. high fluidity, good feeding and low hot tearing tendency. Consequently, the highly castable alloys of the Al-Si family are the most used in HPDC. Of these, AlSi9Cu3(Fe) type alloys (EN AB-46000, comparable with the US designation A380) are the most common, since their compositions provide attractive combinations of cost, strength, hardness, and corrosion resistance in the as-cast state, with excellent fluidity and resistance to hot cracking.

Chapter 3

EFFECTS OF TRACE ELEMENTS

3.1. Introduction

Depending on the purity of the base material, the Al-Si foundry alloys contain varying amounts of impurity elements. Iron, Manganese, Chromium and Bismuth correspond to typical impurities elements in secondary aluminium alloys. The purpose of this chapter is to bring the literature analysis of the effects of these trace elements and their typical intermetallic phases which form in Al-Si die-casting alloys in order to give the reader sufficient background in the interpretation of the results in the articles presented in the part two of this thesis.

3.2. Bismuth

3.2.1. Bismuth source in Al casting alloys

Bismuth is an impurity element in Al-Si casting alloys, and it is normally present in secondary aluminium alloys due to the scrap recycling. Since it is not separately specified in alloy specifications, its limit is describe as *other each*, as reported in Table 2.2¹⁰. The maximum allowable content of Bi in EN AB-46000 alloy is 0.05 wt.%.

Bismuth, as well as other low-melting-point elements, such as Pb, Sn and Cd, makes Al alloys free-machining alloys. These free-machining constituents are insoluble in solid α -Al phase and they form a soft, low-melting phases that promote chip breaking and help to lubricate the cutting tool³². Although lead was the typical element added to conventional wrought aluminium free-cutting alloys, over the last years attention has been paid to reduce and finally eliminate Pb and Pb containing products due to their toxicity^{47,48}. At present the RoHS

directive (*Restriction of Hazardous Substances*) provides that the maximum admissible Pb content in Al alloys is 0.4 wt.%⁴⁸. In order to keep a good free cutting machinability, new lead-free wrought alloys with Bi and Sn have been recently developed. These materials are the main source of Bi in Al foundry alloys, since the chips obtained by machining are mixed with the aluminium scrap. This leading to a steady increase of Bi level in secondary Al alloys, and this mechanism increases with the improvement of the recycling process, as reported in Fig. 3.1.

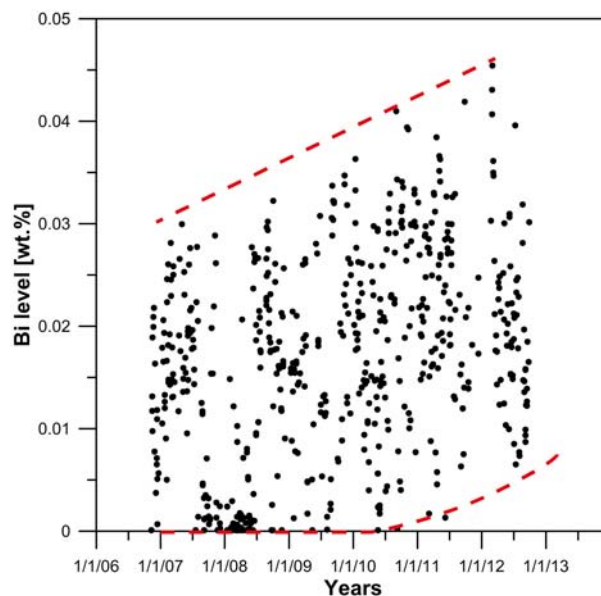


Figure 3.1: Trend of the Bismuth level in secondary EN AB-46000 alloy in Italy. Each point of the graph correspond to a optical emission spectrometer analysis⁴⁹.

3.2.2. Bismuth phase diagrams

Since Bi level increases in secondary aluminium alloys, it is important to analyse the possible intermetallic phases that Bi can form with the commonly alloying elements. The aim of this paragraph is to examine the Bi phase diagrams in order to better understand the Bi-rich phases composition found in HPDC castings^{50,51} (Article 1, pp. 49-60).

3.2.3. Al-Bi phase diagram

Bismuth solubility in Aluminium is assumed to be almost negligible, since it is less than 0.3 wt.% at monotonic temperature (657°C), while solid solubility in the terminal solid solutions, fcc (Al) and rhombohedral (Bi), are extremely

limited, as reported in Fig.3.2⁵². It was observed that homogeneous Al-Bi liquid decomposes into two immiscible liquids, where Bi-rich droplets nucleate and grow by diffusion in the Al-rich matrix melt until the monotectic temperature is reached⁵³.

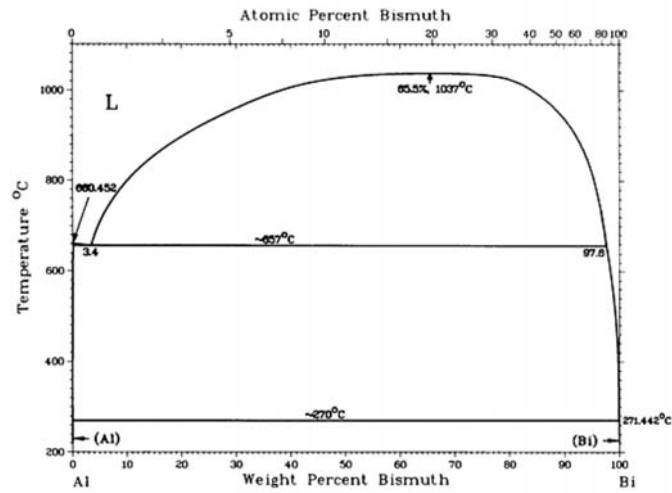


Figure 3.2: The Al-Bi phase diagram⁵².

3.2.4. Mg-Bi phase diagram

Bismuth show no solubility in solid Magnesium and vice versa, as reported in Fig. 3.3. Moreover these two elements forms a Mg_3Bi_2 intermetallic phase with a polymorphic transformation at 703°C. The eutectic point are at 58.9 wt.% of Bi and 553°C (Mg - α - Mg_3Bi_2) and at 99.9 wt.% of Bi and 271.4°C (Bi - α - Mg_3Bi_2)⁵⁴.

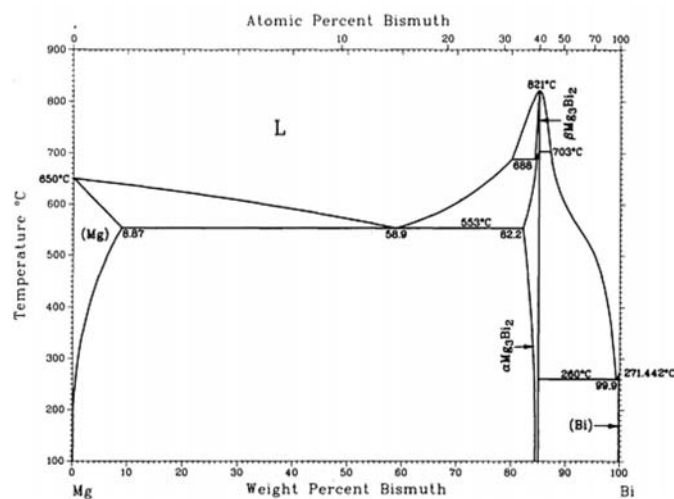


Figure 3.3: The Mg-Bi phase diagram⁵⁴.

3.2.5. Bi-Pb phase diagram

The assessed Bi-Pb phase diagram shown in Fig. 3.4 highlight a very low solubility of Pb in Bi (0.7 wt.%), while up to 20,1 wt.% of Bi is soluble in Pb. No intermetallic compound of unique stoichiometry were found in the Bi-Pb system, and usually they were indicated as ϵ phases or Pb- ϵ ⁵⁵.

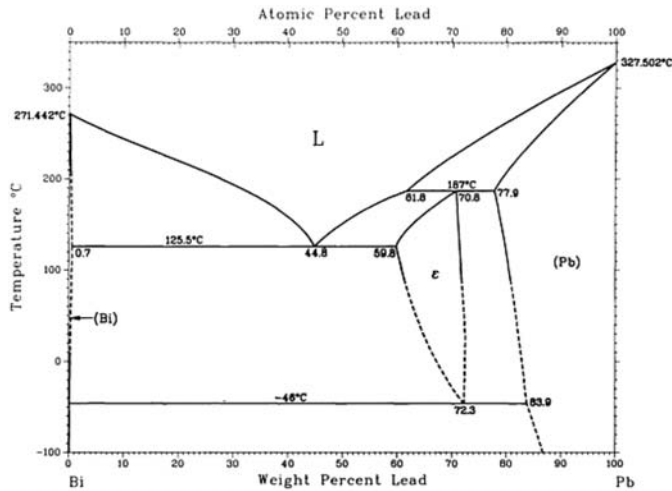


Figure 3.4: The Bi-Pb phase diagram⁵⁵.

3.2.6. Effect of Bismuth in Al-Si casting alloys

Limited research works were done on the Bi effect in Al-Si casting alloy. The main ones are focused on the Bi addition in eutectic and hypoeutectic Al-Si alloys in order to modify the morphology of the eutectic Si phase. Moreover it were analysed the interactions between Bismuth and the other modifier elements (see § 2.3.11).

Pillai and Anantharaman⁵⁶ reported that a Bi amount of 0.20 - 0.25 wt.% could serve as an effective eutectic modifier in an Al-Si eutectic alloy. Since Bi is in group V in the periodic table, they proposed a modifier mechanism similar to Antimony. Farahany et al.⁵⁷ highlight a similar result in AlSi7Mg0.4 alloy. In their work the refinement efficiency of Bi was found increase continuously up to 0.5 wt.% of Bi. Both slow (0.8 °C/sec) and fast (4 °C/sec) cooling rate were analysed, corresponding to sodium silicate bonded CO₂ sand mold and permanent metal mold, respectively. Moreover, the refinement behaviour of Bi showed a continuous decrease in the eutectic growth temperature and an increase in the recalescence temperature with increasing Bi. These

microstructural features as function of Bi content were reported in Fig. 3.5 in order to be compared with HPDC results^{50,51} (Article 1, pp. 49-60)

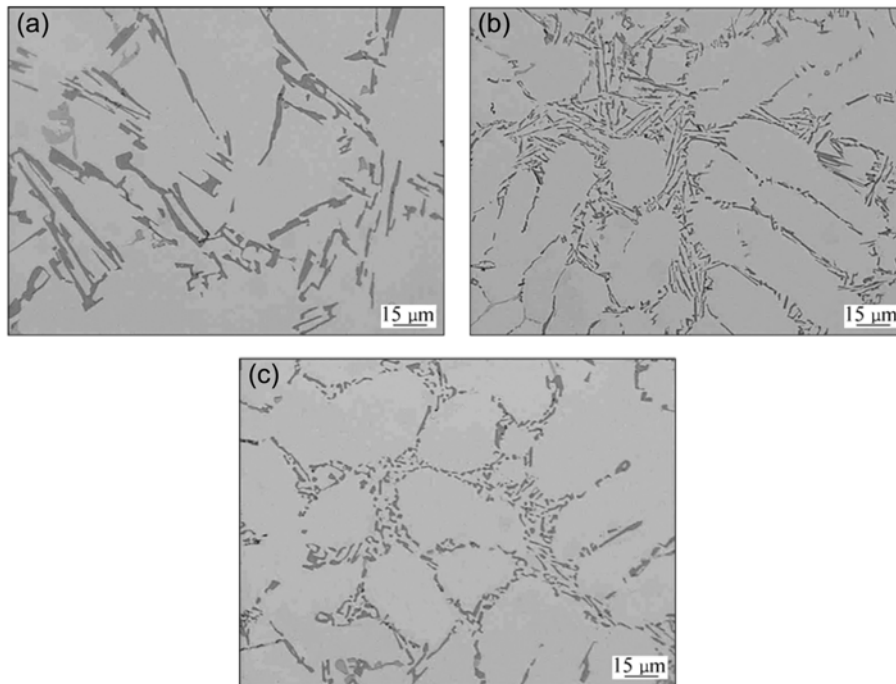


Figure 3.5: Microstructure of AlSi7Mg0.4 alloy solidified in a metal mold (cooling rate: 4°C/sec) as function of Bi content: (a) without Bi; (b) 0.1 wt.% Bi; (c) 0.5 wt.% Bi⁵⁷.

Although Bismuth acts as modifier in Al-Si cast alloys, it was seen that this element interferes with the modification effect of Strontium⁵⁷⁻⁵⁹. According to Cho and Loper⁵⁸, small amount of Bi, as little as 50 ppm, decrease the effect of Sr in a AlSi7Mg0.3 alloy. Sr modification was continuously nullified with increased amounts of Bi addition, up to 0.02 wt.% Bi, e.g., they observed more lamellar and coarser eutectic silicon. The Sr modification effect was completely eliminated by 0.1 wt.% Bi addition. This effect was more significant at slower solidification rates. They presumed that Bi might act quite similarly to that of Sb, by forming ternary and/or binary compounds with Sr, such as Bi₂Mg₂Sr, Bi₃Sr, BiSr, Bi₂Sr, and BiSr₂. Other studies^{57,59} reported that a Sr/Bi mass ratio higher than 0.45 is required when bismuth is present in the melt in order to retain full modification. The surface oxide film of Al-Si cast alloy is also modified by the addition of Bismuth as it disrupts the film's formation by forming a Bi-rich surface covering the liquid alloy⁶⁰. As the oxide skin grows, bismuth disrupts the oxide's integrity as it becomes incorporated into the oxide film.

3.3. Iron, Manganese and Chromium

3.3.1. Fe-rich phases in commercial Al-Si alloys

In commercial aluminium alloys with silicon the most common impurity element is iron, stemming from impurities in bauxite ore and from contamination of scrap aluminium with ferrous metal¹². Since Fe has a very low solubility in aluminium³⁰, it forms a variety of intermetallic compounds with Al, Si and other elements, which have a detrimental effect on the mechanical properties^{12,22-24,61,62} (Article 4, pp. 115-143). Fe cannot readily be removed from molten aluminium by conventional foundry treatment, thus dilution seems to be the only practical, although uneconomic, method to reduce its content in the alloy¹².

In Al-Si cast alloys the Fe compounds crystallize as monoclinic β -Al₅FeSi phase during the solidification, even at low Fe content in the melt⁸. These platelet-like phases, which appear as needles in the microstructure (Fig. 3.6a), act as stress raisers with a general reduction of the plastic properties of the cast alloy^{24,63}. Furthermore, the β -Fe phases block feeding channels earlier due their needle-like morphology, and cause feeding problems and casting porosity^{20,21,64}.

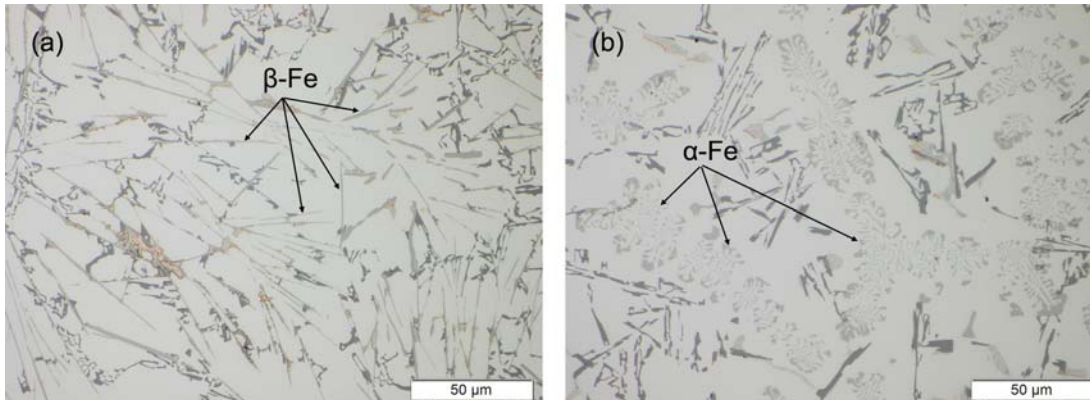


Figure 3.6: Microstructure of secondary Al-Si cast alloys with different amount of Fe, Mn and Cr: (a) the high Fe content results in the nucleation of β -Al₅FeSi as needle phase (β -Fe); (b) the addition of Mn and Cr change the Fe-rich particles' morphologies from β -Fe to α -Fe phases.

Although efforts are made to keep Fe content as low as economically possible in sand and gravity casting alloys, specifications normally permit considerably more iron to be present in alloys commonly used in pressure die-cast, as reported in Table 2.2. The Al-Fe-Si eutectic composition occurs at about

0.8 wt.% Fe. An highest Fe content reduces the solution potential of the molten Al alloy for the steel components of the casting machine and die, and consequently helps to prevent or alleviate the die-soldering^{26,27}.

Manganese and Chromium are present in secondary aluminium alloys as impurity elements, due to the scrap recycling process. However, they also have a beneficial effect in Al-Si cast alloy. Single or in combination, they can neutralize the detrimental effect of the monoclinic β -Al₅FeSi phase by modifying the morphology and type of phase to a less harmful body centred cubic crystal structure, α -Al(Fe,Mn,Cr)Si, which may appear as Chinese script, star-like or polyhedral morphology (Fig. 3.6b)^{25,28-31}. It is reported that if the Fe content exceeds 0.45 wt.%, it is desirable to have Mn present in an amount equal to one half of the Fe⁶⁵. The conversion phenomenon from β -Fe to α -Fe is also reported to occur in absence of alloying elements with a solidification rate higher than 20°C/sec⁶⁶.

3.3.2. The Al-Fe-Si system

In order to better understand the Fe-rich phases formation in Al-Si casting alloys it is important to analyze the Al-Fe-Si system at different amount of alloying element. However, the general Al-Fe-Si phase diagram found in literature is very complicated and difficult to interpret⁶⁷. Besides it shows a wide range of Fe-rich phases which not interest the Al-Si casting alloys due to the chemical compositions and cooling rates used in industrial casting processes.

A simplified version of Al-Fe-Si phase diagram is reported in Fig. 3.7⁸. It shows that the two main Fe-rich phases that occurring in hypo-eutectic Al-Si foundry alloys, even with a low amount of Mn in the melt, are β -Al₅FeSi and α -Al₁₅(Fe,Mn)₃Si₂. The addition of manganese in the alloy expands the α -phase region, and thus the crystallization of α -Fe is possible even at high level of iron, (Fig. 3.7 a-e). The evolution of the solidification process in an alloy with 8 wt.% Si, 0.62 wt.% Fe and 0.4 wt.% Mn is reported in Fig. 3.7 f. According to this chemical composition, the solidification process starts with the formation of α -Al dendrites network (line 1 in Fig. 3.7 f) with the interdendritic liquid that progressively enriches in iron and silicon. The slope of line 1 is calculated according to Scheil's equation, assuming that there is no chemical interference between Si and Fe before they start to form intermetallic particles (with Al and

Mn)^{8,9}. On further solidification, the segregation line penetrates the α -Fe surface and the nucleation of α -Al₁₅(Fe,Mn)₃Si₂ occurs (line 2 in Fig. 3.7 f). Since the α -Fe solidification consumes some Mn, the valley between the α -Fe and β -Fe is soon reach. As a results, the α -Al₁₅(Fe,Mn)₃Si₂ and the β -Al₅FeSi phases precipitate together until the eutectic composition is reached (line 3 in Fig. 3.7 f). When the ternary eutectic valley is obtained, Al, Si and β -Fe phase will precipitate together in the main eutectic reaction (line 4 in Fig. 3.7 f)⁸.

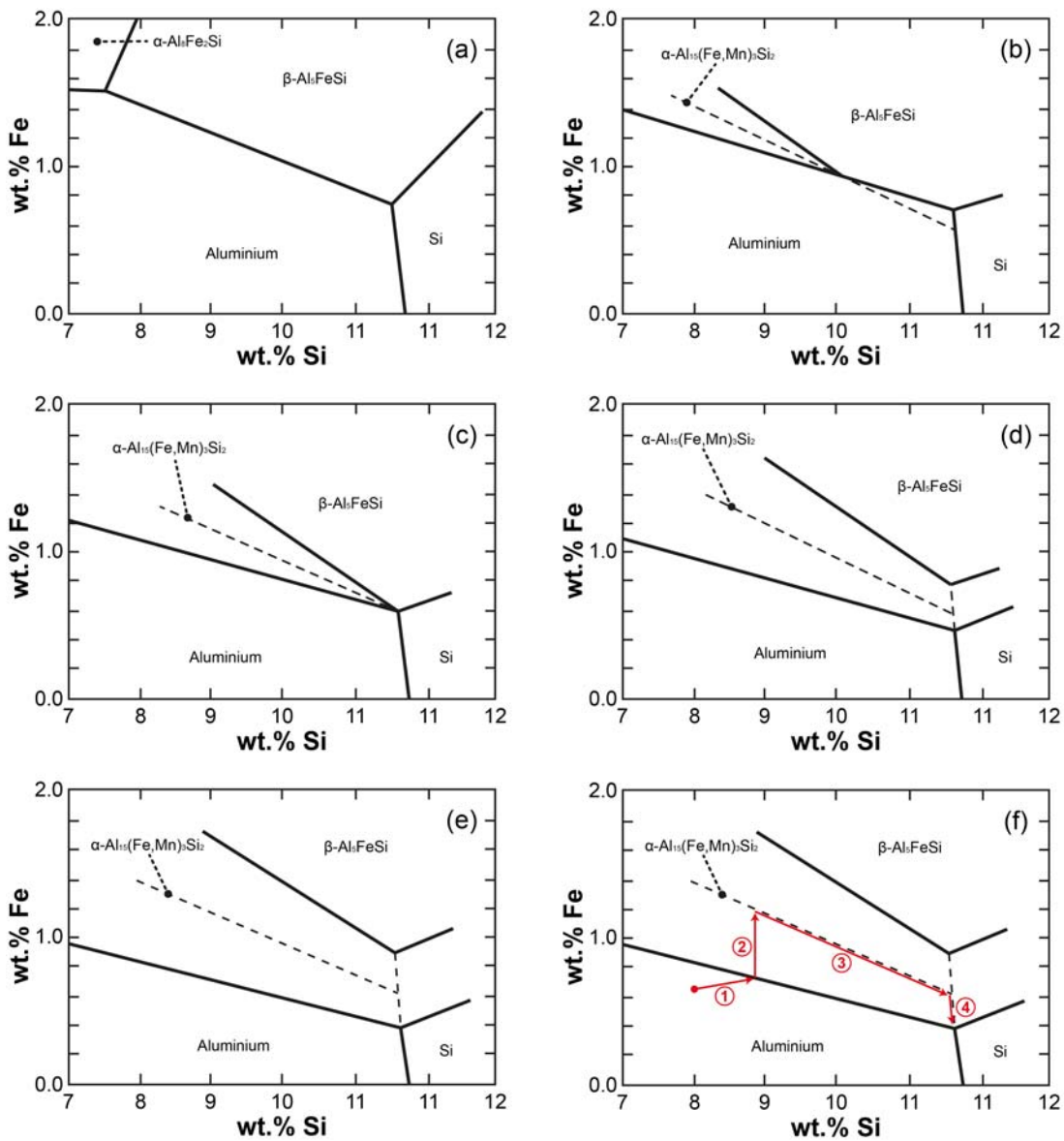


Figure 3.7: Simplified phase diagram of the Al-Fe-Si system at constant Mn levels: (a) 0.0 wt.% Mn; (b) 0.1 wt.% Mn; (c) 0.2 wt.% Mn; (d) 0.3 wt.% Mn; (e) 0.4 wt.% Mn⁸; (f) Evolution of the solidification process in an alloy with 8 wt.% Si, 0.62 wt.% Fe and 0.4 wt.% Mn⁸.

Nevertheless, the α -Fe and β -Fe phases do not have a well defined stoichiometry, since Fe, Mn and Cr have a similar atomic radii and they can substitute to each other in the crystal structure^{25,30}. It was found that the stoichiometry of β -phase correspond to Al_5FeSi where some Fe atoms can be replaced by up to 3.0 wt.% Manganese and Chromium, which are dissolved in the monoclinic crystal structure $\beta-Al_5(Fe,Mn,Cr)Si$ ^{25,68,69}. Moreover the stoichiometry of α -phase are close to $Al_{15}(Fe,Mn,Cr)_3Si_2$ and $Al_{12}(Fe,Mn,Cr)_3Si_2$, depending on the Fe, Mn and Cr content in the alloy and on the phase morphologies (polyhedral, star-like or Chinese script)^{25,29,30,68,70}.

3.3.3. Segregation of primary Fe-rich particles

Modification of Fe-bearing compounds with Mn and Cr addition has also some disadvantages, since they increases the total volume of Fe-rich particles. The complex intermetallic compounds, like α -Fe, can form as primary phases (along line 2 in Fig. 3.7 f), which may appear as Chinese script, star-like or polyhedral morphology, as reported in Fig. 3.8^{25,30,31,68,69} (Article 3, pp. 85-114). They have a high specific gravity and tend to segregate to the bottom of molten alloy and holding furnaces; such primary particles are generally called *sludge*^{25,26,28,71-73}. When sludge crystals are entrained into castings, they decrease the alloy's fluidity and appear as hard inclusions, which can compromise the machining operations and even more degrade the mechanical and physical properties of the component^{12,28,61,62,74-77} (Article 4, pp. 115-143).

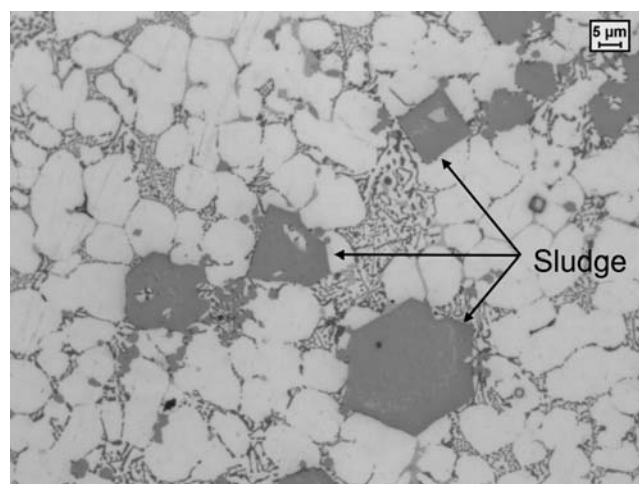


Figure 3.8: Sludge particles in a secondary $AlSi_9Cu_3(Fe)$ die-casting alloy. A comparison of the sludge size to the α -Al cell size reveals that these particles are primary phases⁶⁹.

The problem of sludge formation is often experienced in Al foundries, especially in the die-casting sector where, in order to preserve the die and the tools, the holding and casting temperatures are typically lower than in the other foundry processes²⁸. The formation of sludge particles may also empathise the die-soldering, even if the Al-Si alloys commonly used in HPDC allowed a high Fe content in order to prevent or alleviate this problem^{26,27}. Since sludge crystals are composed mainly of Fe- and Mn- rich compounds, their formation as primary phases causes a depletion of Fe and Mn in the melt²⁶.

Several empirical formulas have been developed in order to predict whether a given alloy composition is likely to cause Fe-rich intermetallic compounds to be formed and to segregate. Based on the Fe, Mn and Cr content in the alloy, a *Sludge Factor (SF)* is calculated (also referred as "iron equivalent value (IEV)", or "sludging factor", or "segregation factor", or "sedimentation factor"). This factor is matched to a suggested minimum holding temperature above which sludge formation would be minimized.

The first Sludge equation might be developed by Glaisher (1951)⁷⁸ using the following formula:

$$\text{Sludge Factor (SF)} = (1 \times \text{wt.\%Fe}) + (1.5 \times \text{wt.\%Mn}) \quad (3.1)$$

In order to calculate the Sludge Factor when the Cr content was considered, the equation (3.1) was implemented as follows⁷⁹:

$$\text{Sludge Factor (SF)} = (1 \times \text{wt.\%Fe}) + (1.5 \times \text{wt.\%Mn}) + (2 \times \text{wt.\%Cr}) \quad (3.2)$$

Parallel to this, another Sludge Factor formula was developed and first published by Dunn (1965)⁸⁰.

$$\text{Sludge Factor (SF)} = (1 \times \text{wt.\%Fe}) + (2 \times \text{wt.\%Mn}) + (3 \times \text{wt.\%Cr}) \quad (3.3)$$

Equation (3.3) is currently the most widespread and accepted, since Gobrecht (1975)⁷³ and Jorstad (1986)²⁸ demonstrated that it well describes the sludge particles segregation in the holding furnace for AlSi9Cu3(Fe) type alloys,

as reported in Fig. 3.9. A common foundry rule is to keep the SF under 1.7-1.8³.

Recently, Shabestari²⁵ found that the initial Fe, Mn and Cr contents as well as the cooling rate significantly affect the morphology, amount and size of the sludge. According to these results, the sludge forming temperature depends especially on the Fe content in the alloy with this relationship:

$$Temperature(^{\circ}C) = 645.7 + 34.2 \times (wt.\%Fe)^2 \quad (3.4)$$

The equation (3.4) highlight a wide differences if compared with the results of equation (3.3). For example, for an alloy containing 1 wt.% Fe, Shabestari equation predicts that sludge can form when the melt is held at 680°C, while the curves given by Gobrecht and Jorstad (Fig. 3.9) predict that for the same iron content, sludge can form only when the holding temperature is below 600°C.

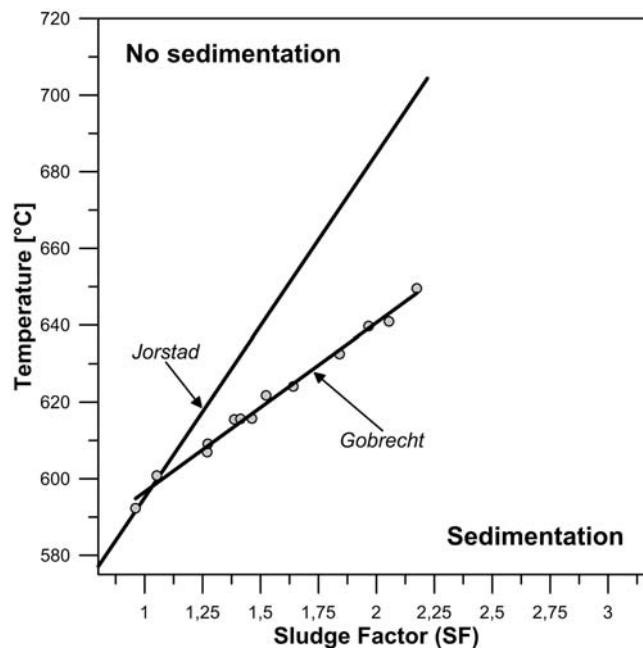


Figure 3.9: Suggested minimum holding temperature to minimize gravity segregation of primary Fe-bearing compounds as function of the *sludge factor* in AlSi9Cu3(Fe) type alloys, according to Gobrecht⁷³ and Jorstad²⁸.

In the work of Gobrecht⁷³ it is indicated that increasing Cu content and lower the Si content will increase the sludge formation temperature. However, the slope of the Gobrecht segregation curve is constant with variations in the chemical composition. The results from Jorstad²⁸ are not in particularly good

agreement with those from Gobrecht for the nominally identical AlSi9Cu3(Fe) alloy. However, this difference may result from different experimental conditions and from a different level of inclusions and oxide films in the molten metal.

When aluminium is melted, it instantaneously forms a thin protective amorphous film on all surface exposed to an atmosphere containing oxygen. This thin film is fairly impermeable to diffusion of metal and oxygen, so the oxide layer tends to inhibit further oxidation⁴³. The type of oxide that forms in Al-Si alloy is widely related to the chemical composition of the alloy. Depending on the Mg content the oxidation reaction can mainly develop alumina oxide (Al_2O_3), magnesium oxide (MgO) or a mixture of these (spinel, $\text{MgO}\cdot\text{Al}_2\text{O}_3$ or Al_2MgO_4). Since the nucleation of Fe-rich intermetallic particles is promoted by double oxide films^{71,81-84} (Fig. 3.10) and inclusions, such as CaO and SiC⁸⁵, a unsatisfactory cleaning treatment of molten metal can increase the sedimentation phenomena of Fe-rich phases. Moreover the aluminium oxide on the surface of the samples acts as a nucleant for sludge particles⁸⁶.

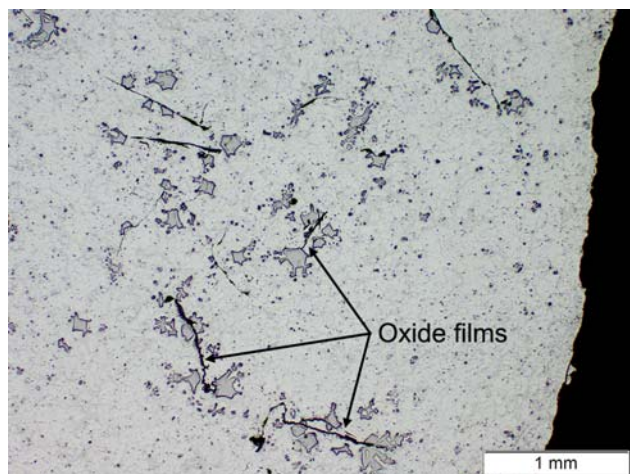


Figure 3.10: Nucleation of sludge particles on oxide film.

The melt temperature influence the crystal structure and lattice parameters of oxide films. A superheat temperature above 850°C results in a transformation of Al_2O_3 from metastable $\gamma\text{-Al}_2\text{O}_3$ (cubic) to the thermodynamically stable $\alpha\text{-Al}_2\text{O}_3$ (hexagonal), also called corundum^{66,83}. This conversion can be used to neutralize the effect of Fe without any addition of elements like Mn or Cr, since the $\gamma\text{-Al}_2\text{O}_3$ act as a nucleant for crystallization of $\beta\text{-Fe}$ phase while $\alpha\text{-Al}_2\text{O}_3$ promoting the formation of $\alpha\text{-Fe}$ phase^{66,71,83,87}.

It is important to note that sludge particles will also form in melts held above the sludge formation temperature when scrap is added into the melt, since local cooling below this critical temperature occurs. Similarly, sludge can be formed near the cold refractory linings of melting furnace. Moreover segregation of sludge may occur when the molten metal cooled down in the ladle during the melt transfer from the holding furnace to the die-casting machine and inside the shoot sleeve^{28,62,69,72}. Since the amount, size and morphologies of Fe-rich particles also depend largely on the cooling condition^{8,24,25,29,30,63}, the thermal condition may also influence the segregation temperature reported in Fig. 3.9 (Article 2, pp. 61-84).

3.3.4. Critical aspects

Wide studies have been conducted over the years on formation of sludge particles in the holding furnace^{8,25,28,71-74,80}. However, there was no full agreement to the relative contributions of different elements to the sludge formation. So, different criteria were formed based on different alloy composition and different experimental condition. In addition the main factors affecting the mechanical and microstructural properties of the aluminium alloys with different levels of Fe, Mn or Cr were described^{22-24,31,61,63,75,76,88-90}. However it lacks a correlation between the sludge formation in the holding furnace and in the ladle during the melt transfer, and the microstructural and mechanical effect of sludge on HPDC casting.

Actually, three critical aspects can be evidenced from the literature^{62,68,69} (Article 3, pp. 85-114; Article 4, pp. 115-143). Firstly, the mechanical and microstructural analysis were developed as function of a single impurity element, or the combination of only two, while sludge particles are (Fe,Mn,Cr)-based intermetallic compounds and therefore it seems important to consider the overall combination of the elements. Further, it is generally referred to primary aluminium alloys with low concentration of trace elements outside of those studied. However sludge is a problem of increasing importance in secondary aluminium alloys, with a higher levels of Fe, Mn and Cr. Finally, the mechanical properties were evaluated on gravity die-cast alloys; sludge formation is however more frequently observed in high-pressure die-casting, where higher cooling rates and different feeding conditions exist⁹¹.

Chapter 4

OBJECTIVES AND SURVEY OF THE ARTICLES

The aim of Article 1 was to study the effects of different Bismuth contents on the microstructure and mechanical properties of secondary AlSi9Cu3(Fe) die-casting alloy. Bismuth is an impurity element in Al-Si casting alloys, and its maximum allowable content in EN AB-46000 alloy is 0.05 wt.%. The main source of Bi is ascribed to the Bi-containing free-cutting wrought Al alloys, which are progressively substitute the lead containing alloys. Limited research works were done on the Bi effect in aluminium casting alloy. The main ones are focused on the Bi addition as modifier element in primary Al-Si gravity die-cast alloys. Since the recycling process of scrap is leading to a steady increase of Bi content in secondary Al alloys, a better understanding of the effects of this element may be necessary, especially under industrial casting conditions commonly used for secondary aluminium alloys, i.e. high-pressure die-casting.

The aim of Article 2 was to enlighten the role of Fe, Mn, and Cr, and the cooling rate on the primary precipitation of sludge particles in secondary AlSi9Cu3(Fe) alloys. The temperature and the evolution of sludge formation were studied by means of differential scanning calorimetry, thermal analysis and interrupt solidification with a rapid quenching technique. The objective of this paper is to allowed the foundry to set the right molten temperature in order to prevent formation and sedimentation of brittle intermetallic particles in the holding furnace and during the melt movement in HPDC machine.

The aim of Article 3 was to study the influence Fe, Mn and Cr additions on the sludge particles in secondary die-cast AlSi9Cu3(Fe) type alloy over three levels of iron (0.80, 1.00, 1.20 wt.%), three levels of manganese (0.25, 0.40, 0.55 wt.%) and two levels of chromium (0.06, 0.10 wt.%). Metallographic and image analysis techniques were used in order to quantitatively evaluate the morphological and dimensional variation of sludge particles occurring with Fe, Mn and Cr addition. In the analysed range of composition, the design of experiment (DOE) methodology and the analysis of variance (ANOVA) were used in order to develop a semi-empirical model that accurately predict the average size and number of sludge particles per unit area as function of the initial chemical composition of the alloy.

The aim of Article 4 was to evaluate the effects of sludge intermetallic particles on the tensile properties of a secondary AlSi9Cu3(Fe) die-casting alloy. Different alloys were produced by systematically varying the Fe, Mn and Cr content within the composition tolerance limits of the standard EN AC-46000. Cast-to-shape specimens were produced using a multicavity die in a cold chamber high-pressure die-casting machine. A statistical approach based on analysis of variance (ANOVA) was implemented in order to develop some functional equations useful to estimate the tensile properties in HPDC as function of the initial chemical composition of the alloy in castings with a wall thickness that ranges from 3 to 6 mm.

Chapter 5

CONCLUSIONS

The following conclusions can be draw from this doctoral thesis work:

- The Bismuth addition up to 0.3 wt.% on secondary die-cast AlSi9Cu3(Fe) type alloy seems to not produce significantly changes in the microstructure and mechanical properties. However, the Weibull statistics show that the addition of Bi leads to less reliable castings, which is mainly associated with an increase of defects, such as old oxide films and microshrinkage. No modification or refinement of eutectic Si particles were revealed, while the high solidification rate typical of HPDC process seems to mainly control the eutectic Si refinement and modification more than Bi content. Fine Bi-rich compounds, mainly distributed in the interdendritic regions and along grain boundaries, were revealed in the die-cast alloys. They are a complex Bi-Bi₂Mg₃ eutectic structure, which presents mainly rod-type and blocky morphology.
- The temperature of sludge formation is closely related to the specific chemical composition of the alloy. An increasing of Fe, Mn and Cr, i.e. the *sludge factor*, shifts sludge nucleation towards higher temperature regardless of the cooling rate. Furthermore, for the same chemical composition, the sludge formation temperature decrease with increasing the cooling conditions. The sludge formation temperature detected will support the foundries to set the right molten metal temperature in order to prevent sludge formation in the holding furnace and during the melt handling to and into plunger system in HPDC machines.

- Any increase of the Fe, Mn and Cr level in aluminium alloys promotes the formation of larger sludge particles, with a polyhedral and star-like morphologies. While Fe and Mn produce an increase on number of Fe-rich particles, Cr addition promotes the formation of a large number of pro-eutectic Fe-rich particles. No relationship has been found between sludge morphology variation, evaluated as roundness, and chemical composition (i.e. Fe, Mn and Cr content), sludge factor or Fe:Mn ratio.
- The Fe, Mn and Cr content, as well as the sludge amount seems to not influence the size and the content of porosity in HPDC casting.
- Even with a proper holding temperature, sludge particles may forms in secondary aluminium alloys mainly in the ladle and in the shot sleeve before the melt entered the die cavity.
- The *sludge factor* is not a reliable parameter to describe the mechanical features of the die-cast Al-Si alloys, because this value does not consider the mutual interaction between the elements.
- In the considered range of composition, the average tensile properties as well as the average size and number of sludge particles per unit area can be well described by a regression model that consider the concentration of Fe, Mn, Cr and the interaction between this elements.

References

- [1] M.E. Schlesinger: *'Aluminum Recycling'*, USA, Taylor & Francis, (2007).
- [2] S.K. Das: *'Designing Aluminum Alloys for a Recycling Friendly World'*, Mater. Sci. Forum, vol.519-521, pp.1239-1244, (2006).
- [3] J.G. Kaufman and E.L. Rooy: *'Aluminum Alloy Castings: Properties, Processes, and Applications'*, pp.340; USA, ASM International, (2004).
- [4] J. Zehnder, R. Pritzlaff, S. Lundberg, and B. Gilmont: *'Aluminium in Commercial Vehicles'*, 9th ed., European Aluminium Association, (1988).
- [5] EAA: *'Aluminium in Cars'*, 1st ed., pp.1-15; European Aluminium Association, (2007).
- [6] J.E. Gruzleski and B.M. Closset: *'The treatment of liquid aluminum-silicon alloys'*, USA, American Foundrymen's Society, Inc., (1990).
- [7] J.L. Murray and A.J. McAlister: *'The Al-Si (Aluminum-Silicon) system'*, Bulletin of Alloy Phase Diagrams, vol.5(1), pp.74-84, (1984).
- [8] L. Backerud, G. Chai, and J. Tamminen: *'Solidification Characteristics of Aluminum Alloys, vol 2: Foundry Alloys'*, pp.266; Stockholm, AFS-Skanaluminium, (1990).
- [9] W. Kurz and D.J. Fisher: *'Fundamentals of solidification'*, 4th ed., pp.305; Switzerland, Trans Tech Publications, (1998).
- [10] Standard EN 1706:2010, *'Aluminium and aluminium alloys - Castings - Chemical composition and mechanical properties'*, (2010).
- [11] J.A.S. Green: *'Aluminum Recycling and Processing for Energy Conservation and Sustainability'*, USA, ASM International, (2007).
- [12] P.N. Crepeau: *'Effect of Iron in Al-Si Casting Alloys: A Critical Review'*, AFS Trans., vol.103, pp.361-366, (1995).
- [13] ASSOFOND: *Report on EU & Italian Foundry in 2011*, Assofond, Milano, (2012).

- [14] Stacast: *1st Public Meeting*, Stacast project - New Quality and Design Standards for Aluminium Alloys Cast Products, Call FP7-NMP-2012-CSA-6, Project Number: 319188, Milano, (2013).
- [15] Standard EN 1676:2010, '*Aluminium and aluminium alloys - Alloyed ingots for remelting - Specifications*', (2010).
- [16] J.L. Jorstad: Proc. of 12th Int. Summer School on '*Light Alloy Castings: from Innovative Design to Advanced Applications*', Vicenza (IT), July 25th - 29th, (2011).
- [17] D. Apelian: *Worldwide Report - Aluminum Cast Alloys: Enabling Tools for Improved Performance*, NADCA, USA, (2009).
- [18] ASM: '*Handbook: Vol.15 Casting*', 9th ed., pp.1256; USA, ASM International, (2002).
- [19] J. Campbell: '*Castings*', 2nd ed., Great Britain, Butterworth-Heinemann, (2003).
- [20] C.M. Dinnis, J.A. Taylor, and A.K. Dahle: '*Iron-related porosity in Al-Si-(Cu) foundry alloys*', Mater. Sci. Eng. A, vol.425(1-2), pp.286-296, (2006).
- [21] L. Lu and A.K. Dahle: '*Iron-rich intermetallic phases and their role in casting defect formation in hypoeutectic Al-Si alloys*', Metall. Mater. Trans. A, vol.36(13), pp.819-835, (2005).
- [22] A.M.A. Mohamed, A.M. Samuel, F.H. Samuel, and H.W. Doty: '*Influence of additives on the microstructure and tensile properties of near-eutectic Al-10.8%Si cast alloy*', Mater. Design, vol.30(10), pp.3943-3957, (2009).
- [23] A.M.A. Mohamed, F.H. Samuel, A.M. Samuel, and H.W. Doty: '*Influence of additives on the impact toughness of Al-10.8% Si near-eutectic cast alloys*', Mater. Design, vol.30(10), pp.4218-4229, (2009).
- [24] S. Seifeddine and I.L. Svensson: '*The influence of Fe and Mn content and cooling rate on the microstructure and mechanical properties of A380-die casting alloys*', Metall. Sci. Technol., vol.27(1), pp.11-20, (2009).
- [25] S.G. Shabestari: '*The effect of iron and manganese on the formation of intermetallic compounds in aluminum-silicon alloys*', Mater. Sci. Eng. A, vol.383(2), pp.289-298, (2004).
- [26] M.M. Makhlof and D. Apelian: '*Casting characteristics of aluminum die casting alloys*', Work Performed Under DOE Contract No. DEFC07-99ID13716, vol., pp.1-46, (2002).
- [27] S. Shankar and D. Apelian: '*Die soldering: Mechanism of the interface reaction between molten aluminum alloy and tool steel*', Metall. Mater. Trans. B, vol.33(3), pp.465-476, (2002).

- [28] J.L. Jorstad: '*Understanding Sludge*', Die Casting Engineer, vol., pp.30-36, (1986).
- [29] G. Gustafsson, T. Thorvaldsson, and G.L. Dunlop: '*The influence of Fe and Cr on the microstructure of cast Al-Si-Mg alloys*', Metall. Trans. A, vol.17(1), pp.45-52, (1986).
- [30] L.F. Mondolfo: '*Aluminium alloys : structure and properties*', Butterworths, (1976).
- [31] G. Timelli and F. Bonollo: '*The influence of Cr content on the microstructure and mechanical properties of AlSi9Cu3(Fe) die-casting alloys*', Mater. Sci. Eng. A, vol.528(1), pp.273-282, (2010).
- [32] G. Timelli and F. Bonollo: '*Influence of tin and bismuth on machinability of lead free 6000 series aluminium alloys*', Mater. Sci. Tech., vol.27(1), pp.291-299, (2011).
- [33] D.E.J. Talbot and C.E. Ransley: '*The addition of bismuth to aluminum-magnesium alloys to prevent embrittlement by sodium*', Metall. Trans. A, vol.8(7), pp.1149-1154, (1977).
- [34] G. Timelli, G. Camicia, and S. Ferraro: '*Effect of Grain Refinement and Cooling Rate on the Microstructure and Mechanical Properties of Secondary Al-Si-Cu Alloys*', J. Mater. Eng. Perform., vol., pp.1-11, (2013).
- [35] P. Schumacher, A.L. Greer, J. Worth, P.V. Evans, M.A. Kearns, P. Fisher, and A.H. Green: '*New studies of nucleation mechanisms in aluminium alloys: implications for grain refinement practice*', Mater. Sci. Tech., vol.14(5), pp.394-404, (1998).
- [36] A.L. Greer, P.S. Cooper, M.W. Meredith, W. Schneider, P. Schumacher, J.A. Spittle, and A. Tronche: '*Grain Refinement of Aluminium Alloys by Inoculation*', Adv. Eng. Mater., vol.5(1-2), pp.81-91, (2003).
- [37] M. Easton and D. StJohn: '*Grain refinement of aluminum alloys: Part I. the nucleant and solute paradigms—a review of the literature*', Metall. Mater. Trans. A, vol.30(6), pp.1613-1623, (1999).
- [38] M. Easton and D. StJohn: '*Grain refinement of aluminum alloys: Part II. Confirmation of, and a mechanism for, the solute paradigm*', Metall. Mater. Trans. A, vol.30(6), pp.1625-1633, (1999).
- [39] A.K. Dahle: Proc. of 12th Int. Summer School on '*Light Alloy Castings: from Innovative Design to Advanced Applications*', Vicenza (IT), July 25th - 29th, (2011).
- [40] D. Apelian and J.L. Jorstad: '*Pressure Assisted Processes for High Integrity Automotive Aluminum Castings - Part 1: Principles and Fundamentals*', 3rd Int. conference High Tech Die Casting, Vicenza (IT), 21-22 September, (2006).

- [41] E.J. Vinarcik: *'High Integrity Die Casting Processes'*, pp.223; USA, Wiley, (2002).
- [42] J.R. Brown: *'Foseco Non-Ferrous Foundryman's Handbook'*, 11th ed., pp.304; Oxford, Butterworth-Heinemann, (1999).
- [43] J. Campbell: *'Complete Casting Handbook: Metal Casting Processes, Metallurgy, Techniques and Design'*, pp.1220; UK, Elsevier Butterworth-Heinemann, (2011).
- [44] G. Timelli, S. Ferraro, F. Grosselle, F. Bonollo, F. Voltazza, and L. Capra: *'Caratterizzazione meccanica e microstrutturale di leghe di alluminio pressocolate'*, La Metallurgia Italiana, vol.101(1), pp.5-17, (2011).
- [45] H.I. Laukli: *'High Pressure Die Casting of Aluminium and Magnesium Alloys - Grain Structure and Segregation Characteristics'*, PhD thesis, Norwegian University of Science and Technology (NTNU), Trondheim, (2004).
- [46] E. Gariboldi, F. Bonollo, and P. Parona: *'Handbook of defects in high pressure diecastings'*, pp.132; Milano (IT), AIM, (2010).
- [47] EU: *'Directive 2000/53/EC- End of Life Vehicles'*, Official Journal of the European Communities, vol.L269, pp.34-42, (2000).
- [48] EU: *'Directive 2011/65/EU - On the restriction of the use of certain hazardous substances in electrical and electronic equipment'*, Official Journal of the European Communities, vol.L174, pp.88-110, (2011).
- [49] S. Capuzzi: *'Sviluppo di trattamenti termici per componenti automotive colati in lega di alluminio secondario allo stato semi-solido'*, MS thesis, University of Padova, Department of Management and Engineering (2012).
- [50] S. Ferraro, G. Timelli, and A. Fabrizi: *'Effects of Bismuth on the microstructure and mechanical properties of AlSi9Cu3(Fe) diecasting alloys'*, Mater. Sci. Forum, vol.765, pp.59-63, (2013).
- [51] G. Timelli, S. Ferraro, and A. Fabrizi: *'Effects of chromium and bismuth on secondary aluminium foundry alloys'*, Int. J. Cast. Met. Res., vol.26(4), pp.239-246, (2013).
- [52] A.J. McAlister: *'The Al-Bi (Aluminum-Bismuth) system'*, Bulletin of Alloy Phase Diagrams, vol.5(3), pp.247-250, (1984).
- [53] P.L. Schaffer, R.H. Mathiesen, L. Arnberg, M. Di Sabatino, and A. Snigirev: *'In situ investigation of spinodal decomposition in hypermonotectic Al-Bi and Al-Bi-Zn alloys'*, New Journal of Physics, vol.10(5), (2008).
- [54] A.A. Nayeb-Hashemi and J.B. Clark: *'The Bi-Mg (Bismuth-Magnesium) system'*, Bulletin of Alloy Phase Diagrams, vol.6(6), pp.528-533, (1985).

- [55] N.A. Gokcen: *'The Bi-Pb (Bismuth-Lead) system'*, JPE, vol.13(1), pp.21-32, (1992).
- [56] R.M. Pillai and T.R. Anantharaman: *'Elements of V Group as Modifiers of Aluminum-Silicon Alloys'*, Trans. Metall. AIME, vol.24(2), pp.2025-2027, (1968).
- [57] S. Farahany, A. Ourdjini, M.H. Idris, and L.T. Thai: *'Effect of bismuth on microstructure of unmodified and Sr-modified Al-7Si-0.4Mg alloys'*, Trans. Nonferr. Metal. soc., vol.21(7), pp.1455-1464, (2011).
- [58] J.I. Cho and C.R. Loper: *'Limitation of Bismuth Residual in A356.2 Aluminum'*, AFS Trans., vol.108, pp.359-367, (2000).
- [59] C.J. Machovec, J.W. Zindel, L.A. Godlewski, and G.E. Byczynski: *'Determining The Effect Of Bi-Sr Interactions On Si Morphology In 319Al'*, Modern Casting, vol.90(6), pp.42-44, (2000).
- [60] A. Papworth and P. Fox: *'The disruption of oxide defects within aluminium alloy castings by the addition of bismuth'*, Mater. Lett., vol.35(3-4), pp.202-206, (1998).
- [61] J. Shouxun, Y. Wenchao, G. Feng, W. Douglas, and F. Zhongyun: *'Effect of iron on the microstructure and mechanical property of Al-Mg-Si-Mn and Al-Mg-Si diecast alloys'*, Mater. Sci. Eng. A, vol.564, pp.130-139, (2012).
- [62] S. Ferraro and G. Timelli: *'Influence of Sludge Particles on the Tensile Properties of Die-cast Secondary Aluminium Alloys'*, Submitted for publication in: Mat. Sci. Eng. A, vol., (2013).
- [63] S. Seifeddine, S. Johansson, and I.L. Svensson: *'The influence of cooling rate and manganese content on the β -Al₅FeSi phase formation and mechanical properties of Al-Si-based alloys'*, Mater. Sci. Eng. A, vol.490(1-2), pp.385-390, (2008).
- [64] J.A. Taylor, G.B. Schaffer, and D.H. StJohn: *'The role of iron in the formation of porosity in Al-Si-Cu-based casting alloys: Part I. Initial experimental observations'*, Metall. Mater. Trans. A, vol.30(6), pp.1643-1650, (1999).
- [65] ASM: *'Handbook: Vol.2 Properties and Selection: Nonferrous Alloys and Special-Purpose Materials'*, pp.1328; USA, ASM International, (2002).
- [66] L.A. Narayanan, F.H. Samuel, and J.E. Gruzleski: *'Crystallization behavior of iron-containing intermetallic compounds in 319 aluminum alloy'*, Metall. Mater. Trans. A, vol.25(8), pp.1761-1773, (1994).
- [67] G. Effenberg, H. Landolt, and S. Ilyenko: *'Ternary Alloy Systems: Phase Diagrams, Crystallographic and Thermodynamic Data'*, pp.292; Springer, (2008).

- [68] A. Fabrizi, S. Ferraro, and G. Timelli: *'The influence of Fe, Mn and Cr additions on the formation of Iron-rich intermetallic phases in an Al-Si die-casting alloy'*, Shape Casting 5: International Symposium, TMS, vol., (2014).
- [69] S. Ferraro, A. Fabrizi, and G. Timelli: *'The influence of Fe, Mn and Cr addition on Sludge in Die-cast Secondary Aluminum Alloys'*, Submitted for publication in: Metall. Mater. Trans. A, vol., (2013).
- [70] M. Warmuzek, W. Ratuszek, and G. Sęk-Sas: *'Chemical inhomogeneity of intermetallic phases precipitates formed during solidification of Al-Si alloys'*, Mater. Charact., vol.54(1), pp.31-40, (2005).
- [71] X. Cao, N. Saunders, and J. Campbell: *'Effect of iron and manganese contents on convection-free precipitation and sedimentation of primary α -Al(FeMn)Si phase in liquid Al-11.5Si-0.4Mg alloy'*, J. Mater. Sci., vol.39, pp.2303-2314, (2004).
- [72] S.G. Shabestari and J.E. Gruzleski: *'Gravity Segregation of Complex Intermetallic Compounds in Liquid Aluminum-Silicon Alloys '*, Metall. Mater. Trans. A, vol.26A, pp.999-1006, (1995).
- [73] J. Gobrecht: *'Schwere seigerungen von Eisen, Mangan und Chrom in Aluminium-Silicium-Gußlegierungen '*, Giesserei, vol.62(10), pp.263-266, (1975).
- [74] X. Cao and J. Campbell: *'Effect of Precipitation of Primary Intermetallic Compounds on the Mechanical Properties of Cast Al 11.5Si 0.4Mg Alloy'*, AFS Trans., vol.108, pp.391-400, (2000).
- [75] H.Y. Kim, S.W. Han, and H.M. Lee: *'The influence of Mn and Cr on the tensile properties of A356-0.20Fe alloy'*, Mater. Lett., vol.60(15), pp.1880-1883, (2006).
- [76] L. Ceschini, I. Boromei, A. Morri, S. Seifeddine, and I.L. Svensson: *'Microstructure, tensile and fatigue properties of the Al-10%Si-2%Cu alloy with different Fe and Mn content cast under controlled conditions'*, J. Mater. Process. Technol., vol.209(15-16), pp.5669-5679, (2009).
- [77] E. Taghaddos, M.M. Hejazi, R. Taghiabadi, and S.G. Shabestari: *'Effect of iron-intermetallics on the fluidity of 413 aluminum alloy'*, J. Alloys Compd., vol.468(1-2), pp.539-545, (2009).
- [78] W.H. Glaiser: *'Segregation of Iron and Manganese in Some Aluminium Casting Alloys'*, Metallurgia, vol., pp.127-131, (1951).
- [79] A. Kaye and A. Street: *'Chapter 8 - Inclusions and hard spots in aluminium alloys'*, in *'Die Casting Metallurgy'*, (eds. A. Kaye, et al.), pp.71-79; (1982), Butterworth-Heinemann.

- [80] R. Dunn: *'Aluminum Melting Problems and Their Influence on Furnace Selection'*, Die Casting Engineer, vol., pp.8-30, (1965).
- [81] X. Cao and J. Campbell: *'The nucleation of Fe-Rich phases on oxide films in Al-11.5Si-0.4Mg cast alloys'*, Metall. Mater. Trans. A, vol.34A, pp.1409-1420, (2003).
- [82] X. Cao: *'Heat Treatment of Liquid Metal - Precipitation and Sedimentation Processing of Liquid Al-11.5Si-0.4Mg Alloy'*, PhD thesis, University of Birmingham, School of Metallurgy and Materials, (2001).
- [83] X. Cao and J. Campbell: *'Effect of melt superheating on convection-free precipitation and sedimentation of primary α -Fe phase in liquid Al-11.5Si-0.4Mg alloy'*, Int. J. Cast. Met. Res., vol.15, pp.595-608, (2003).
- [84] X. Cao and J. Campbell: *'The Solidification Characteristics of Fe-Rich Intermetallics in Al-11.5Si-0.4Mg Cast Alloys'*, Mater. Sci. Eng. A, vol.35A, pp.1425-1435, (2004).
- [85] W. Khalifa, F.H. Samuel, J.E. Gruzleski, H.W. Doty, and S. Valtierra: *'Nucleation of Fe-Intermetallic Phases in the Al-Si-Fe Alloys'*, Metall. Mater. Trans. A, vol.36A, pp.1017-1032, (2005).
- [86] S. Terzi, J.A. Taylor, Y.H. Cho, L. Salvo, M. Suéry, E. Boller, and A.K. Dahle: *'In situ study of nucleation and growth of the irregular α -Al/ β -Al₅FeSi eutectic by 3-D synchrotron X-ray microtomography'*, Acta Mater., vol.58(16), pp.5370-5380, (2010).
- [87] A.M. Samuel, F.H. Samuel, H.W. Doty, and S. Valtierra: *'Effect of Superheat, Cooling Rate and Impurities on the Formation of Iron Intermetallics in Al-Si Die Casting Alloys '*, AFS Trans., vol.109, pp.679-696, (2001).
- [88] S. Seifeddine and I.L. Svensson: *'Prediction of mechanical properties of cast aluminium components at various iron contents'*, Mater. Design, vol.31, pp.S6-S12, (2010).
- [89] J.Y. Hwang, H.W. Doty, and M.J. Kaufman: *'The effects of Mn additions on the microstructure and mechanical properties of Al-Si-Cu casting alloys'*, Mater. Sci. Eng. A, vol.488(1-2), pp.496-504, (2008).
- [90] Z. Ma, A.M. Samuel, F.H. Samuel, H.W. Doty, and S. Valtierra: *'A study of tensile properties in Al-Si-Cu and Al-Si-Mg alloys: Effect of β -iron intermetallics and porosity'*, Mater. Sci. Eng. A, vol.490(1-2), pp.36-51, (2008).
- [91] P. Beeley: *'Foundry Technology, 2nd Edition'*, pp.719; Oxford, United Kingdom, Butterworth-Heinemann, (2001).

PART 2

ARTICLES

ARTICLE 1

EFFECTS OF BISMUTH ON THE MICROSTRUCTURE AND MECHANICAL PROPERTIES OF ALSi9Cu3(Fe) DIECASTING ALLOYS

S. Ferraro¹, G. Timelli¹, A. Fabrizi¹

¹ Department of Management and Engineering - DTG
University of Padua
Vicenza, ITALY

Presented at 6th International Light Metals Technology Conference (LMT 2013)

July 24-26, 2013, Old Windsor, United Kingdom.

Also published in: Materials Science Forum, vol.765, 59-63, 2013

ABSTRACT

In secondary diecast Al alloys, Bismuth is generally considered an impurity element and present as trace element in commercial foundry alloys. In the present work, the influence of different Bi content on the microstructure and mechanical properties of a commercial diecast AlSi9Cu3(Fe) alloy is investigated. The Bi level ranges between 0.015 and 0.3 wt.%. The results show that the presence of Bi seems to not produce significantly changes in the microstructure and mechanical properties. Fine Bi-rich compounds are observed in the diecast alloys and they are mainly distributed in the interdendritic regions and along grain boundaries. TEM investigations revealed a complex Bi-Bi₂Mg₃ eutectic structure, which presents mainly rod-type and blocky morphology.

KEYWORDS

Cast aluminium alloys

Recycling

Bismuth

Microstructure

Mechanical properties

High-pressure die-casting

1. Introduction

Bismuth, as well as other low-melting-point elements (Pb, Sn, Cd), makes Al alloys free-machining alloys. This element shows a very low solubility in solid α -Al phase and it forms a soft, low-melting phase that promotes chip breaking and helps to lubricate the cutting tool [1]. It is known that Bi does not form compounds with aluminium or silicon [2]. The Al-Bi phase diagram evidences how the solubility of Bi is less than 0.24 wt% at the monotectic temperature (657°C), and almost null at the eutectic temperature (270°C) [3].

Bismuth is generally considered an impurity and it is generally present as trace element in commercial foundry alloys. The presence of impurities in the development of the alloy microstructure and mechanical properties can be critical because these elements are often not separately specified in alloy specifications except as *others each* and *others total*. Low-melting elements such as lead, tin, and bismuth may form brittle intergranular compounds. Further, insoluble impurity elements are responsible for decreases in elongation [2].

The main source of Bi contamination in the Al foundry alloys is ascribed to the Bi-containing free-cutting wrought Al alloys, which are progressively substitute the lead containing alloys. This is leading to a steady increase of Bi content in secondary Al alloys.

While the deleterious interactions between Sr and Bi on eutectic silicon modification are well known [4], contradicting results exist regarding the influence of Bi on shrinkage behaviour and microporosity formation; these properties seem to be strongly dependent on Bi concentration [5]. Furthermore, the presence of Bi results in a reduction of ductility and in an effective refinement of eutectic silicon when the amount exceeds 0.2 wt.% in a near-eutectic Al alloy [4,5].

Since the recycled Al alloys may contain impurity elements such as Bi, a better understanding of the effects of this element may be necessary. The aim of this work is to present experimental results on the influence of Bi

content on the microstructure and mechanical properties of AlSi9Cu3(Fe) secondary diecasting alloys.

2. Experimental Procedure

In the present work a secondary AlSi9Cu3(Fe) cast alloy (EN AB-46000) was supplied by Raffineria Metalli Capra as commercial ingots and used as a base-line. The ingots were melted in a 300 kg SiC crucible in a gas-fired furnace set up at $690 \pm 5^\circ\text{C}$. A weighed commercial Al-9Bi waffle ingot was added into the molten alloy to ensure that the Bi level in the melt reached the desired levels. After each start up, 20-25 castings were scrapped to reach a quasi-steady state temperature in the shot chamber and die. Five alloys, besides the base-line alloy (1-Bi), were prepared with a Bi content ranging from 0.0146 to 0.317 wt.%. The level of the metal bath in the furnace was allowed to decrease after each subsequent Al-9Bi addition, i.e. from 2-Bi to 6-Bi alloy. For each composition 40 castings were produced. The chemical composition of the separately poured samples is listed in Table 1.

Table 1: Chemical compositions of the experimental alloys (wt.%). Aluminium content is the remainder.

<i>Alloy code</i>	<i>Fe</i>	<i>Cr</i>	<i>Si</i>	<i>Mg</i>	<i>Mn</i>	<i>Cu</i>	<i>Zn</i>	<i>Ni</i>	<i>Bi</i>
1-Bi (base)	0.872	0.065	8.878	0.316	0.213	2.349	1.041	0.090	0.0146
2-Bi	0.891	0.069	8.893	0.319	0.223	2.295	1.055	0.087	0.0337
3-Bi	0.872	0.066	8.786	0.311	0.217	2.314	1.063	0.088	0.0525
4-Bi	0.890	0.069	8.839	0.311	0.224	2.309	1.059	0.088	0.0794
5-Bi	0.891	0.069	8.786	0.307	0.226	2.277	1.063	0.086	0.1158
6-Bi	0.877	0.066	8.661	0.318	0.221	2.307	1.066	0.087	0.3170

Cast-to-shape specimens were produced using a multicavity die in a cold chamber die-casting machine with a locking force of 2.9 MN. The die provided two cylindrical tensile specimens and two flat tensile specimens, one plate and one Charpy specimen to be cast from each shot. The weight of the aluminium alloy diecasting was 0.9 kg, including the runners, gating and

overflow system. The plunger velocity was 0.2 m s^{-1} for the first phase and 2.7 m s^{-1} for the filling phase; a pressure of 40 MPa was applied when the die cavity was full, to guarantee high-integrity die castings. A detailed description of HPDC machine, casting procedure, and process parameters is given elsewhere [6].

This study only examined cylindrical tensile specimens with a total length of 120 mm, a gauge length of 30 mm, and a diameter of 6 mm. The diecast specimens were stored at room temperature for about seven months before being tested and therefore corresponding to a similar T1-condition. For each alloy, the tensile tests were carried out on the last six castings since the thermal stability of the die was ensured. The experimental data were processed to provide yield stress (YS, actually 0.2% proof stress), ultimate tensile strength (UTS) and elongation to fracture (s_f).

Microstructural investigations were carried out on samples drawn from the cross section of the gauge length by using an optical microscope and a field emission gun scanning electron microscope (FEG-SEM) equipped with an energy-dispersive spectrometer (EDS). Specimens for transmission electron microscopy (TEM) investigations were prepared by ion milling and then examined using a JEOL JEM 2000 EX II electron microscope operated at an accelerating voltage of 200 kV.

3. Results and discussion

The typical microstructures of the diecast alloys with the lowest (0.0146 wt.%) and the highest (0.317 wt.%) Bi content are shown in Fig. 1. Coarse plate-like eutectic silicon and a large amount of angular eutectic Si particles, which are typical of an unmodified Al alloys, are revealed.

In contrast to what is described elsewhere [4,5], the microstructure of the different Bi-added AlSi9Cu3(Fe) alloys does not reveal any modification or refinement of eutectic Si.

Differences in solidification between the wall and the centre of bar section reflect, however, upon dimension and morphology of eutectic Si particles. Along the die wall the nucleation prevails on growing mechanism, due to higher undercooling. Thus, the formation of fine and fibrous eutectic silicon is promoted independently of Bi content, while the eutectic Si particles show a coarse plate-like morphology at the centre of the bars (Fig. 1). It is well known that a rapid solidification can change the eutectic Si morphology similarly to that chemically modified and, in the present work, it seems to control the eutectic Si crystal refinement and modification more than the Bi level.

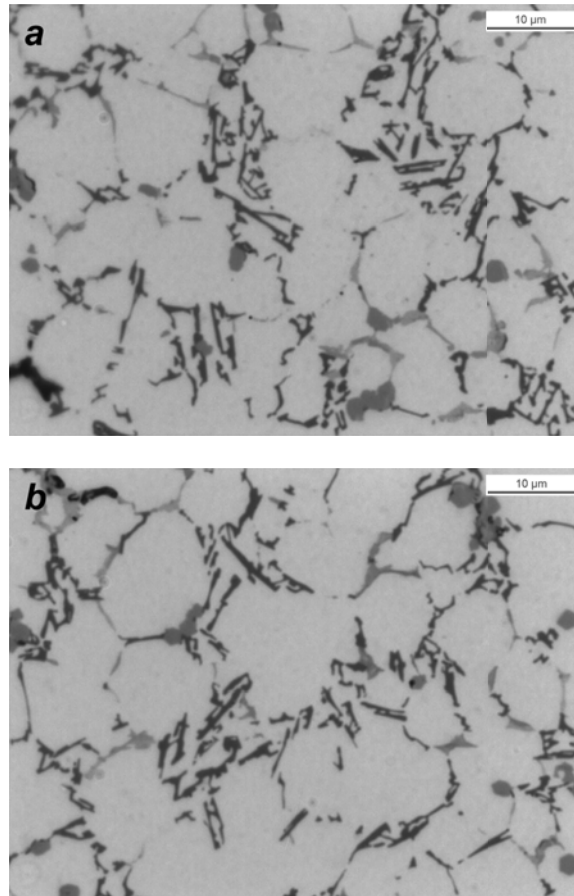


Figure 1: Silicon crystals in the eutectic region of the Bi-added AlSi9Cu3(Fe) alloys: (a) 0.0146 and (b) 0.317 wt.% Bi. Micrographs refer to the centre of round tensile specimens in T1-condition.

Fine Bi-rich particles are observed in all six alloys throughout the microstructure, as confirmed by the EDS analysis (Fig. 2). The size and area fraction of Bi-bearing compounds rise as the Bi content increases. These intermetallic precipitates are mainly distributed in the interdendritic regions and along the grain boundaries.

Due to high solidification rate and low Bi solubility in primary α -Al phase, Bi-rich particles reach sizes lower than one micron and they present two different shapes: rod-type and blocky morphology. The EDS spectra do not reveal any difference of chemical composition between the morphologies. Therefore, no relation seems to exist between the morphology and the chemical composition of these precipitates.

The Bi-bearing particles are mainly found within the Al-Si eutectic and close to the Fe-rich phases, suggesting a good wettability between Bi-bearing precipitates and the Fe-rich particles. As the solid phase continues to form during solidification process, the surrounding liquid progressively enriches in Bi due to poor Bi solubility in the α -Al phase and low-melting point; finally, Bi-rich particles precipitate within the remaining interdendritic voids and at grain boundary. In the work of Schaffer *et al.* [7], it is revealed how from the initial Al-Bi liquid several decompositions take place: firstly, into two immiscible liquids, that is in the case of Al-based hypermonotectic alloys, and further, after the monotectic reaction $L_1 \rightarrow \alpha\text{-Al} + L_2$, Bi solidifies by the reaction $L_2 \rightarrow \alpha\text{-Al} + \text{Bi}$ at 270°C [3].

The distribution of chemical elements inside the Bi-rich particles is analysed by means of EDS line-scan profiles (Fig. 2b). These highlight simultaneous Bi and Mg variation in both rod-type and blocky particles. The Bi-Mg phase diagram [3] shows that this phase can be identified as $\alpha\text{-Bi}_2\text{Mg}_3$.

The presence of Pb, whose content in the investigated alloys is about 0.074 wt.%, is also revealed by EDS besides Bi-rich particles. The EDS profiles highlight that these precipitates are two different phases which are solidified in the same interdendritic voids one next to the other. So the presence of Pb- ϵ intermetallic precipitates is to rule out.

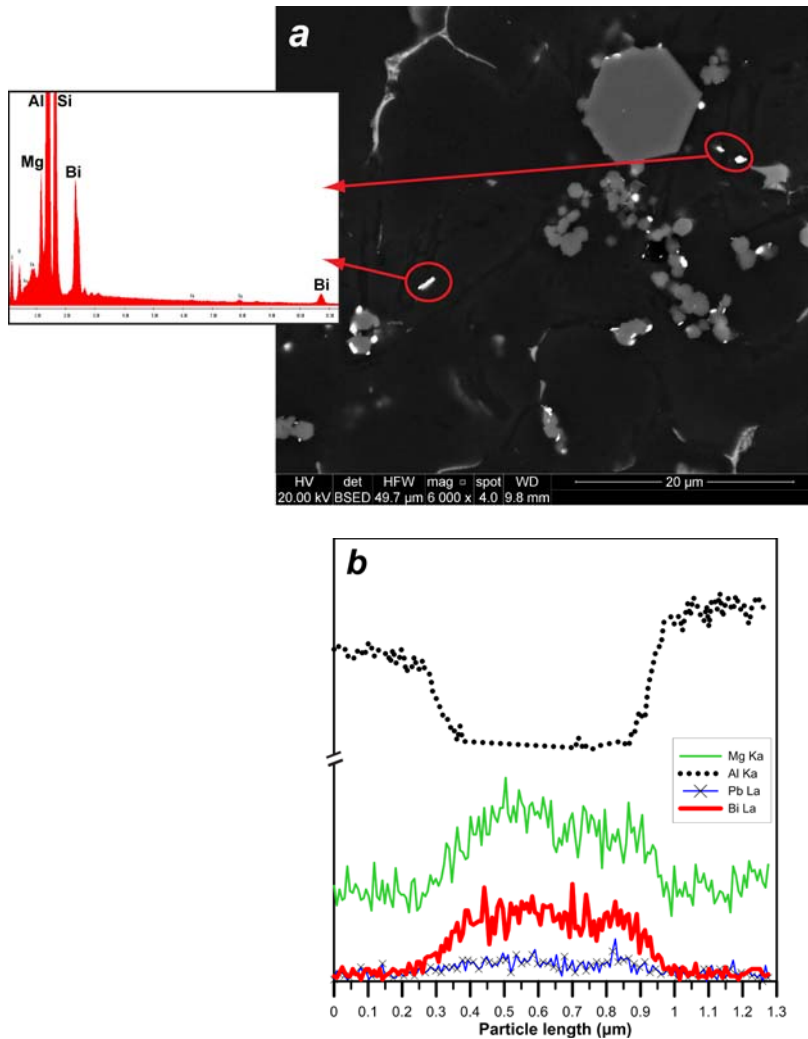


Figure 2: (a) FEG-SEM micrograph of Bi-added AlSi9Cu3(Fe) alloy with Bi-bearing particles, as revealed by EDS spectra. (b) EDS line-scan microanalysis profile of one Bi-rich blocky particle, where the simultaneous variation of Bi and Mg is revealed.

The analysis of Bi-rich particles was also performed by TEM, which confirmed no difference between the observed particles' morphologies. The Bi-rich particles were identified by selected area electron diffraction (SAED) as α -Bi₂Mg₃ phase (hexagonal close-packed, $a = 0.4666$ nm, $c = 0.7401$ nm, with space group P-3m1) [3]. The SAED analysis of Fig. 3 shows the presence of a secondary crystal lattice corresponding to pure Bi. The comparison between the TEM micrographs and the SAED results enables to identify the Bi-rich compounds as a complex Bi-Bi₂Mg₃ eutectic structure. Similar results have been observed by de Haas [8] in wrought free-machining Al alloys.

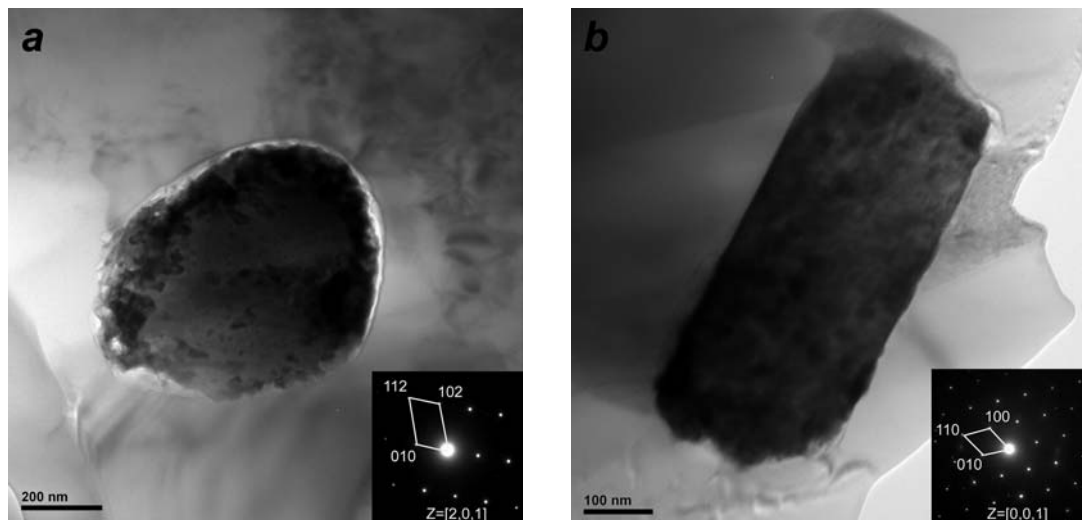


Figure 3: TEM micrographs of Bi-bearing compounds and Bi-rich phase electron diffraction pattern; a) blocky and b) rod-type morphology. The SAED pattern reveals a complex Bi-Bi₂Mg₃ eutectic.

The mean tensile properties such as UTS, YS and s_f for all the Bi-added alloys in T1-condition are steady at about 336 MPa, 179 MPa and 5 %, respectively. These results apparently demonstrate that the presence of Bi does not influence the mechanical properties. The scattering of the tensile test results was evaluated by the Weibull statistics, which revealed a possible interaction between the Bi content and the final reliability of castings (Table 2). The results evidence that the Weibull modulus β shows lower values by increasing the Bi content. Similar results are also observed for s_f . The dispersion of mechanical properties is due to the presence of defects, such as oxide films and porosities. The analysis of the fractures surfaces showed the presence of a great amount of oxide films in the alloys with higher Bi content (Fig. 4). Referring to the thickness and oxidation time, these oxides can be classified as *old oxide films* [9]. Their amount can increase with the holding time in the furnace, therefore they seem to be related to the Bi level as well as to the casting sequence. Generally, the *old oxide films* originate from the thickness growth of the oxidized surfaces of ingots during the melting process and the transport of the liquid metal from the holding furnace into the shot sleeve. If they are not properly removed, they are stochastically entrapped and dragged inside the casting. Furthermore, the oxide films can

obstruct the interdendritic channels preventing the feeding mechanism during the solidification and so promoting micro-shrinkage. This phenomenon is revealed in Fig. 4.

Papworth *et al.* [10] reported how the addition of Bi should reduce, or slow down, the ability of molten Al alloys to produce a surface oxide layer by forming a Bi-rich surface covering the liquid alloy. As the oxide skin grows, Bi becomes incorporated into the oxide film and creates a stress gradient that causes the oxide film to break up. The reduction of the oxide film formation was not observed in this work.

Table 2: Weibull modulus, β , and scale parameter, η , for UTS and s_f values obtained from Bi-added alloys; coefficients of determination, R^2 , are given.

Alloy code	UTS			s_f		
	β	η [MPa]	R^2	β	η [%]	R^2
1-Bi	37.2	334	0.92	15.9	4.5	0.95
2-Bi	19.4	347	0.92	9.6	4.1	0.95
3-Bi	28.6	346	0.97	5.7	5.1	0.93
4-Bi	31.8	340	0.95	8.4	5.3	0.88
5-Bi	15.9	361	0.96	9.8	4.7	0.98
6-Bi	27.8	338	0.93	7.5	4.6	0.97

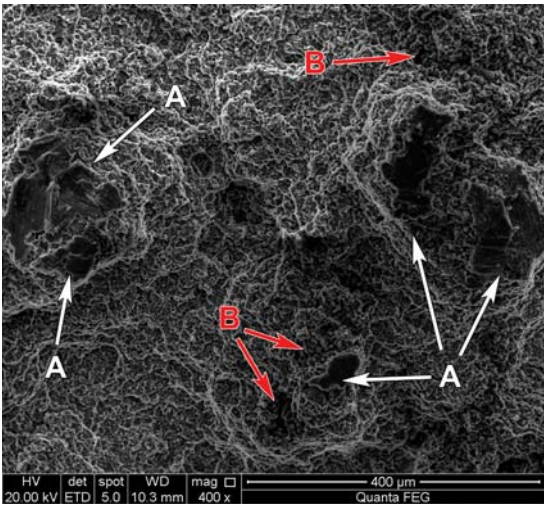


Figure 4: FEG-SEM micrograph of old oxide films (A) and shrinkage porosities (B) as revealed on fracture surface of 6-Bi alloy.

4. Conclusions

The effects of Bi content on the microstructure and tensile properties of a high-pressure die-cast AlSi9Cu3(Fe) have been investigated. The following conclusions can be drawn.

- The Bi contents used in this work do not reveal any modification or refinement of eutectic Si particles; the high solidification rate seems to mainly control the eutectic Si refinement and modification more than Bi.
- Fine Bi-rich particles are mainly distributed in the interdendritic regions and along the grain boundaries. These particles present two different morphologies: rod-type and blocky shape. No differences in the chemical composition between the morphologies are revealed.
- In the analysed alloys, Bi does not solidify as a pure element but it forms a complex Bi-Bi₂Mg₃ eutectic.
- The tensile test results demonstrate that the presence of Bi does not exert any influence on the average mechanical properties.
- Lower Weibull modulus obtained by increasing Bi content reflects poor reliability which is mainly associated with an increase of casting defects, such as old oxide films and microshrinkage.

References

- [1] G. Timelli and F. Bonollo: *'Influence of tin and bismuth on machinability of lead free 6000 series aluminium alloys'*, Mater. Sci. Tech., vol.27(1), pp.291-299, (2011).
- [2] ASM: *'Handbook: Vol.15 Casting'*, 9th ed., pp.1256; USA, ASM International, (2002).
- [3] ASM: *'Handbook: Vol.3 Alloy Phase Diagrams'*, 10th ed., pp.512; USA, ASM International, (1992).
- [4] S. Farahany, A. Ourdjini, M.H. Idris, and L.T. Thai: *'Effect of bismuth on microstructure of unmodified and Sr-modified Al-7Si-0.4Mg alloys'*, Trans. Nonferr. Metal. soc., vol.21(7), pp.1455-1464, (2011).
- [5] J.I. Cho and C.R. Loper: *'Limitation of Bismuth Residual in A356.2 Aluminum'*, AFS Trans., vol.108, pp.359-367, (2000).

- [6] G. Timelli, S. Ferraro, F. Grosselle, F. Bonollo, F. Voltazza, and L. Capra: '*Caratterizzazione meccanica e microstrutturale di leghe di alluminio pressocolate*', La Metallurgia Italiana, vol.101(1), pp.5-17, (2011).
- [7] P.L. Schaffer, R.H. Mathiesen, L. Arnberg, M. Di Sabatino, and A. Snigirev: '*In situ investigation of spinodal decomposition in hypermonotectic Al–Bi and Al–Bi–Zn alloys*', New Journal of Physics, vol.10(5), (2008).
- [8] M.J. de Haas: '*Grain boundary phenomena and failure of aluminium alloys*', PhD thesis, University of Groningen, (2002).
- [9] J. Campbell: '*Castings*', 2nd ed., Great Britain, Butterworth-Heinemann, (2003).
- [10] A. Papworth and P. Fox: '*The disruption of oxide defects within aluminium alloy castings by the addition of bismuth*', Mater. Lett., vol.35(3–4), pp.202-206, (1998).

ARTICLE 2

ON THE FORMATION OF SLUDGE INTERMETALLIC PARTICLES IN SECONDARY ALUMINUM ALLOYS

S. Ferraro¹, A. Bjurenstedt², S. Seifeddine^{2,3}

¹ Department of Management and Engineering - DTG
University of Padua
Vicenza, ITALY

² Department of Mechanical Engineering, Materials and Manufacturing, Casting
Jönköping University,
Jönköping, SWEDEN

³ Swerea SWECAST
Jönköping, SWEDEN

Submitted for publication in: *Metallurgical and Materials Transactions A*, 2013.

ABSTRACT

The primary precipitation of Fe-rich intermetallics in AlSi9Cu3(Fe) type alloys is studied for different Fe, Mn and Cr contents and cooling rates. Differential scanning calorimetry (DSC), thermal analysis (TA) and interrupted solidification with a rapid quenching technique were used in combination in order to assess the nucleation temperature of sludge particles as well as to follow their evolution. The results revealed that the sludge nucleation temperature and the release of latent heat during sludge formation are functions of Fe, Mn and Cr level in the molten alloy (i.e. the *sludge factor*), and the cooling rate. Moreover, it can be concluded that the sensibility to sludge formation is not affected by cooling rate. The sludge formation temperature detected will support the foundries to set the right molten metal temperature in order to prevent sludge formation in the holding furnace and plunger systems.

KEYWORDS

Aluminum alloys

Sludge Factor

Fe-rich intermetallics

DSC

Thermal Analysis

Cooling Rate

1. Introduction

In commercial aluminum-silicon alloys Fe is a common impurity forming brittle intermetallic compounds with Al and other elements that are known to be detrimental to mechanical properties [1]. Even with a low amount of Fe in the melt, the monoclinic particles of $\beta\text{-Al}_5\text{FeSi}$ crystallize during solidification in a platelet-like morphology. These phases act as stress raisers causing a general reduction of the ductility and ultimate tensile strength [1-5]. The formation and amount of porosity is also affected by the Fe content [6-8].

However, Fe in aluminum die-casting alloys is a desirable and necessary element that helps to prevent or alleviate die soldering [9,10]. Therefore, inexpensive secondary alloys with an already relatively high Fe content (in the range of 1 wt.%) are used. The Al–Si–Fe eutectic composition occurs at about 0.8 wt.% Fe. When the Fe content is above this level, the molten metal has little or no tendency to dissolve and solder die steel while the two materials are in intimate contact.

It has been shown that the size and amount of Fe-containing phases is strongly influenced by solidification rate [5,11,12] and that alloying elements such as Mn, Cr, Ni, Mo, Co, Sr, K and Be can change the morphology of the intermetallic phases or enhance the precipitation of phases which are less harmful than $\beta\text{-Al}_5\text{FeSi}$ [5,11-19]. Moreover a cooling rate higher than 20°C/s can suppress the platelet-like morphology and provides a less harmful α -phase form [20]. Mn and Cr, which main source is the recycled aluminum scrap, are normally present in secondary aluminum alloys as impurities. Fe, Mn and Cr can substitute each other in the same crystal structure that is body centered cubic, $\alpha\text{-Al}_{15}(\text{Fe,Mn,Cr})_3\text{Si}_2$, which may appear as Chinese script, star-like or polyhedral morphology [1,21,22]. However, these complex intermetallic compounds have a high specific gravity and tend to segregate to the bottom of aluminum melts and holding furnaces and form solid particles, generally called *sludge*, thus reduce the effective capacity of the furnace [23-26]. Since sludge crystals are hard and brittle compact inclusions [27], they can also compromise the machining operations, with a considerable effects on the cutting tool life, and

even more degrade the mechanical and physical properties of the component [2-4,26,28-30]. The problem of sludge formation is often experienced in aluminum foundries, especially in the pressure die-casting industry where, in order to preserve the die, the melt holding and casting temperatures are typically lower than for other foundry processes [26]. Furthermore, as the use of secondary aluminum alloys becomes more common, sludge is a problem of increasing importance due to the increasing concentration of Fe, Mn and Cr in the scrap cycle.

The tendency of Al-Si-Cu alloys to form primary Fe-rich particles can be predict by *sludge factor* (SF), which represent an attempt to gather the combined effect of Fe, Mn and Cr. The commonly accepted empirical equation of SF is expressed as:

$$\text{Sludge factor } (SF) = (1 \times \text{wt.\%Fe}) + (2 \times \text{wt.\%Mn}) + (3 \times \text{wt.\%Cr}) \quad (1)$$

Dunn, R. [31], Gobrecht, J. [25] and Jorstad, J.L. [26] found an empirical relationship between the SF and the critical precipitation temperature below which Fe-rich particles tend to form in the holding furnaces for several Al-Si-Cu die-casting alloys. However, in these works the cooling conditions used to obtain the samples are not specified, and in addition the analysis of the sludge is carried out only with an indirect measure of the chemical composition.

The aim of the present investigation is to enlighten the role of Fe, Mn, and Cr, and the cooling rate on the primary precipitation of sludge in secondary AlSi9Cu3(Fe) alloys. Differential scanning calorimetry (DSC), thermal analysis (TA) and interrupt solidification with a rapid quenching technique were used in order to obtain the temperature and the evolution of sludge formation. These results can be useful to set the right molten temperature in order to prevent formation and sedimentation of brittle intermetallic particles in the holding furnace and during the melt movement in HPDC machine.

2. Experimental procedure

The chemical composition of the alloys prepared for the study is shown in Table 1. The base-line material, alloy A, was a secondary AlSi9Cu3(Fe) cast alloy (EN AB-46000, comparable with the US designation A380), supplied as commercial ingots. Melts of approximately 6.5 kg were prepared in an electric resistance furnace held at a temperature of $750 \pm 5^\circ\text{C}$ to produce alloy B, C and D by adding Fe, Mn and Cr in the form of commercial Al-10Fe, Al-10Mn and Al-5Cr master alloys. After the addition of the master alloys, the melt was heated in the furnace to $800 \pm 5^\circ\text{C}$ and held for 60 min in order to ensure the homogeneity and dissolution of any intermetallic phases. The temperature of the melt was then gradually decreased by following the furnace inertia down to $750 \pm 5^\circ\text{C}$. The chemical compositions of the alloys were verified by optical emission spectrometry (OES).

Table 1: Chemical composition of the experimental alloys and of alloys referred to in this paper. All the values are in weight percent. The sludge factor SF, according to Eq. (1) are also show for the alloys. Min. and Max. values refer to composition tolerance limits of the European Standard EN 1706:2010 for the alloy EN AB-46000. Aluminum content is the remainder.

Alloy	Si	Cu	Fe	Mn	Cr	Mg	Zn	Ni	Pb	Sn	SF	Fe/Mn
Min.	8.0	2.0	0.6	-	-	0.05	-	-	-	-	-	-
Max.	11.0	4.0	1.3	0.55	0.15	0.55	1.20	0.55	0.35	0.25	-	-
A	8.39	2.60	0.75	0.23	0.02	0.26	1.07	0.03	0.05	0.03	1.27	3.26
B	8.19	2.40	1.25	0.27	0.02	0.25	1.02	0.03	0.05	0.03	1.85	4.63
C	7.72	2.28	1.32	0.58	0.14	0.24	0.96	0.03	0.05	0.03	2.90	2.28
D	7.88	2.15	1.62	0.79	0.16	0.22	0.85	0.03	0.04	0.03	3.68	2.05
B380.1 ^a	9.3	3.42	0.89	0.28	-	0.02	0.76	-	-	-	1.45	3.2
380/7 ^a	8.8	2.40	1.32	0.12	-	0.12	0.50	-	-	-	1.56	11
380/8 ^a	8.7	2.5	1.35	0.48	-	0.12	0.53	-	-	-	2.31	2.8

^{a)} Chemical composition of the 380-type alloys studied by Backerud, L., et al. [32]

For each alloy, cylindrical rods, 18 cm in length and 1 cm in diameter, were cast in a permanent copper mold, preheated to 200°C . In order to produce samples with consistent quality and without element segregation for the DSC analysis, the rods were subsequently remelted in the gradient solidification

equipment [33], which provide a material with low content of oxide films, defects, and a homogeneous and well-fed microstructure over the entire length of the sample. The temperature in the furnace when remelting the rods was set to 800°C and the samples were held at this temperature for 30 minutes under Ar gas atmosphere. The speed of the heating element throughout the cooling channels was 3 mm/s, which generate a secondary dendrite arm spacing (SDAS) of about 7 μm [33]. The chemical composition of the remelted bars were analyzed by OES and were found to correspond to the original compositions.

DSC analysis were performed using a NETZSCH DSC 404C machine, to determining the characteristic temperatures for phase nucleation at different cooling rates for all alloys produced. The samples used for DSC analysis, with a mass of about 40 mg, were melted under a protective Ar gas flow of 50 ml/min. All specimens were selected from the centre of the bars produced with gradient solidification technique. The thermal history of the DSC samples is reported in Fig. 1. Three or more curves were recorded for each cooling rate and alloy, and a new sample was used for every run.

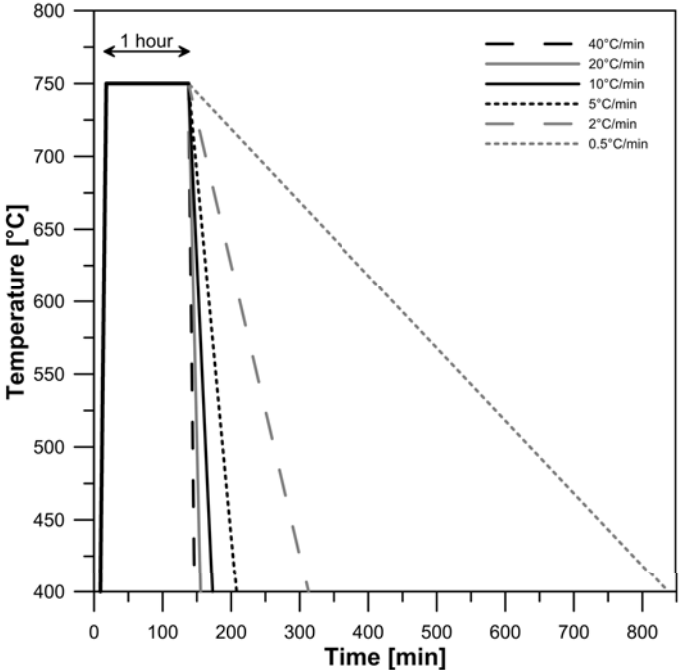


Figure 1: Thermal history of the DSC analysis. A constant heating rate of 40°C/min and a holding time of 1h at 750°C were used for all samples. The cooling rate was varied between 0.5°C/min and 40°C/min.

As for the thermal analysis and interrupted quenching experiments, the alloys were cast into stainless steel tubes (diameter: 30 mm, height: 100 mm) which were preheated at 750°C in order to reduce the thermal shock and to avoid sludge formation during the molten movement. The steel tubes were thereafter immediately placed inside three different cooling media: *steel*, *brick* (similar cooling power to that of sand) and *insulation* (fiberfrax Durablanket®), thereby given three different cooling rates. TA was carried out with the two-thermocouple method developed by Bäckerd *et al.* [32]. The experimental setup includes two N-type (Nicrosil–Nisil) thermocouples, placed inside the casting, one in the centre and one near the wall of the tube. In the experiments, the thermocouples were protected in tightly fitted steel tubes to allow the same thermocouples to be used throughout the experimental plan without the need to remelt the sample between analyses. The data was collected using a data acquisition system with a sampling rate of 4 s⁻¹, linked to a PC. This experimental setup was also used for evaluation of solidification rates as well as for quenching experiments. The quenching was performed by rapidly pouring the liquid metal from steel tubes into a water-10% NaCl solution.

The microstructural investigations were carried out of quenched samples by using an Olympus GX71 inverted metallurgical microscope equipped with Olympus Stream Motion analyzing software. The samples were prepared to a 1-µm finish with diamond paste and, finally, polished with a commercial fine colloidal silica slurry for metallographic investigations. Four samples were analyzed for each alloy, in order to obtain information about the growth of sludge formation and growth during solidification.

3. Results and discussion

3.1. DSC analysis

Fig. 2 shows a typical DSC curve of solidification of alloy B scanned at a cooling rate of 10°C/min. Studying the DSC curves, it is observed that the reaction peaks reflect the specific phase changes and the peak area is proportional to the heat of reaction (ΔH_R) associated with the phase transformation. Positive values of ΔH_R are due to the endothermic reaction of

liquid formation during heating, while negative values result from the latent heat released during solidification. As shown in Fig. 2, there are six reaction peaks during the solidification of this alloy. According to Backerud, L., et al. [32], which have studied the solidification of A380-type alloys, peaks 2 to 7 correspond with the reactions reported in Table 2. These reactions describe the typical phases present in a secondary AlSi9Cu3(Fe) die-casting alloy [34]. With the help of the DSC analysis, one additional reaction, reaction 1, is detected in this study. This reaction, that corresponds to sludge particles formation [21], is added to Table 2.

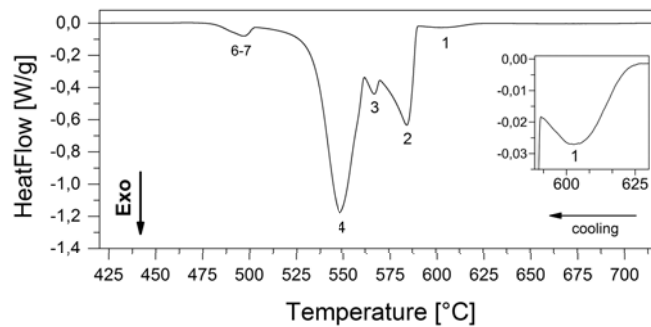


Figure 2: Typical DSC solidification curve of alloy B (SF=1.85) ran at a cooling rate of 10°C/min. The peaks 1-7 refers to reactions reported in Table 2.

Table 2: Solidification reactions of the AlSi9Cu3(Fe) type alloy, according to Backerud, L., et al. [32]. Temperatures are reported in Celsius degree (°C).

N°	Reactions	B380.1 ^{a,b}	380/7 ^{a,c}	380/8 ^{a,c}
1	Precipitation of primary Fe-rich phases (sludge)	-	-	-
2	Development of α -Al dendritic network	575	581	583
3	Precipitation of pro-eutectic Fe-rich phases	573	575	572
4	Main eutectic reaction involving precipitation of Si	564	564	566
5	Precipitation of Mg ₂ Si	-	-	-
6	Precipitation of θ -Al ₂ Cu	505	498	496
7	Formation of complex eutectics, containing Al ₂ Cu and Al ₅ Mg ₈ Si ₂ Cu ₂	492	487	489

^{a)} Chemical composition of the 380-type alloys studied by Backerud, L., et al. [32]

^{b)} Cooling rate: 36°C/min;

^{c)} Cooling rate: 42°C/min

The solidification process of aluminum alloys is well described in the literature. Traditionally, techniques of thermal analysis (TA) with one or two

thermocouples have been used to analyze the solidification process, while more rarely differential thermal analysis (DTA) and differential scanning calorimetry (DSC) have been used. However these techniques have never been used specifically to study the sludge formation in aluminum alloys. In the work of Cao, X. and Campbell, J. [35] it is indicated that the exact nucleation temperature of primary α -Fe particles is not known for alloys with high Fe and Mn contents. They identify the nucleation temperature of sludge in an alloy with high SF (3.8) by means of TA. However, this value is listed as questionable by the authors due to low signal to noise ratio before the solidification of α -Al phase. In the present work the use of DSC makes it easier to identify the reaction peak as well as the heat of reaction associated with the sludge formation, as show in Fig. 2.

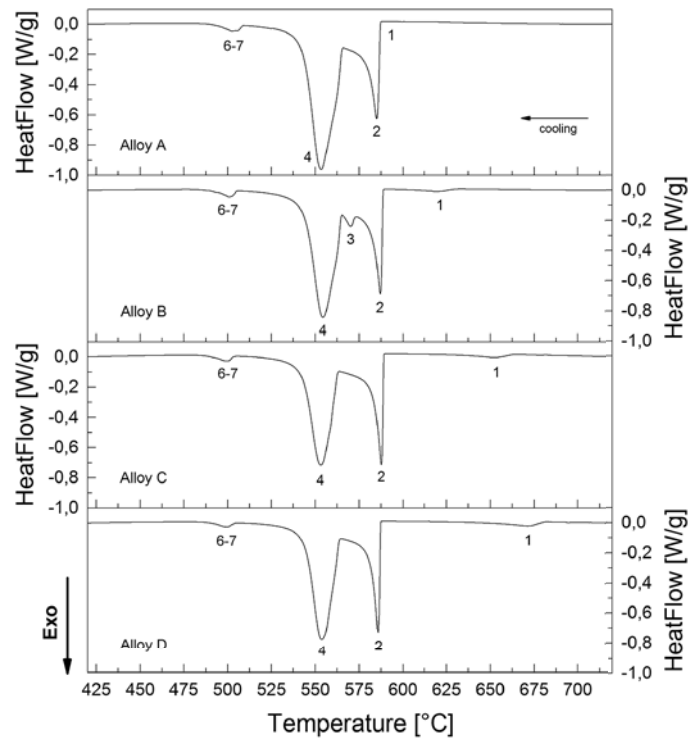


Figure 3: DCS solidification curves of the four alloys, ran at a cooling rate of 5°C/min.

The number on peaks refers to reactions described in Table 2. Solidification temperatures at different cooling rates and the corresponding standard deviations are reported in Table 3.

The DSC plots in Fig.3 show the influence of increasing Fe, Mn and Cr contents on the solidification behavior of AlSi9Cu3(Fe) alloys scanned at a cooling rate of 5°C/min. The most immediately apparent feature is that the

temperature of the peak which corresponds to sludge formation shifts towards higher temperature with an increase of the SF . This corresponds to the work done by Mackay, R.I. and Gruzleski, J.E. [36] where they state that the temperature of pre-dendritic Fe-rich phase precipitation is increased by increasing the Fe content. Gobrecht, J. [25] and Jorstad, J.L. [26] described the dependence of SF on temperature for the sludge sedimentation on Al-Si-Cu type alloys, while Shabestari, S.G. [1] found that the sludge forming temperature strongly depended on the Fe content of the alloy. Furthermore there is an increase of the released heat in reaction number 1 when increasing the Fe, Mn, and Cr concentration. This result is closely related to the volume fraction of Fe-rich particles precipitated from liquid alloy, which depends on the SF [22].

The comparison of the DSC curves in Fig. 3 highlights also the presence of peak 3, which corresponds to the formation of pro-eutectic Fe-rich particles, only visible in alloy B. This is mainly due to the chemical composition of this alloy, which exhibit the highest value of the Fe:Mn ratio (4.63). Here, the content of Mn and Cr is not enough to definitely change the morphology of the Fe-rich phases; therefore, a large number of pro-eutectic platelet particles (β -Al₅FeSi) are promoted. In the other alloys, the eutectic Al-Si and the pro-eutectic Fe-rich particles reactions (peak 3 and 4 respectively in Fig. 2) overlap to such an extent that they are merged in the thermal traces. The separation of this multiple overlapped peaks was performed by means of the application of Gaussian and/or Fraser-Suzuki (asymmetric) type signals and the results were reported in Table 3.

The full analysis of the DSC results is shown in Table 3. It is possible to observe that the increase of the SF increases the nucleation temperature of the sludge regardless of the cooling rate. Moreover the increase of Fe content, without increasing Mn or Cr, as for alloy B in comparison to alloy A, increase the formation temperature of the pro-eutectic β -Al₅FeSi. This result is confirmed by the work of Mackay, R.I. and Gruzleski, J.E. [36], which studied by TA three different commercial aluminum alloys with different Fe content having a maximum level of 2.4 wt.% Fe.

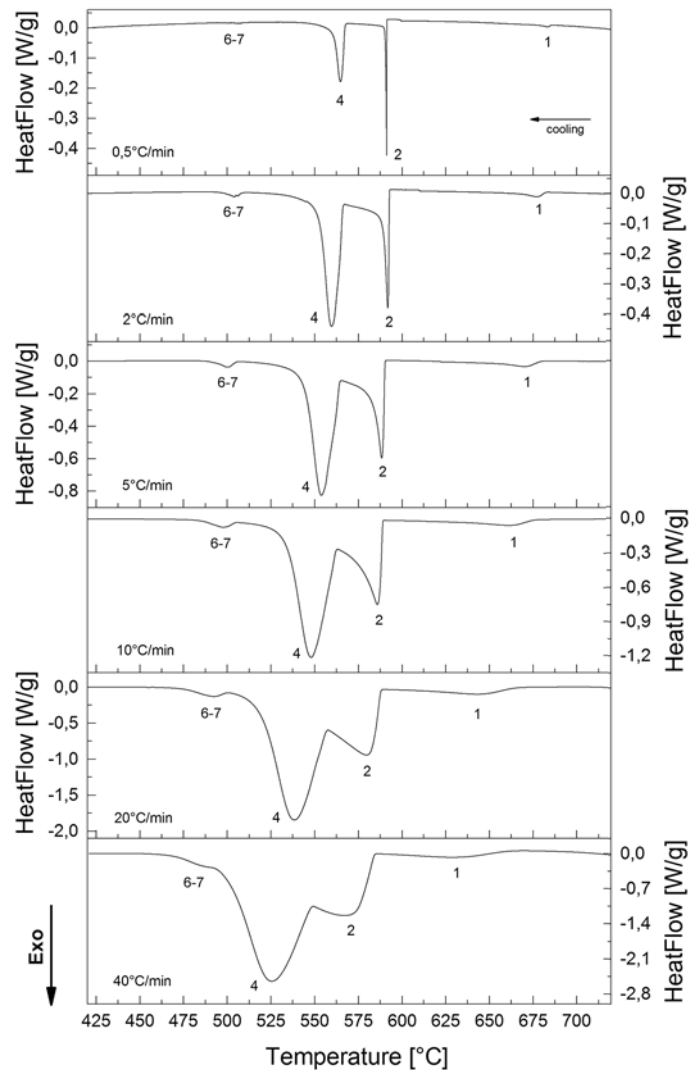


Figure 4: DCS solidification curves of alloy D ran at different cooling rates. The number on the peaks refers to reactions described in Table 2. Several analysis were performed on each experimental alloy and cooling condition, as reported in Table 3.

Fig. 4 highlights the effect of different cooling rates on the solidification behavior of alloy D, which exhibits the highest value of SF (3.68). Similar trends were obtained for the other alloys studied in this work, as show in Table 3. These curves highlight that the nucleation temperature of all reactions decreases with increasing of cooling rate. This effect is most evident for peak 1, which shows a variation of more than 20°C between the highest and lowest cooling rates (0.5 and $40^{\circ}\text{C}/\text{min}$ respectively). Moreover there is a general trend of increased release of latent heat for the reaction associated with peak 1 with increased cooling rate. The fraction of energy released by the sludge formation

was determined by measuring the area under the curve. For alloy D it ranges between -2.75 J/g (cooling rate 0.5°C/min) and -5.75 J/g (cooling rate 40°C/min). This result describes an increase of volume fraction of sludge particles coupled to cooling rate. Due to the higher undercooling, the nucleation prevails as the growth mechanism [37]. Thus, the formation of a large number of primary Fe-rich particles is promoted i.e. the volume increase is mainly related to an increase of the number of particles.

Table 3: Calculated (JMatPro[®]) and experimental DSC solidification temperatures at different cooling rate of the alloys studied in this work. The numbers described in row

R. refer to reactions during solidification reported in Table 2. Sample standard deviations from 3 measurements are listed in parentheses. Temperatures are reported in Celsius degree (°C).

	R.	JMatPro	0.5°C/min	2°C/min	5°C/min	10°C/min	20°C/min	40°C/min
A	1	613.5	609.9 (2.3)	609.1 (1.9)	605.4 (2.6)	602.3 (4.2)	599.7 (2.8)	598.4 (3.7)
	2	593.4	586.2 (0.1)	587.7 (0.4)	587.1 (1.1)	584.9 (1.6)	584.0 (1.4)	574.7 (2.1)
	3	570.8	562.2 (0.6)	561.1 (0.7)	563.0 (0.9)	561.0 (1.1)	-	-
	4	566.4	567.2 (0.2)	571.2 (0.3)	567.4 (0.7)	562.6 (0.5)	558.6 (1.2)	551.2 (2.7)
	6	503.1	510.0 (0.6)	510.0 (0.5)	508.5 (1.0)	506.3 (0.6)	505.4 (1.1)	490.0 (1.9)
	7		506.4 (0.2)	506.6 (0.6)	505.0 (0.3)			
	B	1	632.1	632.6 (3.4)	633.4 (0.8)	624.6 (4.0)	620.3 (0.9)	617.1 (0.2)
2		594.9	588.7 (1.4)	589.2 (0.4)	586.6 (3.3)	587.6 (3.0)	585.0 (2.9)	578.5 (2.0)
3		589.7	580.0 (2.3)	574.0 (4.7)	568.9 (3.0)	572.5 (4.3)	571.2 (2.3)	560.2 (1.7)
4		566.5	566.5 (0.8)	566.3 (1.0)	564.0 (0.8)	561.5 (4.8)	559.2 (1.3)	553.3 (0.9)
6		503.0	509.2 (0.8)	509.5 (1.1)	509.2 (1.0)	500.0 (1.6)	498.4 (1.9)	493.0 (1.8)
7			505.9 (0.1)	507.3 (1.5)	503.4 (1.5)	500.5 (2.1)		
C		1	665.5	668.5 (0.4)	668.1 (3.7)	663.0 (0.1)	658.1 (2.4)	650.3 (2.4)
	2	599.1	590.3 (4.4)	590.2 (2.2)	589.5 (4.2)	589.2 (4.1)	583.3 (4.4)	581.7 (0.4)
	3	584.1	578.2 (2.1)	567.2 (0.7)	565.2 (1.8)	563.3 (0.5)	560.4 (2.1)	549.4 (2.3)
	4	566.3	566.8 (0.4)	565.8 (1.4)	563.6 (1.2)	560.8 (0.7)	555.6 (0.7)	545.3 (0.4)
	6	503.4	510.3 (1.0)	508.7 (0.3)	508.0 (1.1)	501.2 (1.5)	498.6 (2.1)	489.5 (2.8)
	7		504.0 (0.1)	504.4 (0.1)	504.0 (1.1)	494.2 (1.4)		
	D	1	679.4	684.3 (1.8)	682.3 (0.4)	680.4 (0.9)	675.0 (0.9)	666.0 (2.7)
2		598.4	589.8 (2.0)	594.4 (2.4)	587.8 (2.4)	589.1 (1.2)	588.0 (1.7)	583.6 (3.7)
3		587.5	-	568.0 (1.1)	565.2 (0.5)	564.9 (1.9)	560.0 (2.9)	-
4		566.5	565.9 (1.5)	566.7 (0.8)	563.8 (1.0)	561.5 (0.7)	556.6 (1.5)	549.4 (3.5)
6		503.2	508.4 (0.8)	507.9 (0.8)	504.8 (0.9)	503.9 (1.0)	499.3 (0.8)	500.5 (3.5)
7			502.5 (0.2)	506.1 (1.0)	502.6 (1.5)			

Table 3 tabulates the characteristics of the DSC curves of the alloys at different cooling rates. The temperatures of the reactions in alloy A, B and C solidified with a cooling rate of 40°C/min can be compared with those obtained by Bäckerd *et al.* [32], reported in Table 2. The limited difference in temperatures with these authors could be related to the concentration level of elements in the alloys, such as Si, Cu and Mg, as show in Table 1. Nevertheless, there is a substantial difference between the thermal analysis carried out by Bäckerd *et al.* [32] and the DSC tests performed in this work. During the TA experiments, the cooling rate was evaluated at the beginning of the curve, just before the solidification starts. If no crystallization was to occur, cooling rate would gradually decrease by radiation and natural convection to the air surrounding the crucible. The cooling rate is indeed a function of the temperature difference between the sample and its surrounding, so the cooling rate (and the derivative) becomes less in absolute value as time proceeds [32]. On the contrary, the tests conducted with DSC were based on a constant cooling rate of the material. In addition, although the work of Bäckerd *et al.* [32] allows a complete characterization of several aluminum alloys, the thermal analysis used does not allow to identify the nucleation temperature of primary Fe-rich particles (reaction 1 in Table 3). This is mainly due to low signal to noise ratio before the development of α -Al dendritic network, which hides the sludge peak despite the high value of SF .

The temperature of sludge formation in alloy C ($SF=2.90$) and alloy D ($SF=3.68$), cooling rate 2°C/min and 5°C/min, have been compared with the DTA results reported by Warmuzek *et al.* [38], which identified a precipitation temperature of Fe-bearing phases of 669°C in a hypoeutectic alloy with a SF of 3.4 (6%Si, 1.5%Fe, 0.5%Mn, 0.3%Cr, cooling rate: 3.3°C/min). Warmuzek's precipitation temperature is in good agreement with findings here presented, as show in Fig. 5.

The solidification temperatures of experimental alloys has been compared with predicted results using the software JMatPro[®] (acronym for Java[®] based Materials Property software) [39]. These values, reported in Table 3, highlight a good agreement with DSC results obtained with a cooling rate of 0.5°C/min.

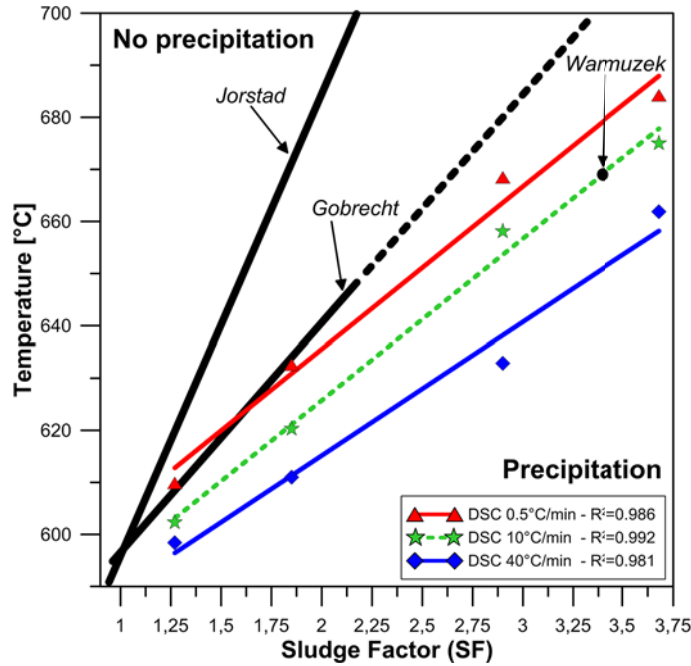


Figure 5: Formation temperatures of Fe-rich intermetallic compounds as function of SF (according to Eq. (1)) and cooling rate for the alloys studied in the present work. The temperature of gravity segregation of sludge according to Jorstad, J.L. [26], Gobrecht, J. [25] and Warmuzek *et al.* [38] is also reported (dashed lines indicated the ideally extension of curve in order to be adapted to the range of SF used here).

The results of DSC analysis reported in Table 3 described the temperature of sludge formation as function of chemical composition (i.e. *sludge factor*) and cooling rate. These values were compared with the temperature of gravity segregation of sludge reported by Gobrecht, J. [25] and Jorstad, J.L. [26], as show in Fig. 5. These two reference curves delineated areas where sludge would form in Al-Si-Cu alloys. In the work of Gobrecht, J. [25] it is indicated that increasing Cu content and lower the Si content will increase the sludge formation temperature. However, the slope of the Gobrecht segregation curve is constant with variations in the chemical composition. The results from Jorstad, J.L. [26] are not in particularly good agreement with those from Gobrecht, J. [25] for the nominally identical AlSi9Cu3(Fe) alloy. However, this difference may result from different experimental conditions. The results presented here (Fig. 5) show temperatures of sludge formation - i.e. segregation - lower than those reported by Gobrecht, J. [25] and Jorstad, J.L. [26]. The main difference with their results is the slope of the segregation curves, which could be correlated

with the cleanness of the liquid metal as well as enough data for producing even better comparisons; which is not found in the studies in Gobrecht, J. [25] and Jorstad, J.L. [26]. It is important to note that in this work the tested material has a reduced content of oxide films and inclusions, and therefore a lower content of sites for heterogeneous nucleation of sludge. This is due to the remelting operations in gradient solidification equipment under Ar atmosphere and the protective Ar gas flow during DSC analysis. It is described in literature that the nucleation of Fe-rich particles are promoted by double oxide films [23,40-42] and inclusions, such as CaO and SiC [43]. Moreover the aluminum oxide on the surface of the samples acts as a nucleant for sludge particles [44]. Consequently, the sludge nucleation is easier in an industrial reverberatory furnace [26] and in a 30kg furnace [25] than in a DSC apparatus.

The DSC results of Fig. 5 highlight that the slope of the experimental segregation curves does not change with cooling rate, i.e. a fast cooling alloy has the same susceptibility to sludge formation when changing the SF as an alloy with lower cooling speed. Increasing the cooling rate from 0.5 to 40°C/min decreases the sludge formation temperature by shifting the curve to a lower value. However it is important to consider the kinetics of the Fe-rich formation, which is faster with increasing of cooling rate. The peak of sludge formation (reaction 1 in Table 3) has a temporal extension of 16 min with a cooling rate of 0.5°C/min, while it is reduced to 90 sec by increasing the cooling rate to 40°C/min. The analysis of the kinetics of sludge formation and the modeling of the phenomenon will be discussed in a future study.

3.2. Thermal analysis (TA) and quenching experiments

The DSC analysis described above highlights the sludge formation at different cooling rates. However, they do not provide any direct information about the microstructure of the alloys. Moreover the closed design of the instrument and the need for perfect thermal balance in the system makes it impossible to carry out quench experiments during solidification. These limitations can be overcome through TA. Fig. 6 shows the cooling curves of the three different cooling media, *steel*, *brick* (similar cooling power to that of sand) and *insulation* (fiberfrax Durablanket[®]), which were used. The cooling rates were determined from the slope of the cooling curves before nucleation temperature

of α -Al dendrite, and correspond to 250, 84 and 29°C/min, respectively. Fig. 7 highlights the cooling curve of alloy D in insulation material with its corresponding first derivative. The thermal data was collected from the wall (T_w) and the centre (T_c) of the sample, and the temperature difference ($T_c - T_w$) was also reported in order to see the "heat waves" produced as new phases form [32].

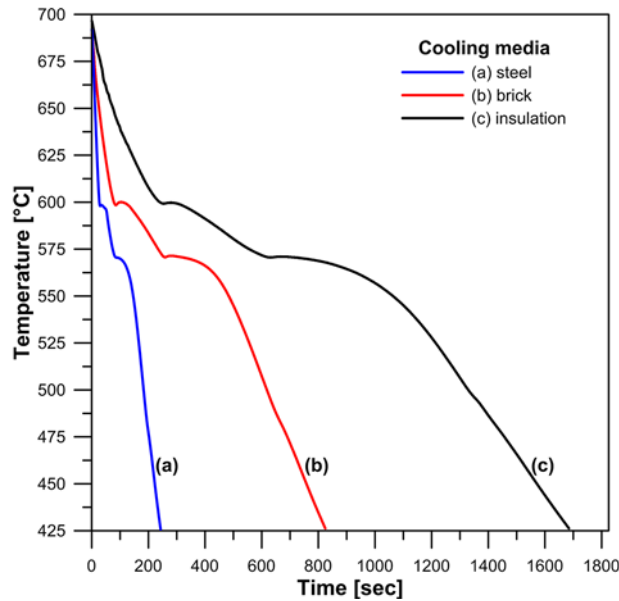


Figure 6: Effect of cooling rate on the solidification behavior of alloy D.

The insulation material with an average cooling rate of 29°C/min was chosen when performing the quench experiment during solidification because of its slower cooling rate. It is worth to bear in mind that the slope of the cooling curve is slightly changing as the temperature is decreasing, why an average is used, see Fig.8. To establish the quench temperatures, the DSC analysis with a cooling rate of 20°C/min was used. Fig. 8 (a) and (b) shows the comparison between the DSC and TA analysis in the temperature range of Fe-rich particles formation, i.e. before the development of α -Al dendritic network. The cooling curve obtained with TA (Fig. 8(b)) highlights a low signal to noise ratio before the solidification of α -Al phase. Consequently, the first derivative and the measured temperature difference do not allow a clear identification of sludge formation despite the high value of the SF .

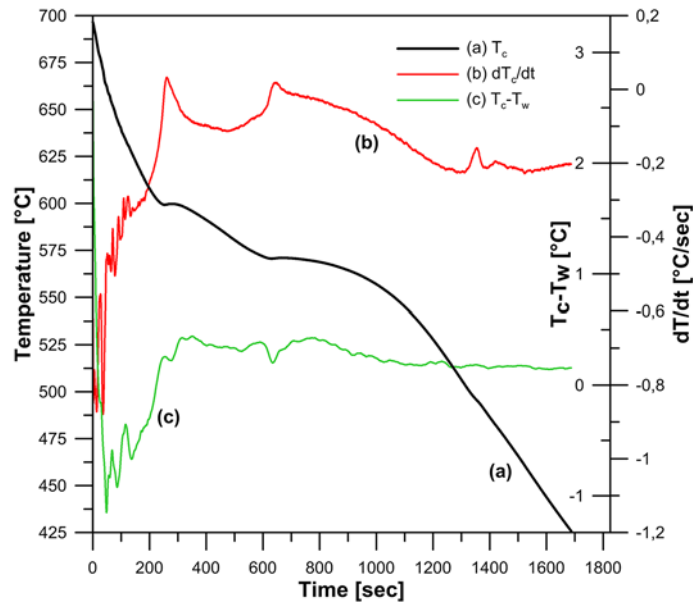


Figure 7: Cooling curve of alloy D in insulation material with its corresponding first derivate (dT_c/dt) and measured temperature difference (T_c-T_w). Thermal data was collected from the wall (T_w) and the centre (T_c) of the same sample.

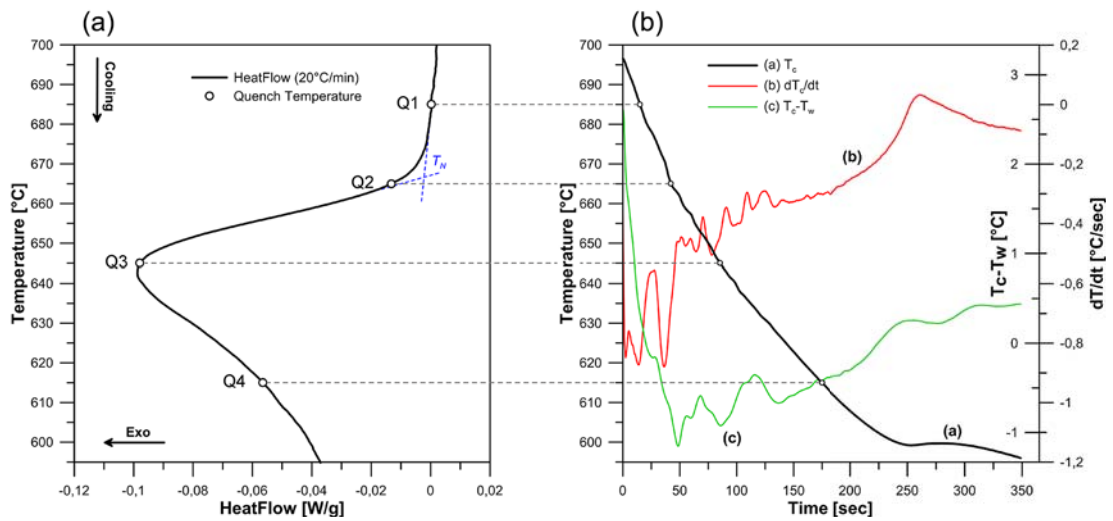


Figure 8: (a) DCS solidification curve of alloy D with a cooling rate of $20^\circ\text{C}/\text{min}$, highlighting the sludge formation. The axes are inverted compared to the DSC diagrams shown above. Q1 to Q4 correspond to the four quench temperatures. T_N is the sludge nucleation temperature; (b) Thermal analysis of alloy D in insulation material before the development of $\alpha\text{-Al}$ dendritic network. First derivate (dT_c/dt) and measured temperature difference (T_c-T_w) are also reported.

The temperatures of four representative quenches, labeled Q1-Q4 in Fig. 8, are reported in Table 4. They vary depending on the alloy studied, in order to describe the evolution of the Fe-rich particles during solidification, according to DSC analysis. The first and the second quench (Q1 and Q2 respectively) were performed before and a few degrees after sludge nucleation, the third (Q3) described the maximum value of heat flow, while the fourth quench (Q4), which corresponds to the last part of peak reaction during DSC, represented the end of sludge growth. The quenching temperatures reported for alloy A were the same as those used for alloy B, due to a limited temperature extension before development of α -Al dendritic network.

Table 4: Quench temperatures used in the present work in order to describe the microstructural evolution of sludge during solidification. Temperatures are reported in Celsius degree ($^{\circ}\text{C}$).

	<i>Sludge evolution</i>	<i>Alloy A</i>	<i>Alloy B</i>	<i>Alloy C</i>	<i>Alloy D</i>
Q1	Before nucleation	640	640	670	685
Q2	Start of nucleation	615	615	650	665
Q3	Nucleation and growth	600	600	635	645
Q4	End of growth	590 ^a	590 ^a	620	620

^{a)} *Development of α -Al dendritic network*

The microstructural characterization of quenched samples highlights equiaxed α -Al dendrites, separated by regions of quenched liquid, as shown in Fig. 9. A comparison of the Fe-rich particles size to the α -Al cell size of the alloys allows identifying if these are primary or pro-eutectic phases. The microstructure examination of the quenched samples is employed to confirm the sludge formation detected in the DSC analysis, at given temperatures.

In Q1 sample, large amounts of small Fe-rich phases were observed. The size, the morphologies and the uniform dispersion of these particles suggest that they are nucleated during the quench experiment or after the development of Al dendritic network, as pro-eutectic phases. Consequently, no sludge particles were formed in the molten aluminum over the nucleation temperature found by means of DSC analysis. The second quench (Q2) shows the presence of large

polyhedral α -Fe particles with an average area of about $3500 \mu\text{m}^2$. These primary sludge particles are surrounded by smaller Fe-rich phases, with sizes and morphologies similar to sample Q1 (Fig.9b). This microstructure could then reveal the starting nucleation temperature of sludge particles (T_N), as highlight in Fig. 8. Large Fe-rich intermetallic particles with polyhedral, star-like and dendritic-like morphologies are recognizable in Fig. 9c, which correspond to third quench (Q3). Their sizes increase compared to condition Q2, and reach an average area of about $8700 \mu\text{m}^2$. Moreover, the amounts of small pro-eutectic Fe-rich phases were assessed to be less than the previous samples. This is assumed to be due to the increased growth of primary sludge particles, which are consuming Fe, Mn and Cr in the molten surrounding. Finally, in the fourth quench (Q4) the microstructure reveals the presence of only large sludge particles with an average area of $13700 \mu\text{m}^2$, with star-like and dendritic-like morphologies, while the pro-eutectic Fe-rich phases are conspicuous by their presence.

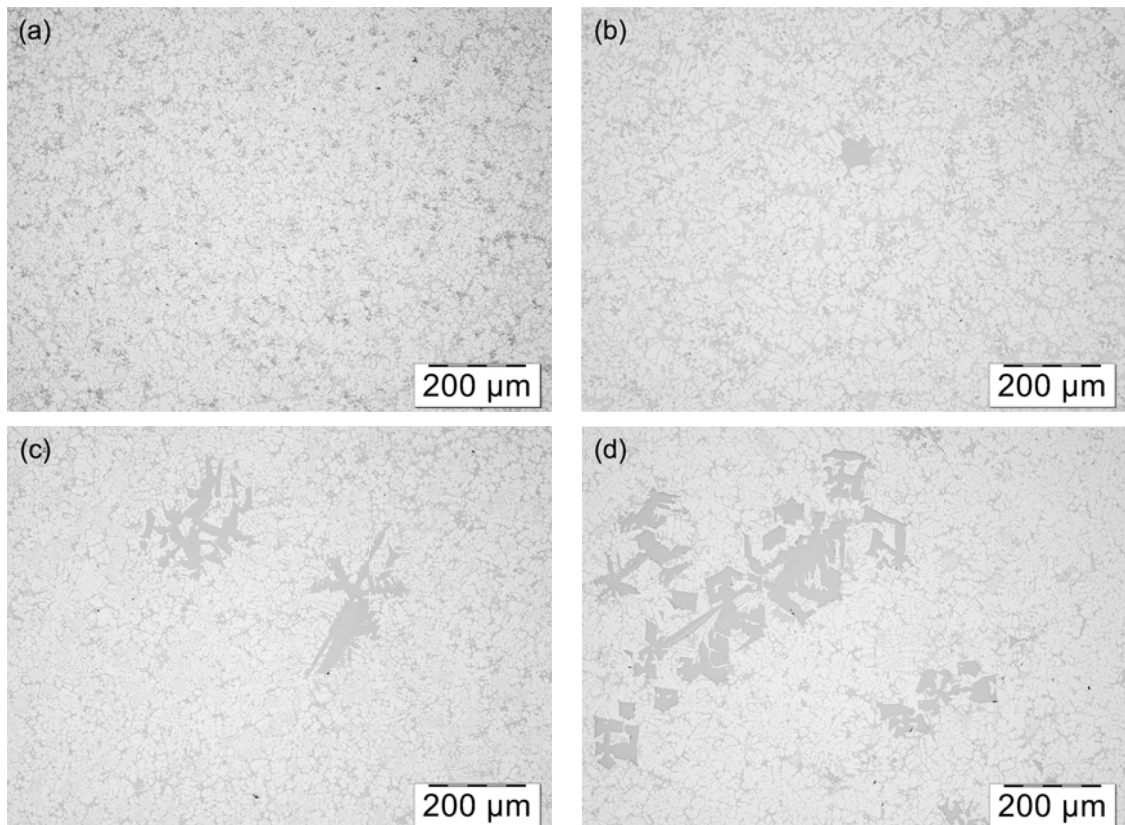


Figure 9: Microstructure evolution of sludge particles during solidification of alloy D. The images refer to quenching temperatures reported in Table 4: (a) Q1; (b) Q2; (c) Q3; (d) Q4.

The amount and dimensions of sludge particles increase with the level of Fe, Mn and Cr in the alloy, according to *sludge factor* value reported in Eq. 1. Moreover, a large number of platelet-like phases were recognizable in alloy B, as an impact of the higher value of Fe:Mn ratio (4.63). Here, the content of Mn and Cr is not enough to definitely change the morphology of the Fe-rich phases; therefore, a large number of needles β -phase coexists with blocky α -phase.

4. Conclusions

The effect of Fe, Mn, Cr and the cooling rate on the sludge formation in secondary AlSi9Cu3(Fe) alloys has been investigated by means of thermal analysis techniques (DSC and TA). Based on the results obtained in the present study, the following conclusions can be drawn.

- The temperature of sludge formation is closely related to the specific chemical composition of the alloy. An increasing of Fe, Mn and Cr, i.e. the *sludge factor*, shifts sludge nucleation towards higher temperature regardless of the cooling rate.
- Sludge nucleation temperature decreases with increasing the cooling rate of the molten material. Moreover, primary Fe-rich particles show large dependency on cooling conditions compared to the typical solidification reactions of the AlSi9Cu3(Fe) type alloy.
- A large number of pro-eutectic platelet particles (β -Al₅FeSi) is promoted in the alloy which exhibits the highest value of the Fe:Mn ratio. The increase of Fe content, without increasing Mn or Cr, increases the formation temperature of these pro-eutectic phases.
- Increasing the cooling rate and/or the Fe, Mn and Cr concentration in the alloy increase the release of latent heat for the sludge formation. This is correlated with an increase of volume fraction of sludge particles coupled to cooling rate.
- Sensibility to sludge formation is not affected by cooling rate.

- The results obtained by thermal analysis and quenching experiments confirm that the solidification of primary phase detected by DSC analysis correspond to sludge formation.
- The solidification temperatures of Fe-rich phases as function of Fe, Mn and Cr content will be support the foundries to set the right molten metal temperature in order to prevent sludge formation in the holding furnace and during the melt handling to and into the plunger system in HPDC machines.

References

1. S.G. Shabestari, *Mater. Sci. Eng. A*, 2004, vol. 383, pp. 289-298.
2. P.N. Crepeau, *AFS Trans.*, 1995, vol. 103, pp. 361-366.
3. A.M.A. Mohamed, A.M. Samuel, F.H. Samuel and H.W. Doty, *Mater. Design*, 2009, vol. 30, pp. 3943-3957.
4. A.M.A. Mohamed, F.H. Samuel, A.M. Samuel and H.W. Doty, *Mater. Design*, 2009, vol. 30, pp. 4218-4229.
5. S. Seifeddine and I.L. Svensson, *Metall. Sci. Technol.*, 2009, vol. 27, pp. 11-20.
6. C.M. Dinnis, J.A. Taylor and A.K. Dahle, *Mater. Sci. Eng. A*, 2006, vol. 425, pp. 286-296.
7. L. Lu and A.K. Dahle, *Metall. Mater. Trans. A*, 2005, vol. 36, pp. 819-835.
8. J.A. Taylor, G.B. Schaffer and D.H. StJohn, *Metall. Mater. Trans. A*, 1999, vol. 30, pp. 1643-1650.
9. S. Shankar and D. Apelian, *Metall. Mater. Trans. B*, 2002, vol. 33, pp. 465-476.
10. M.M. Makhoulouf and D. Apelian, *Work Performed Under DOE Contract No. DEFC07-99ID13716*, 2002, pp. 1-46.
11. S. Seifeddine, S. Johansson and I.L. Svensson, *Mater. Sci. Eng. A*, 2008, vol. 490, pp. 385-390.
12. G. Gustafsson, T. Thorvaldsson and G.L. Dunlop, *Metall. Trans. A*, 1986, vol. 17, pp. 45-52.
13. P. Ashtari, H. Tezuka and T. Sato, *Scripta Mater.*, 2005, vol. 53, pp. 937-942.

14. J.Y. Hwang, H.W. Doty and M.J. Kaufman, *Mater. Sci. Eng. A*, 2008, vol. 488, pp. 496-504.
15. Z. Ma, A.M. Samuel, F.H. Samuel, H.W. Doty and S. Valtierra, *Mater. Sci. Eng. A*, 2008, vol. 490, pp. 36-51.
16. M. Mahta, M. Emamy, A. Daman, A. Keyvani and J. Campbell, *Int. J. Cast. Met. Res.*, 2005, vol. 18, pp. 73-79.
17. S. Murali, K.S. Raman and K.S.S. Murthy, *Mater. Charact.*, 1994, vol. 33, pp. 99-112.
18. S.G. Shabestari, M. Keshavarz and M.M. Hejazi, *J. Alloys Compd.*, 2009, vol. 477, pp. 892-899.
19. Y.-H. Tan, S.-L. Lee and Y.-L. Lin, *Metall. Mater. Trans. A*, 1995, vol. 26, pp. 1195-1205.
20. L.A. Narayanan, F.H. Samuel and J.E. Gruzleski, *Metall. Mater. Trans. A*, 1994, vol. 25, pp. 1761-1773.
21. L.F. Mondolfo: *Aluminium alloys : structure and properties*. (Butterworths, 1976).
22. G. Timelli and F. Bonollo, *Mater. Sci. Eng. A*, 2010, vol. 528, pp. 273-282.
23. X. Cao, N. Saunders and J. Campbell, *J. Mater. Sci.*, 2004, vol. 39, pp. 2303-2314.
24. S.G. Shabestari and J.E. Gruzleski, *Metall. Mater. Trans. A*, 1995, vol. 26A, pp. 999-1006.
25. J. Gobrecht, *Giesserei*, 1975, vol. 62, pp. 263-266.
26. J.L. Jorstad, *Die Casting Engineer*, 1986, pp. 30-36.
27. C.L. Chen, A. Richter and R.C. Thomson, *Intermetallics*, 2010, vol. 18, pp. 499-508.
28. J. Shouxun, Y. Wenchao, G. Feng, W. Douglas and F. Zhongyun, *Mater. Sci. Eng. A*, 2012, vol. 564, pp. 130-139.
29. E. Taghaddos, M.M. Hejazi, R. Taghiabadi and S.G. Shabestari, *J. Alloys Compd.*, 2009, vol. 468, pp. 539-545.
30. Y. Zedan, F.H. Samuel, A.M. Samuel and H.W. Doty, *J. Mater. Process. Technol.*, 2010, vol. 210, pp. 245-257.
31. R. Dunn, *Die Casting Engineer*, 1965, pp. 8-30.
32. L. Backerud, G. Chai and J. Tamminen: *Solidification Characteristics of Aluminum Alloys, vol 2: Foundry Alloys*. (AFS-Skanaluminium, Stockholm, 1990).

33. S. Seifeddine: *Characteristics of cast aluminium-silicon alloys - microstructures and mechanical properties. Ph.D. Thesis - Dissertation No. 1058.* (Linköping Studies in Science and Technology, Sweden, Linköping, 2006).
34. A. Fabrizi, S. Ferraro and G. Timelli, *Mater. Charact.*, 2013, vol. 85, pp. 13-25.
35. X. Cao and J. Campbell, *Mater. Sci. Eng. A*, 2004, vol. 35A, pp. 1425-1435.
36. R.I. Mackay and J.E. Gruzleski, *Int. J. Cast. Met. Res.*, 1997, vol. 10, pp. 131-145.
37. J.E. Gruzleski and B.M. Closset: *The treatment of liquid aluminum-silicon alloys.* (American Foundrymen's Society, Inc., USA, 1990).
38. M. Warmuzek, W. Ratuszek and G. Sęk-Sas, *Mater. Charact.*, 2005, vol. 54, pp. 31-40.
39. Z. Guo, N. Saunders, J.P. Schillé and A.P. Miodownik, *Mater. Sci. Eng. A*, 2009, vol. 499, pp. 7-13.
40. X. Cao and J. Campbell, *Metall. Mater. Trans. A*, 2003, vol. 34A, pp. 1409-1420.
41. A.M. Samuel, F.H. Samuel, H.W. Doty and S. Valtierra, *AFS Trans.*, 2001, vol. 109, pp. 679-696.
42. X. Cao and J. Campbell, *Int. J. Cast. Met. Res.*, 2003, vol. 15, pp. 595-608.
43. W. Khalifa, F.H. Samuel, J.E. Gruzleski, H.W. Doty and S. Valtierra, *Metall. Mater. Trans. A*, 2005, vol. 36A, pp. 1017-1032.
44. S. Terzi, J.A. Taylor, Y.H. Cho, L. Salvo, M. Suéry, E. Boller and A.K. Dahle, *Acta Mater.*, 2010, vol. 58, pp. 5370-5380.

ARTICLE 3

EVOLUTION OF SLUDGE PARTICLES IN SECONDARY DIE-CAST ALUMINUM ALLOYS AS FUNCTION OF FE, MN AND CR CONTENTS

S. Ferraro¹, A. Fabrizi¹, G. Timelli¹

¹ Department of Management and Engineering - DTG
University of Padua
Vicenza, ITALY

Submitted for publication in: *Metallurgical and Materials Transactions A*, 2013.

ABSTRACT

The evolution of sludge particles in a secondary high-pressure die-cast AlSi9Cu3(Fe) alloy has been investigated over three levels of iron (0.80, 1.00, 1.20 wt.%) and manganese (0.25, 0.40, 0.55 wt.%), and two levels of chromium (0.06, 0.10 wt.%). Metallographic and image analysis techniques have been used in order to quantitatively evaluate the morphological and dimensional variations of sludge with different Fe, Mn and Cr contents. The results indicate that any increase of the Fe, Mn and Cr level promotes the formation of coarser sludge, with polyhedral and star-like morphologies. Fe and Mn produce an increase on the number of primary Fe-rich particles, while Cr promotes the formation of a large number of secondary Fe-rich particles. No relationship is revealed between the morphological variation of sludge and the Fe, Mn or Cr contents, as well as between the *sludge factor* and the Fe:Mn ratio. In the analyzed range of composition, the design of experiment methodology and the analysis of variance have been used in order to develop statistical models that accurately predict the average size and number of sludge particles in the AlSi9Cu3(Fe) diecasting alloys.

KEYWORDS

Aluminum alloys

Sludge Factor

Fe-rich intermetallics

High-pressure die-casting

Microstructure

ANOVA

1. Introduction

In the automotive and aerospace industry, aluminum-silicon foundry alloys are widely used due to their excellent castability, high strength to weight ratio, good corrosion resistance and recycling properties [1]. Iron is one of the most detrimental impurity of these alloys, since it forms brittle and complex intermetallic compounds that have long been known to reduce the mechanical properties and to increase the porosity content [2-8]. The monoclinic $\beta\text{-Al}_5\text{FeSi}$ ($\beta\text{-Fe}$) particles crystallize during the solidification even at low Fe content in the melt, due to low Fe solubility in solid $\alpha\text{-Al}$ phase [9]. Due to the sharp edges of these needle-like phase, a severe stress concentration is introduced to the alloy's matrix with a general reduction of the plastic properties of the material [7,10].

Since Fe is inevitable and cannot be economically removed from the molten aluminum [4], different solutions have been developed to neutralize its negative effects. The $\beta\text{-Al}_5\text{FeSi}$ phase can be modified to a less harmful and more compact morphology by addition of alloying elements such as Mn, Cr, Ni, Mo, Co, Sr, K and Be [8,11,16-23]. The amount, size and shape of these Fe-rich particles also depend largely on the cooling condition [7-11]. Cooling rates higher than 20°C/s can suppress the platelet-like morphology and provide a less harmful α -phase shape [12].

Manganese is the most common alloying element to suppress the development of needle particles by promoting the formation of a thermodynamically stable α -phase [4,8,13]. Generally, alloying with a Fe:Mn ratio lower than 2 is recommended to encourage the α -phase precipitation [14]; nevertheless, it is reported that the formation of Fe-rich needles is still not totally inhibited even at high Mn level and Fe:Mn ratio up to 1 [10].

It has been shown that Cr has similar effect of Mn [9,11,15]. These two elements are normally present in secondary Al foundry alloys as impurities due to the recycling process of aluminum scraps. Fe, Mn and Cr can substitute each other in the same bcc crystal structure, $\alpha\text{-Al}(\text{Fe,Mn,Cr})\text{Si}$ ($\alpha\text{-Fe}$), which may appear with Chinese script, star-like or polyhedral morphology [8,9,15].

Fe-bearing compounds can nucleate and grow at temperature higher than the α -Al dendrites. These primary Fe-rich particles, commonly called *sludge* [8,16-21], have high specific density and tend to segregate to the bottom of molten alloy and holding furnace. Further, the sludge decreases the alloy's fluidity and can be entrapped and dragged into the castings. Since sludge crystals are hard and brittle [22], they can compromise the machining operations with a considerable effects on the cutting tool life, and even more degrade the mechanical and physical properties of components [4-6,14,20,23,24].

The tendency of Al-Si-Cu alloys to form primary Fe-rich particles can be predicted by the *sludge factor (SF)* equation, which represents an attempt to gather the combined effects of Fe, Mn and Cr. The accepted empirical equation of *SF* is expressed as [19,20,25]:

$$\text{Sludge Factor (SF)} = (1 \times \text{wt.\%Fe}) + (2 \times \text{wt.\%Mn}) + (3 \times \text{wt.\%Cr}) \quad (1)$$

Dunn [25], Gobrecht [19] and Jorstad [20] found an empirical relationship for Al-Si-Cu alloys between the *SF* and the critical precipitation temperature below which Fe-rich particles tend to form in the holding furnaces.

Recently, Shabestari [8] found that the initial Fe, Mn and Cr contents as well as the cooling rate significantly affect the morphology, amount and size of sludge. According to these results, the temperature of sludge formation depends especially on the Fe content following this relationship:

$$\text{Temperature}(\text{°C}) = 645.7 + 34.2 \times (\text{wt.\%Fe})^2 \quad (2)$$

It is also well described in literature that the precipitation and sedimentation of Fe-rich particles may directly related to size and quantity of oxide films [16,26,27] and inclusions in the Al melt, e.g. CaO and SiC [28]. The Al oxide covering the bath surface can also act as a nucleant for sludge [29]. Moreover, the melt temperature influences the morphology of Fe-rich particles by changing the type of oxide. When the melt is superheated to high temperature ($\geq 850\text{°C}$), the metastable $\gamma\text{-Al}_2\text{O}_3$ (cubic), which acts as nucleant for the $\beta\text{-Fe}$ phase,

transforms into the thermodynamically stable $\alpha\text{-Al}_2\text{O}_3$ (hexagonal) and promotes the formation of $\alpha\text{-Fe}$ compounds [12,16,26,27].

Although the negative effects of Fe, this element is desirable and necessary in aluminum die-casting alloys because it increases the high-temperature properties of the alloy and it helps to prevent or alleviate the die soldering [17,30]. The problem of sludge formation is often experienced in Al foundry, especially in high-pressure die-casting (HPDC) foundries where, in order to preserve the die and tools, the holding and casting temperatures are typical lower than in the other foundry processes [20].

The literature well describes the effects of Fe, Mn and Cr on the formation of sludge in the holding furnace [8,13,16,18-20,25,27]. However, generally the microstructural investigations were performed on separately *gravity* cast samples, while sludge formation is frequently observed in HPDC where higher cooling rates and different feeding conditions exist respect to gravity die-casting [20]. Since sludge shape is dependent on the cooling rate [7-11], Fe-bearing morphologies that form during die-casting process may not necessarily form under other casting conditions [21].

In this work, the evolution of sludge particles in a secondary high-pressure die-cast AlSi9Cu3(Fe) alloy has been investigated as function of different Fe, Mn and Cr contents. The Fe, Mn and Cr levels were varied in order to correlate the amount and morphologies of Fe-bearing particles with the sludge factor. A statistical approach based on the analysis of variance (ANOVA) was implemented to develop functional equations useful to estimate the size and amount of sludge as function of the initial chemical composition of the alloy.

2. Experimental procedure

A secondary AlSi9Cu3(Fe) cast alloy (EN AB-46000, equivalent to the US designation A380) was supplied by Raffineria Metalli Capra and used as a baseline. The chemical composition of the base EN AC-46000 alloy and the composition tolerance limits of the Standard EN 1706:2010 [31] are listed in Table 1.

Table 1: Chemical composition of the supplied alloy (wt.%); the composition limits of the EN AC-AlSi9Cu3(Fe) alloy (EN AC-46000) is also reported according to the EN standard 1706:2010 [31]; the upper limit of the elements not listed in the table is 0.05 wt.%, with a total amount of 0.25 wt.%.

<i>Alloy</i>		<i>Si</i>	<i>Fe</i>	<i>Cu</i>	<i>Mn</i>	<i>Mg</i>	<i>Cr</i>	<i>Ni</i>	<i>Zn</i>	<i>Pb</i>	<i>Sn</i>	<i>Ti</i>	<i>Al</i>
EN AC-46000	<i>Min.</i>	8.0	0.6	2.0	-	0.05	-	-	-	-	-	-	<i>Bal.</i>
	<i>Max.</i>	11.0	1.3	4.0	0.55	0.55	0.15	0.55	1.20	0.35	0.25	0.25	
supplied (base-line)		8.40	0.72	2.43	0.21	0.19	0.06	0.05	1.05	0.09	0.03	0.04	<i>Bal.</i>

The experimental alloys were prepared from the supplied material by progressively adding Fe, Mn and Cr, in the form of commercial Al-25Fe, Al-25Mn and Al-10Cr master alloys, inside a 300 kg holding furnace. After addition, the molten metal was heated up to $760 \pm 5^\circ\text{C}$ and held for 30 min. The temperature was then decreased to $690 \pm 5^\circ\text{C}$, that is the holding temperature commonly used for AlSi9Cu3(Fe) type alloys.

Eighteen different alloys were prepared by varying the Fe, Mn and Cr contents according three levels of Fe (0.80 - 1.00 - 1.20 wt.%) and Mn (0.25 - 0.40 - 0.55 wt.%), and two levels of Cr (0.06 - 0.10 wt.%). Table 2 shows the targeted and the achieved contents of Fe, Mn and Cr in the experimental alloys, while the concentrations of the other alloying elements remain almost similar to the base alloy. According to alloys' compositions, the *SF* was varied between 1.32 and 2.90. In order to avoid any type of sedimentation and to guarantee the homogeneity of the molten bath, the material was periodically skimmed and stirred, and the chemical composition was verified on samples separately poured at the beginning and at the end of every set of casting.

Cast-to-shape specimens were produced using a multicavity die in a cold chamber die-casting machine. A detailed description of HPDC machine, casting procedure and geometry, and process parameters is given elsewhere [32]. After each start up, 20-25 castings were scrapped to reach a quasi-steady state temperature in the shot chamber and die. The die temperature was maintained at ~230°C by circulating oil through channels in the die. The melt was transferred in 15 sec from the holding furnace and poured into the shot sleeve by means of a cast iron ladle coated with a ceramic paste.

Microstructural investigations were carried out on the cross section of the cylindrical specimens (\varnothing 6 mm) drawn from the die-castings, and analyzed by means of an optical microscope (OM) and a field emission gun-scanning electron microscope (FEG-SEM), equipped with an energy-dispersive spectrometer (EDS). The samples were mechanically prepared to a 3- μ m finish with diamond paste and, finally, polished with a commercial fine colloidal silica slurry for metallographic observations. The polished specimens were etched in a 70°C heated solution of 10% sulphuric acid in water, to easily analyze the Fe-rich particles by image analysis software. Only Fe-rich particles with an area greater than 10 μm^2 were considered for the microstructural characterization of sludge by means of OM. The analysis was performed on three different samples for each alloy, covering a total area of about 20 mm^2 . Some samples were also deeply etched in a concentrated NaOH solution in order to reveal the 3D morphology of Fe-rich phases.

The effects of Fe, Mn, Cr and their interaction on the microstructural evolution of sludge were also studied through a statistical approach based on the analysis of variance (ANOVA). Each independent variable (Fe, Mn and Cr content) was analyzed at two different levels, and thus a simplified model, if compared to the entire experimental campaign, was carried out. A detailed description of the statistical method used in this work is given elsewhere [33,34].

Table 2: and achieved (in parentheses) levels (wt.%) of Fe, Mn and Cr in the experimental alloys. The sludge factor SF, calculated according to Eq. (1), and the Fe:Mn ratio are also indicated for each alloy.

<i>Alloy No.</i>	<i>Fe</i>	<i>Mn</i>	<i>Cr</i>	<i>SF</i>	<i>Fe:Mn</i>
1	0.80 (0.72)	0.25 (0.22)	0.06 (0.056)	1.48 (1.32)	3.20 (3.33)
2	0.80 (0.72)	0.25 (0.22)	0.10 (0.102)	1.60 (1.47)	3.20 (3.29)
3	0.80 (0.73)	0.40 (0.43)	0.06 (0.061)	1.78 (1.77)	2.00 (1.70)
4	0.80 (0.71)	0.40 (0.39)	0.10 (0.105)	1.90 (1.81)	2.00 (1.83)
5	0.80 (0.72)	0.55 (0.59)	0.06 (0.058)	2.08 (2.07)	1.45 (1.22)
6	0.80 (0.72)	0.55 (0.56)	0.10 (0.104)	2.20 (2.14)	1.45 (1.29)
7	1.00 (1.01)	0.25 (0.22)	0.06 (0.057)	1.68 (1.62)	4.00 (4.62)
8	1.00 (1.03)	0.25 (0.22)	0.10 (0.099)	1.80 (1.76)	4.00 (4.74)
9	1.00 (1.04)	0.40 (0.43)	0.06 (0.059)	1.98 (2.08)	2.50 (2.40)
10	1.00 (1.05)	0.40 (0.43)	0.10 (0.108)	2.10 (2.24)	2.50 (2.43)
11	1.00 (1.01)	0.55 (0.57)	0.06 (0.056)	2.28 (2.31)	1.82 (1.77)
12	1.00 (1.01)	0.55 (0.57)	0.10 (0.094)	2.40 (2.42)	1.82 (1.77)
13	1.20 (1.22)	0.25 (0.21)	0.06 (0.055)	1.88 (1.82)	4.80 (5.71)
14	1.20 (1.38)	0.25 (0.22)	0.10 (0.099)	2.00 (2.11)	4.80 (6.33)
15	1.20 (1.25)	0.40 (0.40)	0.06 (0.054)	2.18 (2.21)	3.00 (3.14)
16	1.20 (1.39)	0.40 (0.43)	0.10 (0.100)	2.30 (2.54)	3.00 (3.24)
17	1.20 (1.27)	0.55 (0.53)	0.06 (0.056)	2.48 (2.51)	2.18 (2.38)
18	1.20 (1.42)	0.55 (0.59)	0.10 (0.103)	2.60 (2.90)	2.18 (2.40)

3. Results and discussion

3.1. Microstructural analysis

In general, the microstructure of die-cast AlSi9Cu3(Fe) alloy consists of equiaxed and less-branched α -Al dendrites, surrounded by Al-Si eutectic and intermetallic particles. Figure 1 shows typical as-polished macrostructure: a large number of compact particles are observed in the macrostructure of all the analyzed alloys. By comparing their dimensions with the α -Al cell size, it results that these are primary particles with a polyhedral morphology, as evidenced in the zoomed area of Fig. 1. These particles are generally described in literature as Fe-rich phases and they are termed sludge in the die-casting industry [20].

The dash-lines mark an area of positive eutectic segregation, commonly called *defect band*, which follows the casting contour. This is a typical microstructural feature observed in Al-Si die-castings [35-37]. The defect band can be easily seen as dark band in etched condition, as reported in previous works [15,32,38]. This segregation area contains higher solute content than the surroundings, higher eutectic fraction [15] and intermetallics, which form late during solidification such as Al(Mn,Fe)Si particles [36]. In the present work, only a few primary polyhedral Fe-rich particles was seen within the defect band (Fig. 1), while primary β -Al₅FeSi particles were observed in the alloys with higher Fe:Mn ratio.

The sludge intermetallics are mainly located in the central region of samples' cross section, within the defect band, while the surface layer displays a lower content. This is mainly related to the primary Fe-rich phase formation during alloy solidification. Since sludge may form before the mold filling [18,20], it is a mixture of solid particles surrounded by liquid metal in shoot chamber. Consequently, the segregation mechanism of sludge particles can be described in a similar way to that suggested for the entrapment of the externally solidified crystals (ESCs) [15]. Due to high shear developed near the die wall, the sludge particles migrate during the die filling from regions of high to low shear rate, i.e. toward the casting centerline. Concurrently, the effective liquid cross-section thickness decreases due to the rapid growth of a surface skin during the die filling. The microstructure scale of this surface layer is smaller than the size of primary Fe-rich particles, and consequently the mechanical entrapment of these particles is difficult [15,35-37]. Thus, the surface layer displays a lower content of Fe-rich phases, while greater fraction of sludge is observed in the centre, without any segregation within the defect band.

The microstructures of the AlSi9Cu3(Fe) alloy with different Fe, Mn and Cr contents are compared in Fig. 2. The micrographs refer to the centre of the round specimen. Large Fe-rich intermetallic particles with polyhedral and star-like morphologies are visible. Their amount and dimensions increase with the increase of Fe, Mn and Cr levels in the alloy, according to *SF* value obtained through Eq. (1).

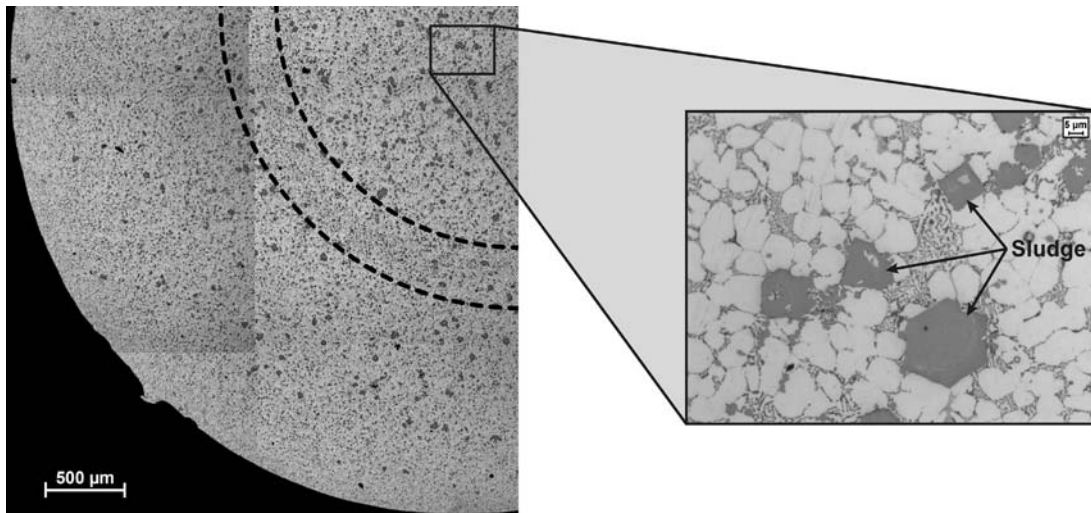


Figure 1: One quarter cross-section of the 6mm-diameter specimen, Alloy 16 (SF = 2.54); the dash-lines define the defect band. The inset better shows sludge particles, which are mainly located in the center region of the sample.

In the Alloy 1 (Fig. 2a), corresponding to the base-line material, few primary polyhedral α -Fe particles appear, while the needle-like β -Fe phase is absent. Upon increasing the Fe amount (Alloy 13, Fig. 2b) both primary polyhedral and star-like morphologies are recognized. The microstructure shows also the presence of primary β - Al_5FeSi particles, as better evidenced in Fig. 3. As the Mn and Cr contents are enhanced (Alloys 9 and 18), both the amount and the dimension of α -Fe compounds significantly increase if compared to the supplied AlSi9Cu3(Fe) alloy (Figs. 2c and 2d). The shape of sludge seems to degenerate, and a large number of star-like and irregular morphologies appear. The presence of pro-eutectic β -Fe phase is also observed, although it results to be smaller in comparison to the same phase in the Alloy 13.

Secondary fine polyhedral α -Fe particles are also revealed in the microstructures, as reported in Fig. 3. These pro-eutectic intermetallics, recognizable in all the experimental alloys, are mainly distributed at grain boundary and in the interdendritic channels, showing a clustering behavior. Due to their small size compared to the α -Al cell size, these particles were not considered primary, i.e. they do not contribute to the sludge.

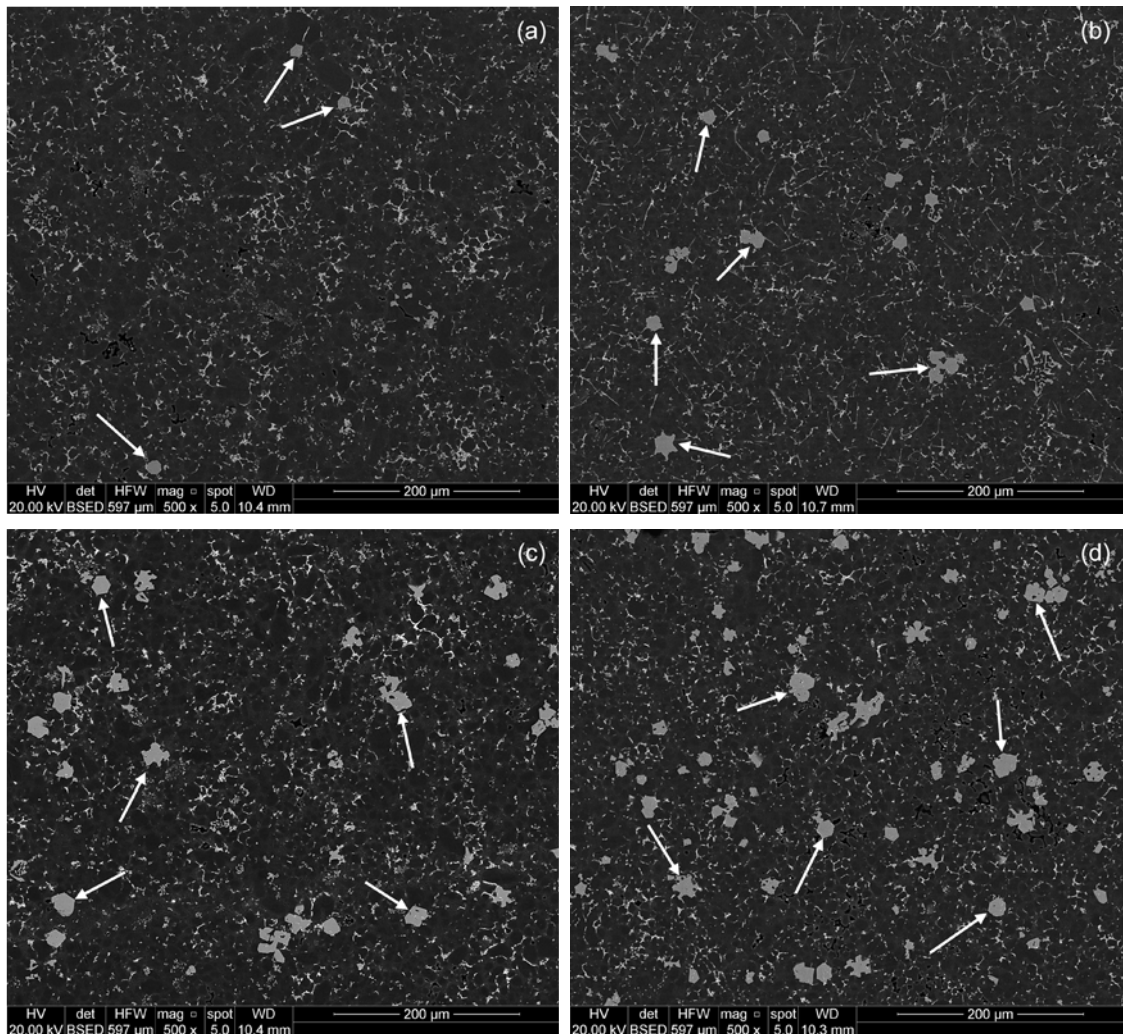


Figure 2: Backscattered FEG-SEM images of die-cast AlSi9Cu3(Fe) alloy with different amount of Fe, Mn and Cr. The micrographs, referred to the centre of cross section of the 6mm-diameter cylindrical specimen, are ordered according to the sludge factor: (a) Alloy 1, SF = 1.32; (b) Alloy 13, SF = 1.82; (c) Alloy 9, SF = 2.08; (d) Alloy 18, SF = 2.90. Sludge particles are indicated with arrows.

The variation of the Fe-rich particles' morphology from needle-like into polyhedral and irregular shapes can be described by the Gibbs-Wulff theorem [39,40]. The surface free energy of crystals is generally anisotropic and consequently the equilibrium crystal shape will not be spherical. The favorite growing planes correspond to the lowest surface energy and can be influenced by the chemical composition of the alloy. In the present work, mainly polyhedral and star-like morphologies were observed (Fig. 2). The most β -Fe enriched alloys were revealed to be the alloys with the relative higher Fe content, i.e. Alloys 13 and 14 that show a Fe:Mn ratio of 5.71 and 6.33, respectively. Here,

the content of Mn and Cr is not sufficient to definitely change the morphology of the Fe-rich particles; therefore, a large number of needles coexists with blocky compounds.

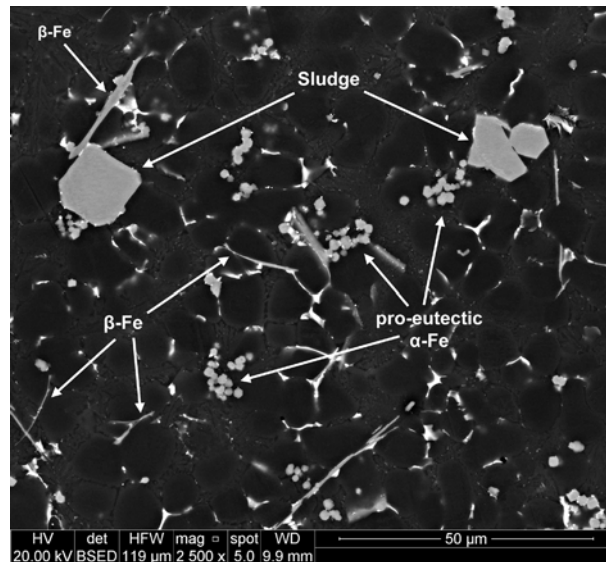


Figure 3: Backscattered FEG-SEM image of Alloy 13, SF = 1.82. A large number of β -Fe needles coexists with polyhedral sludge particles due to the high Fe:Mn ratio (5.71).

As previously described, sludge particles are Fe/Mn/Cr-containing phase. Shabestari [8] reported that the stoichiometry of the polyhedral, star-like and branched particles are α - $\text{Al}_{12}(\text{Fe},\text{Mn},\text{Cr})_3\text{Si}_2$, while Mondolfo [9] described these compounds as a solid solution of Fe and Cr in the $\text{Al}_{15}\text{Mn}_3\text{Si}_2$ phase with a cubic lattice, where 90% of Mn atoms can be substituted by Fe and Cr atoms, with a final α - $\text{Al}_{15}(\text{Fe},\text{Mn},\text{Cr})_3\text{Si}_2$ stoichiometry. Contrary, the results obtained by Warmuzek et al. [41] highlighted a wide range of the variability of the Fe, Mn and Cr concentration in the Fe-rich precipitates, with a stoichiometry that is closely related to the chemical composition of the alloy and the morphologies of the particles. The formation process of the α -Al(Fe,Mn,Cr)Si phase is controlled by the initial chemical composition of the alloy, but in the case of non-equilibrium conditions, such as in HPDC, the local fluctuations of the Fe, Mn, Cr and Si concentrations may influence the phase precipitation [42,43].

The Mn and Cr contents influence the composition of the needle-like particles, generally reported as monoclinic β - Al_5FeSi [9] phase. Shabestari [8]

found that the stoichiometry of the β -phase generally corresponds to Al_5FeSi but some Fe atoms can be replaced by 3.0 wt.% maximum of Mn and Cr, which are dissolved in the monoclinic crystal structure $\beta\text{-Al}_5(\text{Fe},\text{Mn},\text{Cr})\text{Si}$.

The chemical compositions of primary Fe-rich intermetallics were here studied by EDS and the results are reported in Fig. 4. Gradual changes in the chemical composition are recorded when the morphology degenerates from compact structures (polygonal or star-like) to Chinese script: a reduction of the Al, Mn and Cr levels with a corresponding increase of Si and Fe occurs for all the α -Fe phases in the experimental alloys, as reported in [44]. Since the literature shows no clarity about the composition of sludge, and considering that in this study the alloys were produced by systematically changing the Fe, Mn and Cr content, a generic $\alpha\text{-Al}_x(\text{Fe},\text{Mn},\text{Cr})_y\text{Si}_z$ is used to describe the stoichiometry of the sludge particles.

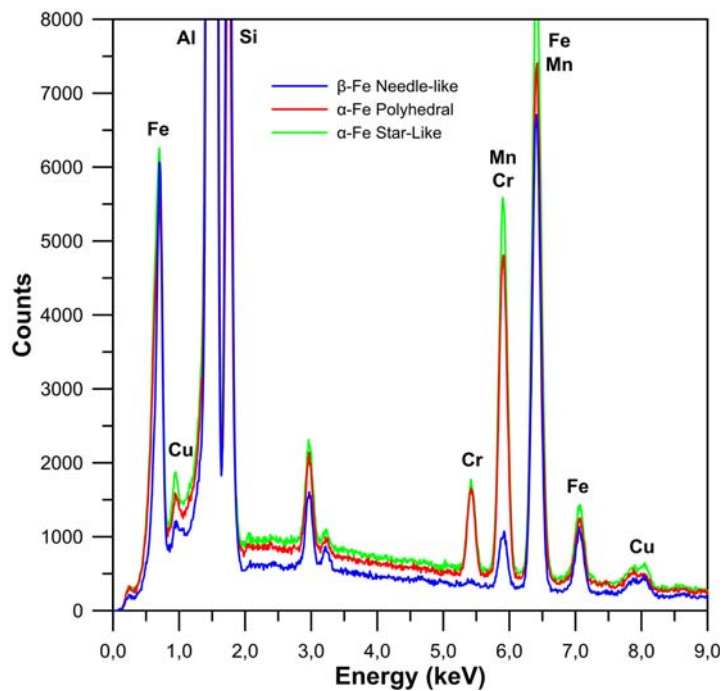


Figure 4: EDS spectra of primary Fe-rich intermetallics as function of their morphology. Peaks not specified correspond to the "ghost" of the main peaks.

3.2. Distribution of Sludge particles

The number of primary Fe-rich particles as well as their size and roundness were estimated by image analysis after chemical etching. The size of the sludge particles, reported here as equivalent circle diameter was found to follow the 3-parameter lognormal distribution:

$$f(x) = \frac{1}{\sigma(x-x_0)\sqrt{2\pi}} \cdot \exp\left[\frac{-(\ln(x-x_0)-\mu)^2}{2\sigma^2}\right] \quad (3)$$

where x is the equivalent circle diameter, x_0 is the threshold, μ and σ are the location parameter and the scale parameter, respectively [45].

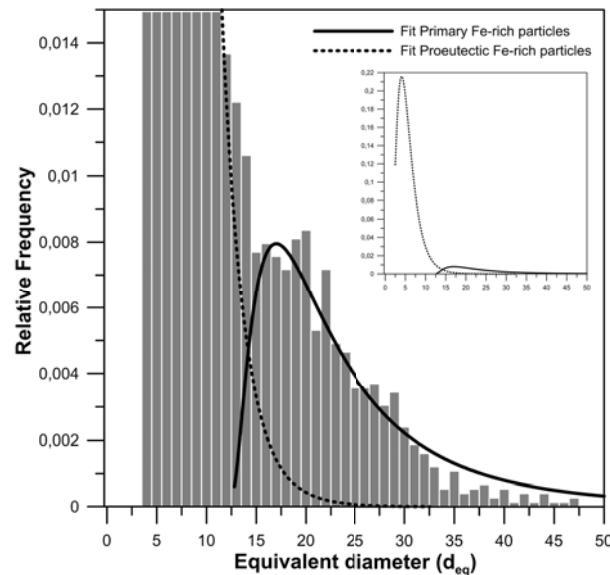


Figure 5: Distribution of the dimension of Fe-rich particles in Alloy 18, SF = 2.90, with associated the 3 parameter log-normal fit curves, which shows a bimodal distribution.

The probability density function reported in Fig. 5 highlight a bimodal distribution of equivalent circle diameter of Fe-rich particles. The two different modes, which appear as distinct peaks (local maxima), refer to Fe-rich pro-eutectic and sludge particles, respectively. By fitting the two modes with a 3-parameter lognormal curves, the average size of Fe-rich pro-eutectic and sludge particles are estimated. In particular, it results that the minimum dimension of primary Fe-rich particles for all the alloys, corresponds to about

12 μm . This particles size appears in good agreement with the typical $\alpha\text{-Al}$ grain size in HPDC [46].

The average sludge area and the number of particles per unit of area were reported in Fig. 6 as function of *sludge factor*. The data for each alloy corresponds to the expected value of log-normal distribution. These results well evidence that under these process conditions, the *SF* of the alloy accurately predicts the area and the density of sludge particles. The variation of the alloy's chemistry, especially the increasing of the concentration of Fe, Mn and Cr, promotes the formation of a larger number of Fe-rich particles, with gradually larger area, as show in Fig. 2.

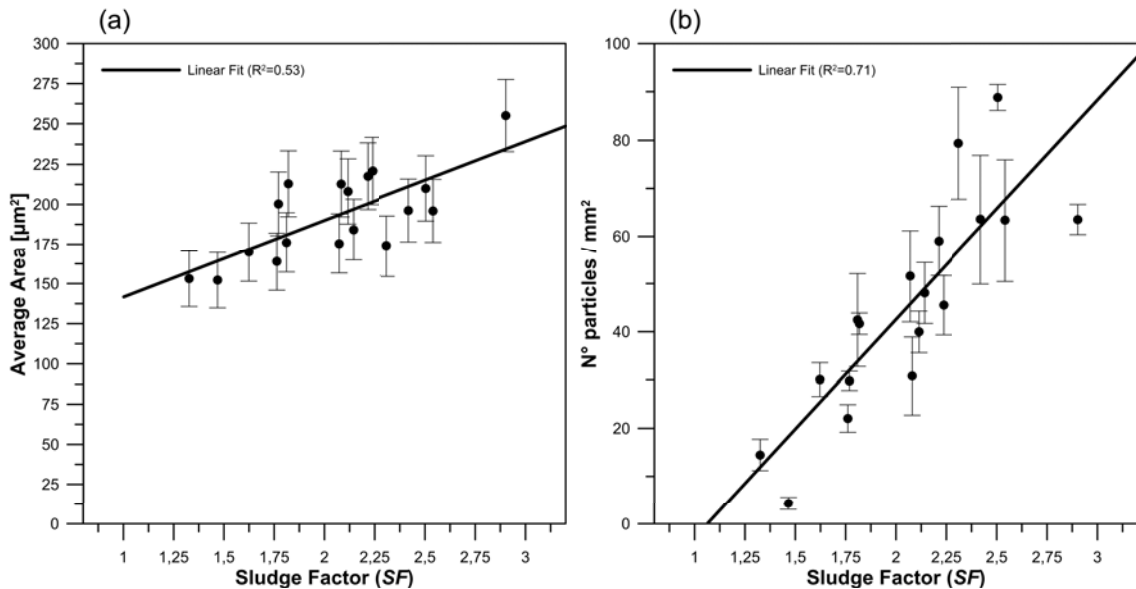


Figure 6: (a) Average size and (b) density, defined as number of particles per unit area, of sludge particles as function of sludge factor. Standard deviations are given as error bars.

The sludge particles density is plotted as parametric curves, as show in Fig. 7, in order to analyze the influence of each single element (Fe, Mn and Cr) on the sludge density. According to Table 2, the targeted values of chemical composition were used to simplify the reading of the diagrams. The variation of Fe and Mn content in the AlSi9Cu3(Fe) alloy produces a progressive increase of number of particles per unit area (Fig. 7a and b). On the contrary, the Cr addition does not reveal a marked effect, with a quasi-steady mean values (Fig. 7c). This is in disagreement with those reported in [15]. However, the results are closely

related to the minimum equivalent circle diameter used to identify the sludge particles. By adopting $3.6 \mu\text{m}$ as the lower limit size for sludge particles as reported by Timelli et al. [15] (that corresponding to an area of $\sim 10 \mu\text{m}^2$) the parametric curves show an increasing of Fe-rich particles density with the Cr content (Fig. 8), and the results are comparable [15]. Thereby, it can be proposed that the increase of Cr level promotes the formation of a large number of small Fe-rich particles (diameter less than $12 \mu\text{m}$), here described as pro-eutectic particles. To the contrary, the Fe and Mn parametric curves show the same trend by setting a size limit of both 3.6 and $12 \mu\text{m}$.

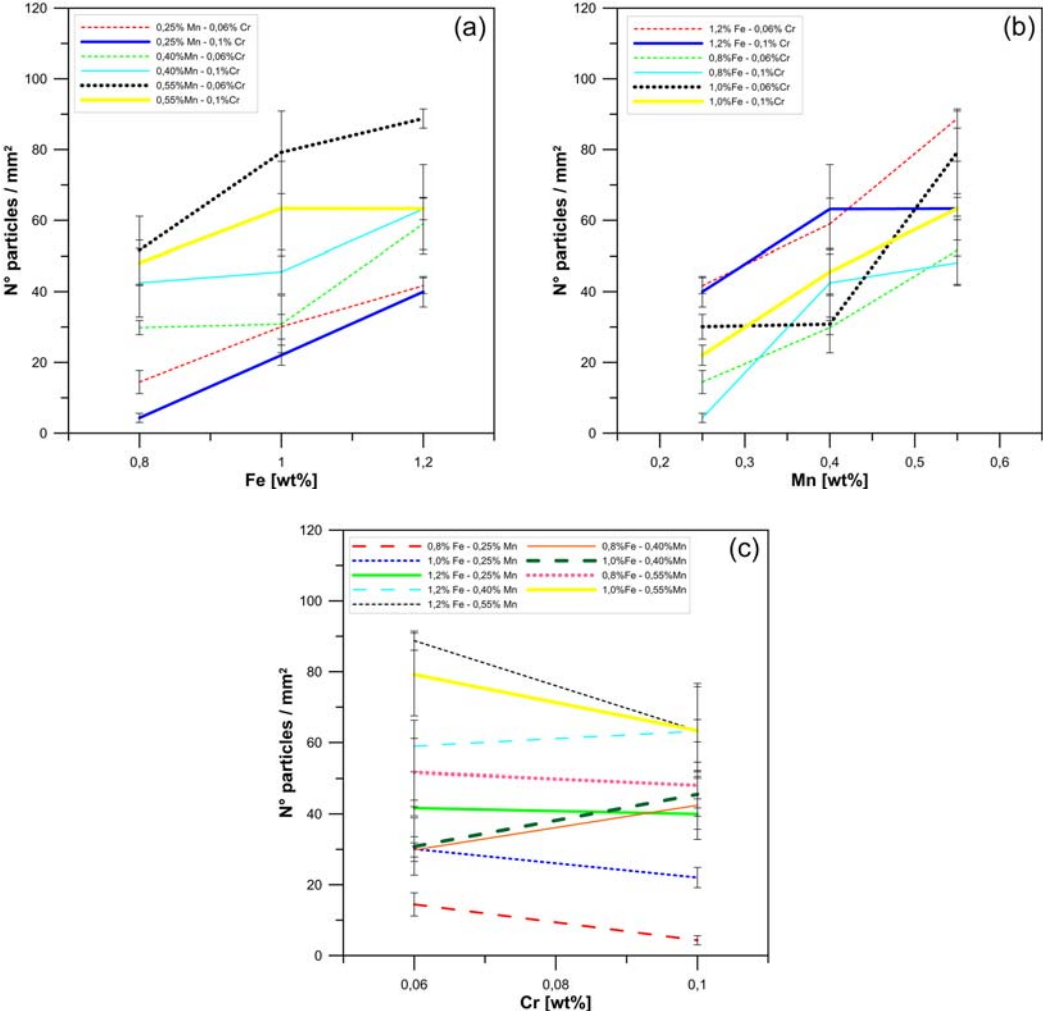


Figure 7: Parametric curves displaying the influence of nominal (a) Fe, (b) Mn and (c) Cr levels on sludge particles' density (number of particles per unit area); standard deviations are given as error bars. The concentration of the alloying elements refer to the targeted values of Table 2.

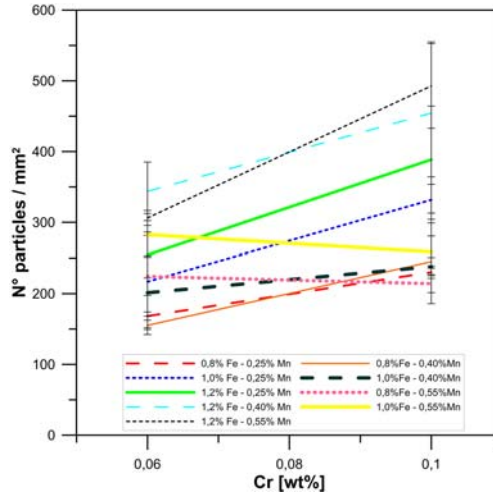


Figure 8: Parametric curves displaying the influence of nominal Cr levels on Fe-rich particles' density (both pro-eutectic and primary particles were considered); standard deviations are given as error bars. The Cr concentration refer to the targeted values of Table 2.

The mean area fraction of primary Fe-rich precipitates formed in each alloy was plotted as a function of sludge factor, as show in Fig. 9. The relationship was estimated by a linear regression analysis ($R^2=0.87$) as follows:

$$\text{Sludge fraction (\%)} = 1.5 \times (SF) - 1.9 \quad (4)$$

The results well evidence that under these process conditions, the SF of the alloy accurately predicts the sludge formation. According to Eq. (4), no sludge particles form in an AISi9Cu3(Fe) alloy with a sludge factor less than 1.27. A similar critical value (1.25) was obtained in a previous work [15] by varying the Cr content under similar experimental conditions. However, the slope of the fitting curve found in [15] was larger than the present result (see Fig. 3) and this may be due to higher Cr concentration (0.15 wt.%) and the threshold limit used to identify primary Fe-rich particles in the image analyzer.

Shabestari [8] and Taghaddos et al. [23] found the critical SF for sludge formation to be ~ 1.15 and ~ 0.35 , respectively for an A413 type alloys poured in permanent molds with short holding times (Fig. 9). Nevertheless, beside the *sludge factor*, the amount of primary Fe-rich intermetallics is strictly related to the holding temperature and time [17-20,25] and the cleanness of the melts

[16,26-28]. In addition, the cooling rate, related to the casting technologies and the content of Si and Cu, influences the nucleation temperature of sludge [13,19,47], and consequently the nucleation and growth mechanism. While in the present investigation a HPDC technology with an holding temperature of 690°C was used, the works of Shabestari [8] and Taghaddos et al. [23] were carried out by means of gravity casting with initial temperature of the melt of 720 and 670°C, respectively. Another important factor affecting the measurement of the area fraction of intermetallics is the threshold limit settings of Fe-bearing particles in the image analyzer, which was not reported in [8,23].

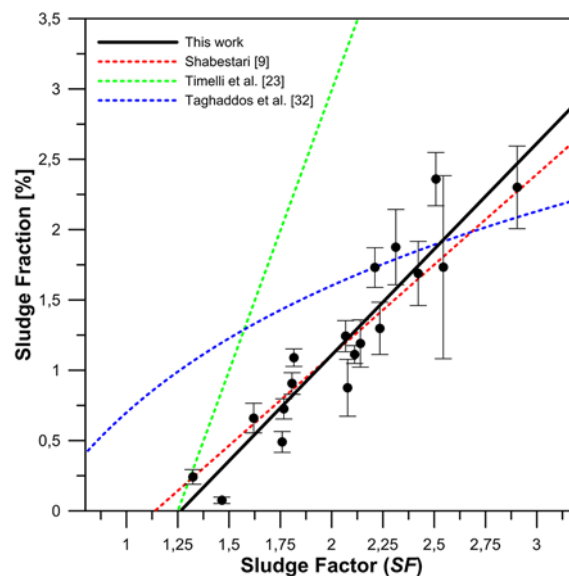


Figure 9: Average area fraction (%) of sludge particles as function of sludge factor calculated according to Eq.(1); standard deviations are given as error bars. The results of Shabestari [8], Timelli et al. [15] and Taghaddos et al. [23] are also reported.

3.3. Morphological analysis of Sludge

It has been reported that high Mn content leads Fe-rich phases to Chinese script morphology, while higher Cr promotes the formation of polyhedral, star-like and blocky particles [8,17,21]. However, there is not a systematic *quantification* of the sludge particles' morphology in the literature.

In order to study the effects of different content of Fe, Mn and Cr on the shape variation, the roundness of each sludge particle was calculated as follows:

$$\text{Roundness} = \frac{P^2}{4\pi A \cdot 1.064} \quad (5)$$

where P is the perimeter and A is the area of each particle. According to the Eq. (5), the minimum value of roundness is 1 corresponding to a circle shape.

Table 3: Mean roundness values of sludge particles for the experimental alloys. The concentration of the alloying elements refer to the targeted values of Table 2. The alloys were organized according to increasing roundness value.

<i>Alloy No.</i>	<i>Fe</i>	<i>Mn</i>	<i>Cr</i>	<i>SF</i>	<i>Fe:Mn</i>	<i>Roundness</i>
4	0.71	0.39	0.11	1.81	1.83	1.69
3	0.73	0.43	0.06	1.77	1.70	1.79
13	1.22	0.21	0.06	1.82	5.71	1.84
7	1.01	0.22	0.06	1.62	4.62	1.87
11	1.01	0.57	0.06	2.31	1.77	1.90
1	0.72	0.22	0.06	1.32	3.33	1.94
8	1.03	0.22	0.10	1.76	4.74	1.98
6	0.72	0.56	0.10	2.14	1.29	1.99
5	0.72	0.59	0.06	2.07	1.22	2.04
2	0.72	0.22	0.10	1.47	3.29	2.05
15	1.25	0.40	0.05	2.21	3.14	2.21
17	1.27	0.53	0.06	2.51	2.38	2.26
16	1.39	0.43	0.10	2.54	3.24	2.30
9	1.04	0.43	0.06	2.08	2.40	2.36
12	1.01	0.57	0.09	2.42	1.77	2.62
14	1.38	0.22	0.10	2.11	6.33	2.62
10	1.05	0.43	0.11	2.24	2.43	2.85
18	1.42	0.59	0.10	2.90	2.40	3.53

The roundness distributions were found to follow the lognormal distribution, according to the Eq.(3). The mean roundness value for the experimental alloys, reported in Table 3, ranges from 1.7 to 3.5, pointing out a morphological variation. However, the results indicate no relationship between the roundness of primary Fe-rich particles and the Fe, Mn or Cr contents, as well as between roundness and sludge factor (or Fe:Mn ratio).

Cao et al. [27] found a roundness value between 1.45 and 2.91 in a superheated and slow cooled A360 alloy with a SF of 3.3. However, they didn't observe a correlation of these values with high Mn levels (~ 1.1 wt.%) or with different superheating temperatures and times. Timelli et al. [15] demonstrated that an increasing Cr content, from 0.06 to 0.15 wt.%, does not change the morphology of Fe-bearing compounds in a die-cast AlSi9Cu3(Fe) alloy with 0.75 wt.% Fe and 0.20 wt.% Mn.

In order to better understand the sludge morphology, the α -Al matrix was dissolved by deep etching. The FEG-SEM investigations revealed the 3D morphology of the polyhedral primary α -Fe particles, which correspond to a regular rhombic dodecahedron (Fig. 10a) [44]. The same polyhedral structure of primary α -Fe phase was revealed by using time-resolved radiography in a synchrotron radiation facility [48]. In some cases, the rhombic dodecahedron structures show hollows in the center of the 12 rhombic facets, as shown in Fig. 10b. The different cross-sections of the hollowed shape seem to well approximate the star-like and branched morphologies of sludge, which appear in the OM micrographs (Fig. 11). A detailed description of the different sludge morphologies and the growth mechanism of hollowed α -Fe particles is reported elsewhere [44].

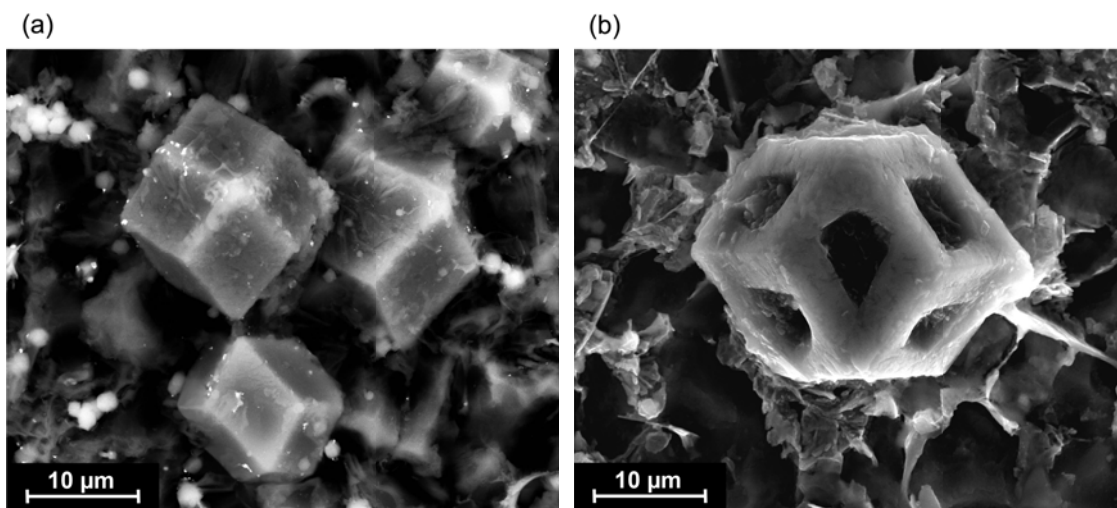


Figure 10: 3D FEG-SEM micrograph of a deep etched sample with primary α -Fe particles [44]: (a) regular rhombic dodecahedron structure, (b) hollowed rhombic dodecahedron structure.

The roundness value of arbitrary cross-sections of hollowed rhombic particles of Fig. 11 ranges from about 1.1 to 5. This highlights that a 2D shape factor of the sludge particle, such as 2D roundness, depends largely on the sectioning of the sample during the metallographic preparation. Contrary, a wide range of sludge morphologies, as reported in Fig. 2, can be related to the same 3D structure.

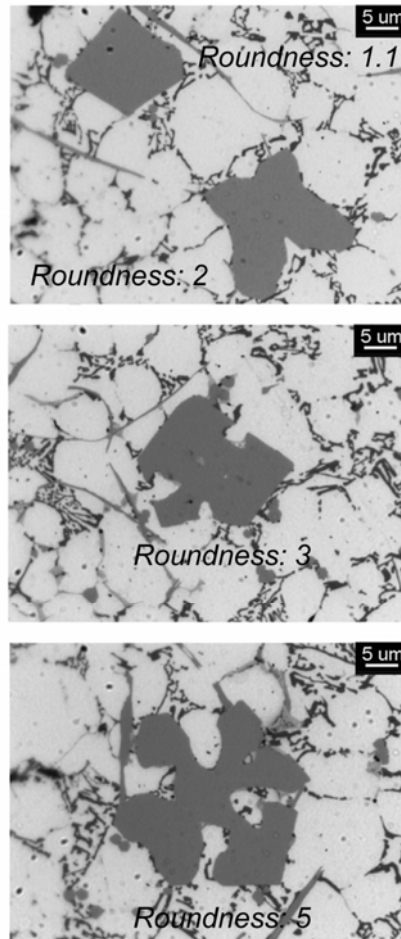


Figure 11: Micrographs of typical star-like and branched morphologies of sludge particles which correspond to cross-sections of the hollowed rhombic dodecahedron [44]. The different roundness values are also indicated.

Further studies will be performed in order to understand more clearly the 3D morphologies of sludge particles. Anyway, the authors suggest that a three-dimensional shape factors should be used to explain the morphology evolution of compact α -Fe particles; for instance the *sphericity*, which is a measure of how round is an object, and it is described as:

$$\Psi = \frac{\pi^{\frac{1}{3}} \cdot (6 \cdot V_p)^{\frac{2}{3}}}{A_p} \quad (6)$$

where V_p and A_p are the volume and the surface area of the particle, respectively. The sphericity of a sphere is 1 and any other morphologies will have sphericity less than 1.

3.4. Design of experimental matrix and ANOVA

The *design of experiments* (DOEs) is a statistical approach to the experimental investigation that allows to analyze which process input have a significant impact on the process output. An *analysis of variance* (ANOVA) should be performed by considering the independent factors (inputs) and their interaction that influence the response (output). The ANOVA is a statistical methodology that enables to investigate and to model the relationship between the output and one or more input variables [33,34].

In the present investigation, a factorial ANOVA approach was implemented in order to investigate the effects of Fe, Mn and Cr contents (*independent variables*) on size and density of sludge particles (*dependent variables*).

In order to realize the DOE matrix, independent variables were analysed at two levels each. The targeted compositions of resulting eight alloys used in the statistical approach are listed in Table 4.

Besides Fe, Mn and Cr contents as independent variables, four interactions were also considered, namely Fe·Mn, Fe·Cr, Mn·Cr and Fe·Mn·Cr.

The results of the ANOVA procedure can be represented in the *normal probability plots* (see Fig. 12), where each point represents the independent factor or their interaction on a dependent variable. The p -value is used to determine whether a factor is statistically significant: higher the p level, lower the probability that the observed relation between two variables in a single sample is a reliable indicator of the relation between the respective variables in the population. The straight line of Fig.12 is a reference line drawn for a p -value of 0.05, which corresponds to a 5% probability that the relation between the variables is fortuitous. The *normal probability plots* allow to highlight simultaneously the magnitude and the direction of variables on response.

Consequently, the input variables that produce considerable effects on the response are far from the reference line, while the negligible ones tend to have a standard effect close to zero.

The analysis of the data by means of ANOVA was applied on average size and density of sludge (Figs. 12a and 12b, respectively), in order to reveal a complete and exhaustive evaluation of the relationship between microstructural features of these intermetallics compounds and the level of Fe, Mn and Cr in the experimental alloys.

While it is clear that Fe and Mn are the two main factors that increase the number and the dimension of sludge particles (factors *A* and *B* in Fig. 12), the effect of Cr depends on the specific microstructural feature analyzed (factor *C* in Fig. 12). Increasing the Cr content, the average area of sludge particles increase, whereas the number of particles per unit area decreases. As previously described (Fig. 8), the latter effect is closely related to the equivalent circle diameter value used to discriminate primary and pro-eutectic Fe-rich particles.

In addition to the single effect of the elements, it is important to analyse the results concerning the relationships among them. The interactions between Mn and Cr (Mn·Cr, also *BC* factor in Fig. 12) seem to have a similar effect of Cr, with a decrease in the number and an increase of the average size of sludge. The effects of other relationships among the elements, i.e. Fe·Mn and Fe·Cr (*AB* and *AC*, respectively), appear statistically insignificant, with a *p*-value higher than 0.05 for both the microstructural features analyzed.

Table 4: Targeted levels (wt.%) of Fe, Mn and Cr in the eight experimental alloys used to perform the DOE. The alloy numbers refer to Table 2.

<i>Alloy No.</i>	<i>Fe</i>	<i>Mn</i>	<i>Cr</i>
1	0.80	0.25	0.06
2	0.80	0.25	0.10
5	0.80	0.55	0.06
6	0.80	0.55	0.10
13	1.20	0.25	0.06
14	1.20	0.25	0.10
17	1.20	0.55	0.06
18	1.20	0.55	0.10

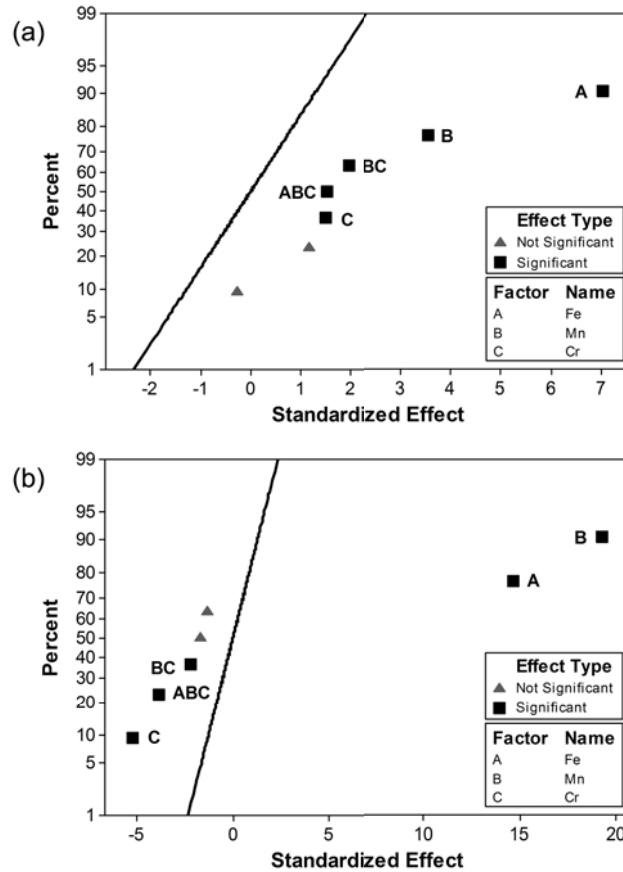


Figure 12: . Normal probability plots concerning the effects of Fe, Mn and Cr, and their interaction, on (a) the sludge size and (b) density. The straight lines points out a p-value of 0.05.

On the basis of the significance level provided by the ANOVA analysis, a regression model can be developed describing the relationship between the response and the predictor variables. The reliability of the model is based on the coefficient of determination, R^2 . It measures the quality of the least-squares fitting to the original full experimental alloy, described in Table 2.

In the considered range of composition, the average size and number of sludge particles per unit area can be described by the following semi-empirical equations:

$$\text{Sludge size} = 84.8 + 130.2 \times (\text{Fe}) - 107.5 \times (\text{Mn}) - 696.3 \times (\text{Cr}) + 2441 \times (\text{Mn} \cdot \text{Cr}) \quad (7)$$

$$\frac{N^\circ \text{ sludge}}{\text{mm}^2} = -80.9 + 72 \times (\text{Fe}) + 183.3 \times (\text{Mn}) + 30.5 \times (\text{Cr}) - 714 \times (\text{Mn} \cdot \text{Cr}) \quad (8)$$

where Fe, Mn and Cr are in wt.%. In order to verify the reliability of the regression models of Eqs.(7) and (8), the Fe, Mn and Cr content of the achieved chemical composition (Table 2) were used to predict the microstructural features of sludge particles. These results were compared with the measured ones to describe the quality of the developed models by means of goodness coefficients, which are 0.80 and 0.89 for the average sludge size and density of sludge particles, respectively. As a result, the Eqs. (7) and (8), that consider the specific chemical composition of the alloy, show a higher reliability compared to the linear regression of Fig. 6., where only one variable, i.e. the sludge factor, was considered.

4. Conclusion

The evolution of sludge particles in a secondary high-pressure die-cast AlSi9Cu3(Fe) alloy has been investigated as function of Fe, Mn and Cr contents. The following conclusions can be drawn from this work.

- The microstructure of die-cast AlSi9Cu3(Fe) alloy with different Fe, Mn and Cr content shows primary $\alpha\text{-Al}_x(\text{Fe},\text{Mn},\text{Cr})_y\text{Si}_z$ particles with polyhedral and star-like morphologies. At the highest Fe:Mn ratio the presence of primary $\beta\text{-Al}_5\text{FeSi}$ particles is also revealed.
- The sludge particles mainly segregate to the central region of the casting, while the surface layer displays lower content. Only few polyhedral sludge particles are observed within the positive eutectic segregation band, while in the same area pro-eutectic $\beta\text{-Al}_5\text{FeSi}$ compounds with a needle-shape are detected.
- The size distribution of Fe-rich particles in the alloy evidences two different modes, which refer to pro-eutectic (secondary) and primary particles, respectively. Any increase of the Fe, Mn and Cr level promotes the formation of coarser sludge particles; while the primary particles' density is more related to Fe and Mn levels, the Cr addition promote the formation of pro-eutectic Fe-rich compounds.

- In the considered range of composition, the average size and number of sludge can be well described by regression models that consider the concentration of Fe, Mn, Cr and the interactions among the elements.
- The area fraction of sludge particles can be estimated from the sludge factor by a linear relationship, while the sludge morphology seems to not be related to chemical composition, sludge factor or Fe:Mn ratio.

Acknowledgements

This work was developed with the financial support of Raffineria Metalli Capra SpA (Brescia, Italy). The authors would like to acknowledge the skilful contribution of Toolcast Snc (Brugine, Italy) for high-pressure die-casting of the tensile test specimens.

References

1. J.G. Kaufman and E.L. Rooy: *Aluminum Alloy Castings: Properties, Processes, and Applications*. (ASM International, USA, 2004).
2. C.M. Dinnis, J.A. Taylor and A.K. Dahle, *Mater. Sci. Eng. A*, 2006, vol. 425, pp. 286-296.
3. L. Lu and A.K. Dahle, *Metall. Mater. Trans. A*, 2005, vol. 36, pp. 819-835.
4. P.N. Crepeau, *AFS Trans.*, 1995, vol. 103, pp. 361-366.
5. A.M.A. Mohamed, A.M. Samuel, F.H. Samuel and H.W. Doty, *Mater. Design*, 2009, vol. 30, pp. 3943-3957.
6. A.M.A. Mohamed, F.H. Samuel, A.M. Samuel and H.W. Doty, *Mater. Design*, 2009, vol. 30, pp. 4218-4229.
7. S. Seifeddine and I.L. Svensson, *Metall. Sci. Technol.*, 2009, vol. 27, pp. 11-20.

8. S.G. Shabestari, *Mater. Sci. Eng. A*, 2004, vol. 383, pp. 289-298.
9. L.F. Mondolfo: *Aluminium alloys : structure and properties*. (Butterworths, 1976).
10. S. Seifeddine, S. Johansson and I.L. Svensson, *Mater. Sci. Eng. A*, 2008, vol. 490, pp. 385-390.
11. G. Gustafsson, T. Thorvaldsson and G.L. Dunlop, *Metall. Trans. A*, 1986, vol. 17, pp. 45-52.
12. L.A. Narayanan, F.H. Samuel and J.E. Gruzleski, *Metall. Mater. Trans. A*, 1994, vol. 25, pp. 1761-1773.
13. L. Backerud, G. Chai and J. Tamminen: *Solidification Characteristics of Aluminum Alloys, vol 2: Foundry Alloys*. (AFS-Skanaluminium, Stockholm, 1990).
14. J. Shouxun, Y. Wenchao, G. Feng, W. Douglas and F. Zhongyun, *Mater. Sci. Eng. A*, 2012, vol. 564, pp. 130-139.
15. G. Timelli and F. Bonollo, *Mater. Sci. Eng. A*, 2010, vol. 528, pp. 273-282.
16. X. Cao, N. Saunders and J. Campbell, *J. Mater. Sci.*, 2004, vol. 39, pp. 2303-2314.
17. M.M. Makhlof and D. Apelian, *Work Performed Under DOE Contract No. DEFC07-99ID13716*, 2002, pp. 1-46.
18. S.G. Shabestari and J.E. Gruzleski, *Metall. Mater. Trans. A*, 1995, vol. 26A, pp. 999-1006.
19. J. Gobrecht, *Giesserei*, 1975, vol. 62, pp. 263-266.
20. J.L. Jorstad, *Die Casting Engineer*, 1986, pp. 30-36.
21. L. Wang, D. Apelian and M.M. Makhlof, *AFS Trans.*, 1999, vol. 107, pp. 231-238.
22. C.L. Chen, A. Richter and R.C. Thomson, *Intermetallics*, 2010, vol. 18, pp. 499-508.
23. E. Taghaddos, M.M. Hejazi, R. Taghiabadi and S.G. Shabestari, *J. Alloys Compd.*, 2009, vol. 468, pp. 539-545.
24. Y. Zedan, F.H. Samuel, A.M. Samuel and H.W. Doty, *J. Mater. Process. Technol.*, 2010, vol. 210, pp. 245-257.
25. R. Dunn, *Die Casting Engineer*, 1965, pp. 8-30.
26. A.M. Samuel, F.H. Samuel, H.W. Doty and S. Valtierra, *AFS Trans.*, 2001, vol. 109, pp. 679-696.
27. X. Cao and J. Campbell, *Int. J. Cast. Met. Res.*, 2003, vol. 15, pp. 595-608.

28. W. Khalifa, F.H. Samuel, J.E. Gruzleski, H.W. Doty and S. Valtierra, *Metall. Mater. Trans. A*, 2005, vol. 36A, pp. 1017-1032.
29. S. Terzi, J.A. Taylor, Y.H. Cho, L. Salvo, M. Suéry, E. Boller and A.K. Dahle, *Acta Mater.*, 2010, vol. 58, pp. 5370-5380.
30. S. Shankar and D. Apelian, *Metall. Mater. Trans. B*, 2002, vol. 33, pp. 465-476.
31. Standard EN 1706:2010, *Aluminium and aluminium alloys - Castings - Chemical composition and mechanical properties*, 2010.
32. G. Timelli, S. Ferraro, F. Grosselle, F. Bonollo, F. Voltazza and L. Capra, *La Metallurgia Italiana*, 2011, vol. 101, pp. 5-17.
33. D.C. Montgomery: *Design and Analysis of Experiments* 8ed. (John Wiley & Sons, 2012).
34. F. Grosselle, G. Timelli and F. Bonollo, *Mater. Sci. Eng. A*, 2010, vol. 527, pp. 3536-3545.
35. C.M. Gourlay, H.I. Laukli and A.K. Dahle, *Metall. Mater. Trans. A*, 2007, vol. 38, pp. 1833-1844.
36. H.I. Laukli, C.M. Gourlay, A.K. Dahle and O. Lohne, *Mater. Sci. Eng. A*, 2005, vol. 413-414, pp. 92-97.
37. S. Otarawanna, C.M. Gourlay, H.I. Laukli and A.K. Dahle, *Metall. Mater. Trans. A*, 2009, vol. 40, pp. 1645-1659.
38. G. Timelli, S. Ferraro and A. Fabrizi, *Int. J. Cast. Met. Res.*, 2013, vol. 26, pp. 239-246.
39. S. Murali, K.S. Raman and K.S.S. Murthy, *Mater. Charact.*, 1994, vol. 33, pp. 99-112.
40. D.A. Porter, K.E. Easterling and Y.S. Mohamed: *Phase Transformations in Metals and Alloys*. 3rd ed. (Taylor & Francis, Boca Raton, FL, 2009).
41. M. Warmuzek, W. Ratuszek and G. Sęk-Sas, *Mater. Charact.*, 2005, vol. 54, pp. 31-40.
42. R. Jeniski, B. Thanaboonsombut and T.H. Sanders, *Metall. Mater. Trans. A*, 1996, vol. 27, pp. 19-27.
43. M. Warmuzek, G. Mrówka and J. Sieniawski, *J. Mater. Process. Technol.*, 2004, vol. 157-158, pp. 624-632.
44. A. Fabrizi, S. Ferraro and G. Timelli, *Shape Casting 5: International Symposium, TMS*, 2014.
45. M. Tiryakioğlu, *Mater. Sci. Eng. A*, 2008, vol. 473, pp. 1-6.
46. A. Fabrizi, S. Ferraro and G. Timelli, *Mater. Charact.*, 2013, vol. 85, pp. 13-25.

47. R.I. Mackay and J.E. Gruzleski, *Int. J. Cast. Met. Res.*, 1997, vol. 10, pp. 131-145.
48. B.H. Kim, S.M. Lee and H. Yasuda, *Mater. Sci. Forum*, 2010, vol. 654-656, pp. 974-977.

ARTICLE 4

INFLUENCE OF SLUDGE PARTICLES ON THE TENSILE PROPERTIES OF DIE-CAST SECONDARY ALUMINIUM ALLOYS

S. Ferraro¹, G. Timelli¹

¹ Department of Management and Engineering - DTG
University of Padua
Vicenza, ITALY

Submitted for publication in: *Materials Science and Engineering: A*, 2013.

ABSTRACT

The effects of sludge intermetallic particles on the mechanical properties of a secondary AlSi9Cu3(Fe) die-casting alloy has been studied. Different alloys have been produced by systematically varying the Fe, Mn and Cr content within the composition tolerance limits of the standard EN AC-46000 alloy. The microstructure shows primary $\alpha\text{-Al}_x(\text{Fe,Mn,Cr})_y\text{Si}_z$ sludge particles, with polyhedral and star-like morphologies, although the presence of primary $\beta\text{-Al}_5\text{FeSi}$ phase is also observed at the highest Fe:Mn ratio. The volume fraction of primary compounds increases as the Fe, Mn and Cr content increases and this can be accurately predicts from the *sludge factor* by a linear relationship. The sludge amount seems to not influence the size and the content of porosity in the die-cast material. Furthermore, the sludge factor is not a reliable parameter to describe the mechanical properties of the die-cast AlSi9Cu3(Fe) alloy, because this value does not consider the mutual interaction between the elements. In the analysed range of composition, the design of experiment methodology and the analysis of variance have been used in order to develop a semi-empirical model that accurately predict the mechanical properties of the die-cast AlSi9Cu3(Fe) alloys as function of Fe, Mn and Cr concentration.

KEYWORDS

Aluminium alloys

Sludge Factor

Fe-rich intermetallics

High-pressure die-casting

Mechanical characterization

ANOVA

1. Introduction

Iron is one of the most common impurity elements in Al-Si foundry alloys. Actually, dilution seems to be the only practical, although uneconomic, method to reduce the Fe content in the alloy [1]. The maximum solubility of Fe in solid Al is between 0.03 and 0.05 wt.% at 655°C and is less than 0.01 wt.% at 427°C [2]. Consequently, in commercial Al-Si foundry alloys, Fe forms intermetallic compounds with Al and other elements, that have long been known to be detrimental to mechanical properties [3-8]. A wide range of Al-Fe-Si particle types is reported in literature [2,9,10]. These can be generally grouped into three different morphologies: polyhedral crystals, Chinese script, or thin platelets.

Even at low Fe content in the melt, the monoclinic β -Al₅FeSi particles crystallize during the solidification. This platelet-like phase, which appears as needle in the microstructure, acts as stress raiser with a general reduction of the plastic properties of the cast alloy [3-5]. The formation and amount of porosity is also dependent on Fe-needles' content [11-13].

Iron in Al die-casting alloys is a desirable and necessary element that helps to prevent or alleviate the die soldering [14]. Generally, a Fe content higher than 0.8 wt.% reduces the solution potential of the molten Al alloy for steel components of the casting machine and die [14,15]. Therefore, secondary alloys with higher Fe content (in the range of 1 wt.%) than primary ones are used.

It has been shown that the size and amount of Fe-containing phases is strongly influenced by the solidification rate [4,5,16] and that alloying elements such as Mn, Cr, Ni, Mo, Co, Sr, K and Be can change the morphology of the phases or enhance the precipitation of Fe-rich particles which are less harmful than β -Al₅FeSi [4-6,16-22]. Manganese and Chromium are normally present in secondary Al alloys as impurities due to the recycling process of aluminium scraps. Mn and Cr can also be intentionally added to the alloy because, singly or in combination, they neutralize the effect of Fe-needle particles by modifying the morphology and type of phase [2,9]. Fe, Mn and Cr can substitute each other in the same bcc crystal structure, α -Al₁₅(Fe,Mn,Cr)₃Si₂, which may appear as

Chinese script, star-like or polyhedral morphology [2,9,23].

Modification of Fe-bearing compounds with Mn and Cr addition has also some disadvantages. The complex intermetallic compounds, like primary $\alpha\text{-Al}_{15}(\text{Fe},\text{Mn},\text{Cr})_3\text{Si}_2$, have a high specific gravity and tend to segregate to the bottom of molten alloy and holding furnaces; such particles are generally called *sludge* [9,15,24-27]. When sludge crystals are entrained into castings, they decrease the alloy's fluidity and appear as hard inclusions, which can compromise the machining operations and even more degrade the mechanical and physical properties of the component [1,27-32].

The problem of sludge formation is often experienced in Al foundries, especially in high-pressure die-casting foundry where, in order to preserve the die and tools, the holding and casting temperatures are typical lower than in the other foundry processes [27].

Sludge formation has been shown to be dependent on the alloy's chemistry, melting and holding temperature and time. Dunn [33], Gobrecht [26] and Jorstad [27] have defined a *sludge factor* (*SF*) for Al-Si-Cu alloys. This factor is calculated from the Fe, Mn, and Cr contents in the alloy as follows:

$$\text{Sludge Factor } (SF) = (1 \times \text{wt.\%Fe}) + (2 \times \text{wt.\%Mn}) + (3 \times \text{wt.\%Cr}) \quad (1)$$

Gobrecht [26] and Jorstad [27] described the relationship between the *SF* and the holding temperature in Al-Si-Cu alloys by defining the critical process conditions where sludge forms (further discussed in § 3.1).

Recently, Shabestari [9] found that the initial Fe, Mn and Cr contents as well as the cooling rate significantly affect the morphology, amount and size of the sludge. According to these results, the sludge forming temperature depends especially on the Fe content according the relationship:

$$\text{Temperature } (^{\circ}\text{C}) = 645.7 + 34.2 \times (\text{wt.\%Fe})^2 \quad (2)$$

The literature results well illustrated the effects of Fe, Mn and Cr on formation of sludge particles in the holding furnace [9,10,24-28,33]. In addition the main factors affecting the mechanical properties of the aluminium alloys with

different levels of Fe, Mn or Cr were described [3-8,18,23,29-31]. However, it lacks a correlation between these two aspects, that is the influence of sludge particles on the mechanical properties of HPDC component. Actually, three critical aspects can be evidenced from the literature:

- The mechanical and microstructural analysis were developed as function of a single impurity element, or the combination of only two; sludge particles are however (Fe,Mn,Cr)-based compounds and therefore it seems important to consider the overall combination of the elements.
- The mechanical properties referred generally to primary cast Al alloys with low concentration of trace elements outside of those studied.
- The mechanical properties were evaluated on gravity die-cast alloys; sludge formation is however more frequently observed in high-pressure die-casting, where higher cooling rates and different feeding conditions exist [34].

In this study, the influence of sludge on the tensile properties of a secondary die-cast AlSi9Cu3(Fe) alloy was investigated. Different contents of Fe, Mn and Cr were studied in order to correlate the mechanical results with the *sludge factor*. A statistical approach based on analysis of variance (ANOVA) was implemented in order to develop equations useful to estimate the mechanical properties in HPDC as function of the initial chemical composition of the alloy in castings with a wall thickness that ranges from 3 to 6 mm.

2. Experimental procedure

A secondary AlSi9Cu3(Fe) cast alloy (EN AB-46000, equivalent to the US designation A380) was supplied by Raffineria Metalli Capra as commercial ingots and used as a base-line. The chemical composition of the base EN AC-46000 alloy and the composition tolerance limits of the Standard EN 1706:2010 [35] are listed in Table 1. The experimental material was prepared by adding Fe, Mn and Cr in the form of commercial Al-25Fe, Al-25Mn and Al-10Cr master alloys, which were added to the molten metal as waffle ingots.

Table 1: Chemical composition of the supplied base-line alloy (wt.%); the composition limits of the EN AC- AlSi9Cu3(Fe) alloy (EN AC-46000) is also reported according to the EN standard 1706:2010 [35]; the upper limit of the elements, not reported in the table, is 0.05 wt.%, with a total amount of 0.25 wt.%.

<i>Alloy</i>		<i>Si</i>	<i>Fe</i>	<i>Cu</i>	<i>Mn</i>	<i>Mg</i>	<i>Cr</i>	<i>Ni</i>	<i>Zn</i>	<i>Pb</i>	<i>Sn</i>	<i>Ti</i>	<i>Al</i>
EN AC-46000	<i>Min.</i>	8.0	0.6	2.0	-	0.05	-	-	-	-	-	-	<i>Bal.</i>
	<i>Max.</i>	11.0	1.3	4.0	0.55	0.55	0.15	0.55	1.20	0.35	0.25	0.25	
supplied (base-line)		8.4	0.72	2.43	0.21	0.19	0.06	0.05	1.05	0.09	0.03	0.04	<i>Bal.</i>

The alloys were melted in a 300 kg SiC crucible in a gas-fired furnace. After the addition of the master alloys, the melt was heated in the furnace at $760 \pm 10^\circ\text{C}$ and held for 30 min at this temperature in order to ensure the homogeneity and dissolution of the present intermetallics. After this operation, the temperature was gradually decreased by following the furnace inertia up to $690 \pm 5^\circ\text{C}$, which is the holding temperature commonly used for EN AB-46000 type alloys. Periodically, the molten metal was manually skimmed and stirred with a coated paddle to avoid any type of sedimentation.

Eighteen different alloys were prepared considering the intersection points of an experimental matrix designed with three levels of Fe (0.8 - 1.0 - 1.2 wt.%), three levels of Mn (0.25 - 0.4 - 0.55 wt.%) and two levels of Cr (0.06 - 0.1 wt.%). Within these ranges, the *SF* varied between 1.48 and 2.60. Table 2 shows the targeted and the achieved level of Fe, Mn and Cr in the experimental alloys, while the concentration of the other alloying and trace elements is similar to the base-line alloy. The chemical composition of the melt was measured by optical emission spectrometer on three samples separately poured at the beginning and at the end of every set of casting.

Cast-to-shape specimens were produced using a multicavity die in an Itaipresse IP300 cold chamber die-casting machine with a locking force of 2.9 MN. For each alloy composition, at least 50 castings were produced. The casting, whose geometry is shown in Fig. 1, provided a cylindrical tensile specimens and two flat tensile specimens, a sample for stress corrosion cracking, one plate and one Charpy specimen to be cast from each shot. Moreover it was obtained a tapered appendix that provides information about the

castability of the alloy. The weight of the Al alloy die-casting was 0.9 kg, including the runners, gating and overflow system.

A detailed description of HPDC machine, casting procedure, and process parameters is given elsewhere [36]. After each start up, 20-25 castings were scrapped to reach a quasi-steady state temperature in the shot chamber and die. The die temperature was maintained at $\sim 230^{\circ}\text{C}$ by circulating oil through channels in the die. The melt was transferred in 15 sec from the holding furnace and poured into the shot sleeve by means of a cast iron ladle coated with a ceramic paste. The fill fraction of the shot chamber, with a 70 mm inner diameter, was kept at 0.28. The plunger velocity was 0.2 m s^{-1} for the first phase and 2.7 m s^{-1} for the filling phase; a pressure of 40 MPa was applied when the die cavity was full.

Table 2: Targeted and achieved (in parentheses) levels (wt.%) of Fe, Mn and Cr in the experimental alloys. The *sludge factor* SF , calculated according to Eq. (1), and the Fe/Mn ratio are also indicated for each alloy.

<i>Alloy No.</i>	<i>Fe</i>	<i>Mn</i>	<i>Cr</i>	<i>SF</i>	<i>Fe/Mn</i>
1	0.80 (0.72)	0.25 (0.22)	0.06 (0.056)	1.48 (1.32)	3.20 (3.33)
2	0.80 (0.72)	0.25 (0.22)	0.10 (0.102)	1.60 (1.47)	3.20 (3.29)
3	0.80 (0.73)	0.40 (0.43)	0.06 (0.061)	1.78 (1.77)	2.00 (1.70)
4	0.80 (0.71)	0.40 (0.39)	0.10 (0.105)	1.90 (1.81)	2.00 (1.83)
5	0.80 (0.72)	0.55 (0.59)	0.06 (0.058)	2.08 (2.07)	1.45 (1.22)
6	0.80 (0.72)	0.55 (0.56)	0.10 (0.104)	2.20 (2.14)	1.45 (1.29)
7	1.00 (1.01)	0.25 (0.22)	0.06 (0.057)	1.68 (1.62)	4.00 (4.62)
8	1.00 (1.03)	0.25 (0.22)	0.10 (0.099)	1.80 (1.76)	4.00 (4.74)
9	1.00 (1.04)	0.40 (0.43)	0.06 (0.059)	1.98 (2.08)	2.50 (2.40)
10	1.00 (1.05)	0.40 (0.43)	0.10 (0.108)	2.10 (2.24)	2.50 (2.43)
11	1.00 (1.01)	0.55 (0.57)	0.06 (0.056)	2.28 (2.31)	1.82 (1.77)
12	1.00 (1.01)	0.55 (0.57)	0.10 (0.094)	2.40 (2.42)	1.82 (1.77)
13	1.20 (1.22)	0.25 (0.21)	0.06 (0.055)	1.88 (1.82)	4.80 (5.71)
14	1.20 (1.38)	0.25 (0.22)	0.10 (0.099)	2.00 (2.11)	4.80 (6.33)
15	1.20 (1.25)	0.40 (0.40)	0.06 (0.054)	2.18 (2.21)	3.00 (3.14)
16	1.20 (1.39)	0.40 (0.43)	0.10 (0.100)	2.30 (2.54)	3.00 (3.24)
17	1.20 (1.27)	0.55 (0.53)	0.06 (0.056)	2.48 (2.51)	2.18 (2.38)
18	1.20 (1.42)	0.55 (0.59)	0.10 (0.103)	2.60 (2.90)	2.18 (2.40)

This study examined cylindrical tensile specimens with a total length of 120 mm, a gauge length of 30 mm, and a diameter of 6 mm [37]; flat tensile specimens with a total length of 90 mm and a gauge dimensions of 30 × 10 × 3 mm. The die-cast specimens were stored at room temperature for about seven months before being tested and therefore corresponding to a similar T1-condition. For each alloy, the mechanical properties were carried out on the last eight castings since the thermal stability of the die was ensured.

In order to assure an acceptable level of soundness before mechanical testing and to localize the porosity distribution, all samples were analysed by means of a Bosello SRE 80 industrial machine equipped with a Hamamatsu microfocus X-ray set up at 50–70 kV and 60 μ A.

The tensile tests were done on an MTS 810 tensile testing machine. The crosshead speed used was 2 mm/min and the strain was measured by means of a 25 mm extensometer. The experimental data were collected and processed to provide yield stress (YS, actually 0.2% proof stress), ultimate tensile strength (UTS) and elongation to fracture (EI).

In order to study the effects of Fe, Mn, Cr and their interaction on mechanical properties, a statistical approach based on the analysis of variance (ANOVA) upon mechanical properties was implemented. Each independent variable (Fe, Mn and Cr content) was analysed at two levels, and therefore a reduced model compared to the experimental tests was made. A detailed description of the statistical method used is given elsewhere [38-40].

Microstructural investigations were carried out on samples drawn from the cross section of the gauge length of round bars by using a Leica DM2500 optical microscope equipped with a Leica QWin image analyzer software. The samples were mechanically prepared to a 3- μ m finish with diamond paste and, finally, polished with a commercial fine colloidal silica slurry for metallographic investigations. The investigations of porosity and sludge were done in a cross-section located at the centre of the gauge length. Three samples were analysed for each alloy, in order to obtain a statistical average value. For each specimen a series of 35 micrographs were taken and analysed with the image analyzer. In order to better contrast the morphologies and the amount of Fe-rich

particles, the polished specimens were etched in a heated solution of 10% sulphuric acid in water [41].

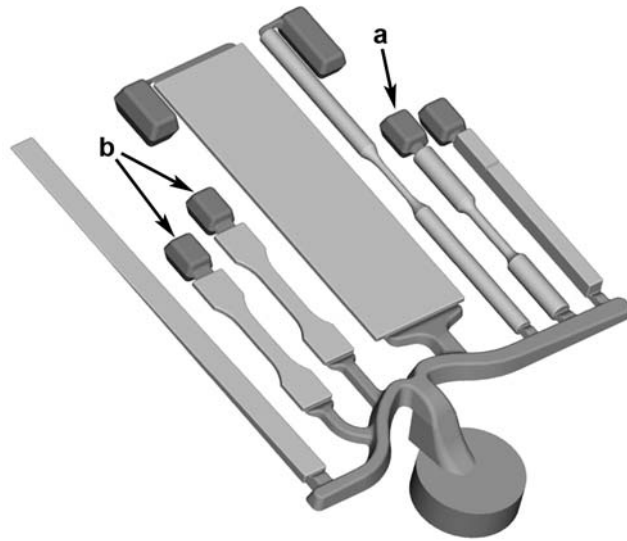


Figure 1: Test multispecimen casting for mechanical testing. The arrows indicate the investigated (a) round and (b) flat specimens for static tensile testing.

3. Results and discussion

3.1. Microstructure observations

The etched microstructures of the AlSi9Cu3(Fe) alloy with different Fe, Mn and Cr content are shown for comparison in Fig. 2. It consists in primary α -Al grains with equiaxed morphology surrounded by Al-Si eutectic. The micrographs refer to the centre of the round tensile bar. Large polyhedral and star-like particles are observed in the microstructure and they appear as dark particles due to the chemical etching. These particles are mainly located along the grain boundaries. A comparison of the particle size to the α -Al cell size of the alloys reveals that these particles are primary phases. These compounds formed by Fe, Mn, and Cr are commonly termed *sludge* in the die-casting industry [27]. Shabestari [9] reported that the stoichiometry of polyhedral, star-like and exploded sludge particles are α -Al₁₂(Fe,Mn,Cr)₃Si₂. Contrary, the results obtained by Warmuzek et al. [42] highlighted a wide range of the variability of the Fe, Mn and Cr concentration in the Fe-rich precipitates, with a stoichiometry that is closely related with the chemical composition of the alloy. Since the

literature shows no clarity about the composition of sludge, and considering that in this study the alloys were produced by systematically changing the Fe, Mn and Cr content, a generic $\alpha\text{-Al}_x(\text{Fe,Mn,Cr})_y\text{Si}_z$ is used to describe the stoichiometry of the sludge particles.

The microstructures show also the presence of primary $\beta\text{-Al}_5\text{FeSi}$ phase in the alloys with higher Fe:Mn ratio. In particular, the most critical alloys were revealed to be the Alloy 13 (see Fig. 2c) and the Alloy 14, which show a Fe:Mn ratio of 5.71 and 6.33, respectively. Here, the content of Mn and Cr is not enough to definitely change the morphology of the Fe-rich phases; therefore, a large number of needles β -phase coexists with blocky α -phase.

The sludge intermetallics are mainly located in the central region of samples' cross section, while the surface layer displays lower content. This segregation mechanism is similar to that suggested for the entrapment of the externally solidified crystals (ESC) [23,43-46]. Due to high shear developed near the die wall, the sludge particles migrate towards the central regions of the casting, where there exist the highest velocity and lowest shear. Concurrently, a surface skin rapidly grows during die filling altering the flow behaviour by reducing the effective cross-section thickness. The structure of this surface layer is relatively finer compared to the size of sludge and this makes the mechanical entrapment more difficult. Thus, a greater fraction of sludge particles is observed at the centre of the castings.

The sludge fraction depends largely on the alloy's chemistry, in particular the concentration of Fe, Mn and Cr, according to Eq. (1). The mean area fraction of primary Fe-rich precipitates formed in each alloy was plotted as a function of sludge factor, as show in Fig. 3. Only large Fe-rich particles with an equivalent diameter higher than 12 μm were considered sludge. The relationship was estimated by a linear regression analysis ($R^2=0.87$) as follows:

$$\text{Sludge fraction (\%)} = 1.5 \times (SF) - 1.9 \quad (3)$$

The results well evidence that under these process conditions, the SF of the alloy accurately predicts the sludge formation. According to Eq. (3), no sludge particles form in an AlSi9Cu3(Fe) alloy with a sludge factor less than

1.27. A similar critical value (1.25) was obtained in a previous work [23] by varying the Cr content under similar experimental condition. However, the slope of the fitting curve found in [23] is larger than the present result (see Fig. 3) and this may be due to higher Cr concentration (0.15 wt.%) and the threshold limit used to identify primary Fe-rich particles in the image analyzer.

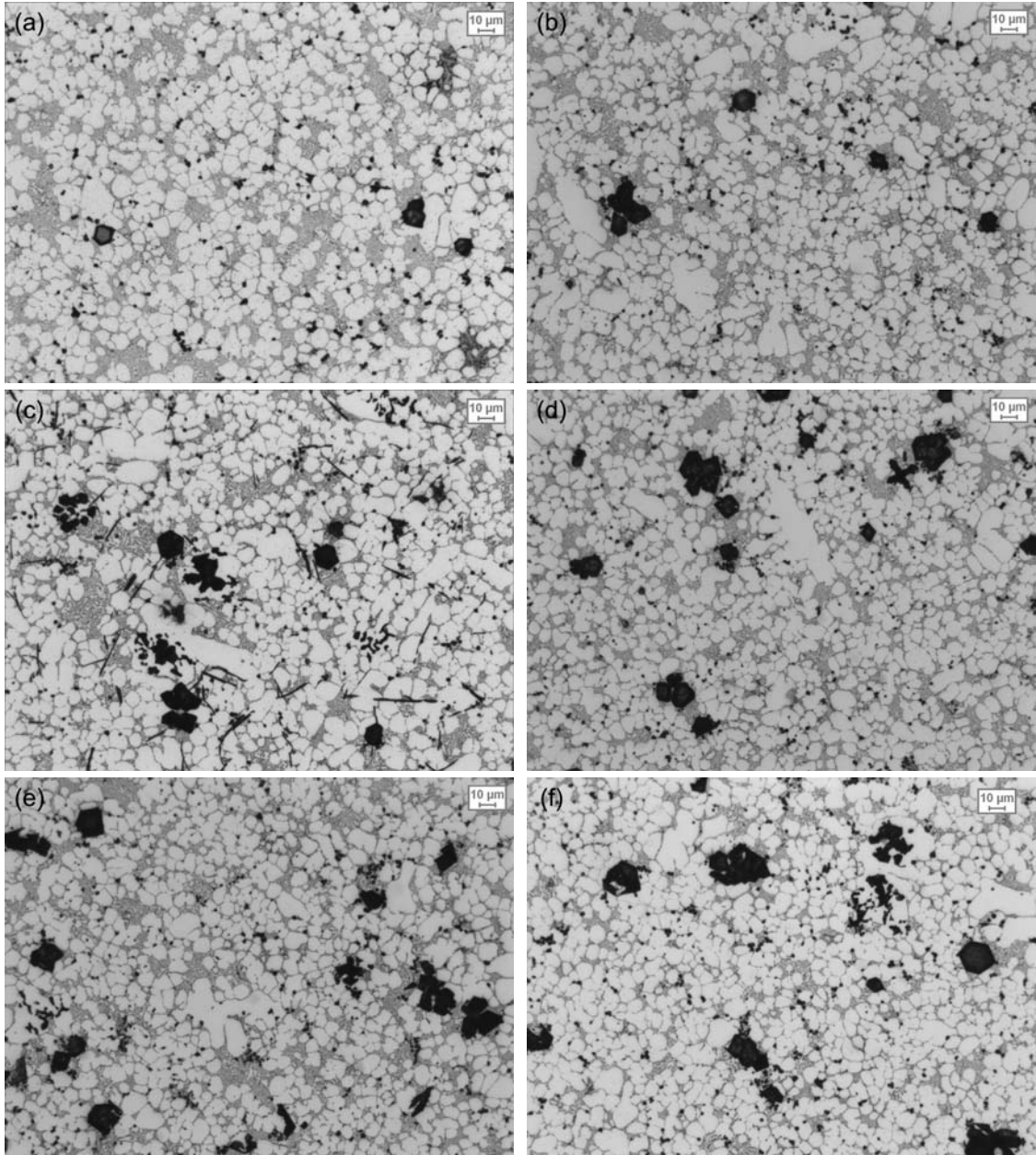


Figure 2: Etched microstructure of AlSi9Cu3(Fe) alloy with different amount of Fe, Mn and Cr. The micrographs, referred to the centre of round tensile specimens, are ordered according to the sludge factor: (a) Alloy 1, SF = 1.32; (b) Alloy 3, SF = 1.77; (c) Alloy 13, SF = 1.82; (d) Alloy 5, SF = 2.07; (e) Alloy 11, SF = 2.31; (f) Alloy 17, SF = 2.51. The Fe-rich particles appear dark, whereas α -Al, eutectic Al-Si, and other intermetallic phases are unetched.

Shabestari [9] and Taghaddos et al. [32] found the critical SF for sludge formation to be ~ 1.15 and ~ 0.35 , respectively for an A413 type alloys poured in permanent mold with short holding times (Fig. 3). Nevertheless, beside the sludge factor, the amount of primary Fe-rich intermetallics is strictly related to the holding temperature and time [15,25-27,33] and the cleanness of the melts [24,28]. In addition, the cooling rate, related to the casting technologies and the content of Si and Cu, influences the nucleation temperature of sludge [10,26,47] and consequently the nucleation and growing mechanism. While in the present investigation a HPDC technology with an holding temperature of $690\text{ }^{\circ}\text{C}$ was used, the works of Shabestari [9] and Taghaddos et al. [32] were carried out by means of gravity casting with initial temperature of the melt of 720 and 670°C respectively. Another important factor affecting the measurement of the area fraction of intermetallics is the threshold limit settings of Fe-bearing particles in the image analyzer.

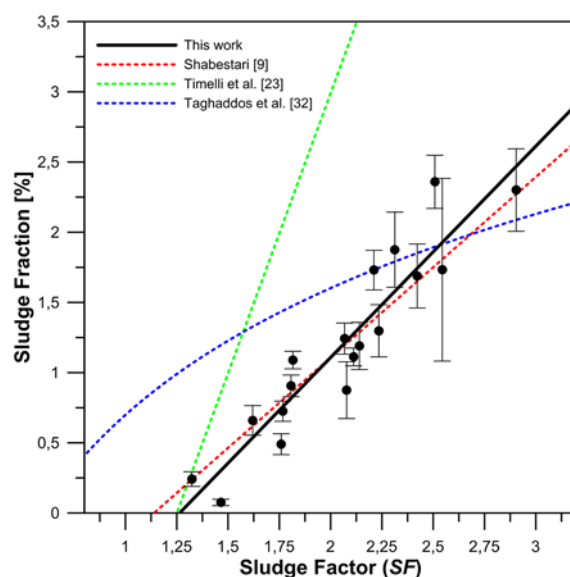


Figure 3: Average area fraction (%) of sludge particles as function of sludge factor calculated according to Eq.(1); standard deviations are given as error bars. The results of Shabestari [9], Timelli et al. [23] and Taghaddos et al. [32] are also reported.

The relationship between the *SF* and the holding temperature for the sludge formation is reported in Fig. 4 according to works of Gobrecht [26] and Jorstad [27], which refers to *SF* in the range 1:2.2 and 0.8:2.4 respectively.

These graphical results delineate the fields where sludge can form in AlSi9Cu3(Fe) alloys. Both the curves were ideally extended (dashed lines) in order to be adapted to the range of *sludge factor* used in the present work. According to these results, the holding temperature used ($690 \pm 5^\circ\text{C}$) is high enough so that sludge should not form in the holding furnace for the alloys with a $SF < 3$ (according to [26]) and $SF < 2$ (according to [27]), respectively. However, the molten metal cooled down in the ladle during the melt transfer from the holding furnace to the die-casting machine and inside the shoot sleeve as described in [27]. The temperature measurements evidenced a continuous dissipation of the melt superheat of about 50°C . Therefore, these thermal conditions, with a reduced melt temperature before injection, promoted the nucleation of sludge crystals in all the analysed alloys (see Fig. 2), even at low SF values. Referring to melting operations in foundry or in the secondary smelters, sludge can also form similarly when ingots or scraps are added directly into the molten metal producing a local cooling below the critical temperature of sludge formation.

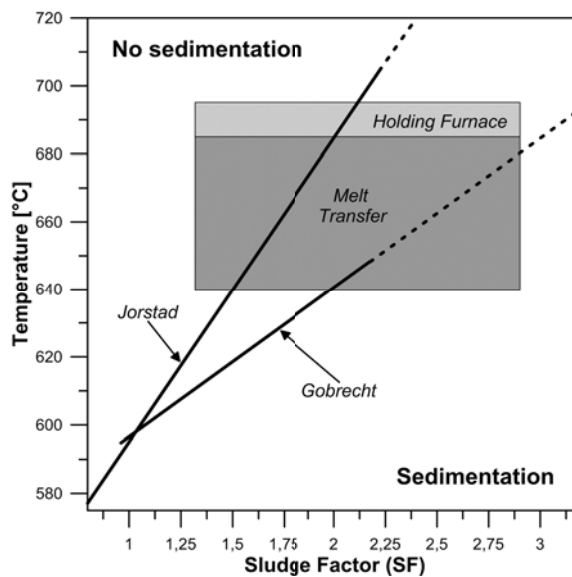


Figure 4: Temperature of gravity segregation of primary Fe-bearing compounds as function of the sludge factor in AlSi9Cu3(Fe) type alloys, according to Gobrecht [26] and Jorstad [27]; the curves are ideally extended (dashed lines) to be adapted to the range of sludge factor used here. The range of working temperatures in the holding furnace and during the melt transfer to the shoot sleeve are also indicated.

3.2. Porosity characterization

In order to assure an acceptable level of soundness before mechanical testing, the influence of Fe, Mn and Cr content on the porosity level was analysed. The preliminary X-ray image, carried out on each specimen, revealed a low amount of porosity, mainly concentrated in the grip regions of tensile test bars, which is closely related to the geometry of the multicavity die used [23,36].

The optical macrograph in Fig. 5 shows the full cross-section located at the centre of the gauge length of round specimens die-cast with Alloy 17 ($SF=2.51$). The size and the amount of porosity seems to be higher at the centre of the cross-section where, due to the higher solidification time compared to the surface layer, air bubbles were entrapped.

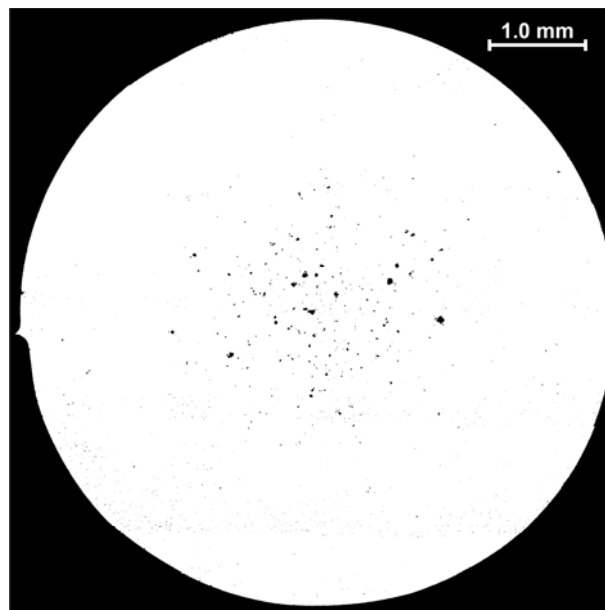


Figure 5: Cross-section of a round tensile specimen (Alloy 17, $SF=2.51$) where the size and the distribution of pores are evidenced by increasing the image contrast.

In the present work, the specimens showed a good integrity level; this is reasonable to expect from their geometry and the process parameters used. A good filling behaviour of the die cavity was obtained with a reduced gas entrapment and porosity size within the castings. The mean porosity content

measured in the round tensile specimens varied from about 0.02 to 0.17%, which is a lower range if compared to the general defects' level in die-castings [48]. These results, plotted in Fig. 6 as function of the *sludge factor*, highlight that there exists no relationship between the concentration of Fe, Mn and Cr and the defects' content. On the contrary, the porosity level seems to be physiologically due to the HPDC process and it is unlikely to be completely eliminated, *i.e. zero defects* [49]. A detailed observations of the pores' morphology, with an average aspect ratio of 2.06 ± 0.2 , evidenced that most of them is due to air/gas entrapment. These results are in contrast with data reported in literature, which refers to gravity casting [5,7,12,13]. It has been shown that Fe facilitates porosity formation and this seems to be associated with the formation of coarse $\beta\text{-Al}_5\text{FeSi}$ platelets. These particles are expected to cause severe feeding difficulties during solidification, since they block the interdendritic flow channels [12,13]. The Mn addition, which helps to replace the $\beta\text{-Fe}$ needle with a more compact $\alpha\text{-Fe}$ phase, causes no significant change in casting porosity level [5,7,13]. Generally, the HPDC induces an over-pressure on the liquid metal during the solidification in order to reduce the shrinkage defects. This over-pressure and the polyhedral morphology of Fe-rich particles can reduce feeding problems and, consequently, the level of porosity [34].

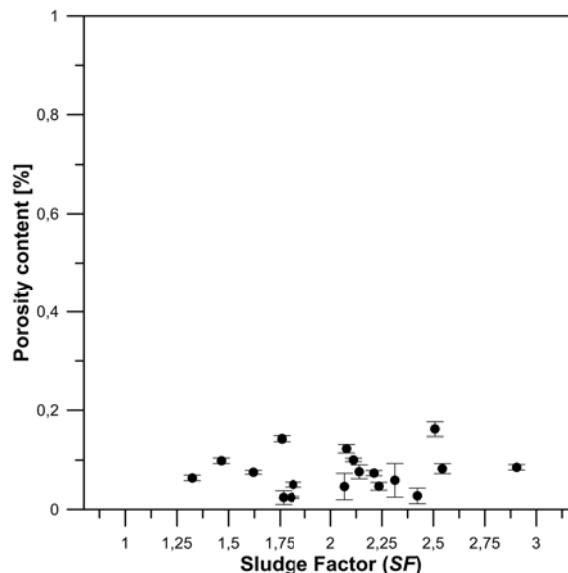


Figure 6: Average porosity content (%) as function of sludge factor; standard deviations are given as error bars. The maximum value of Y-axis was voluntary set to 1%, which is a typical porosity content in die-castings [48].

3.3. Tensile properties

The average tensile properties of the experimental alloys in the T1-condition are shown in Fig. 7 as function of the *sludge factor*. Both the cylindrical and flat tensile specimens have been considered.

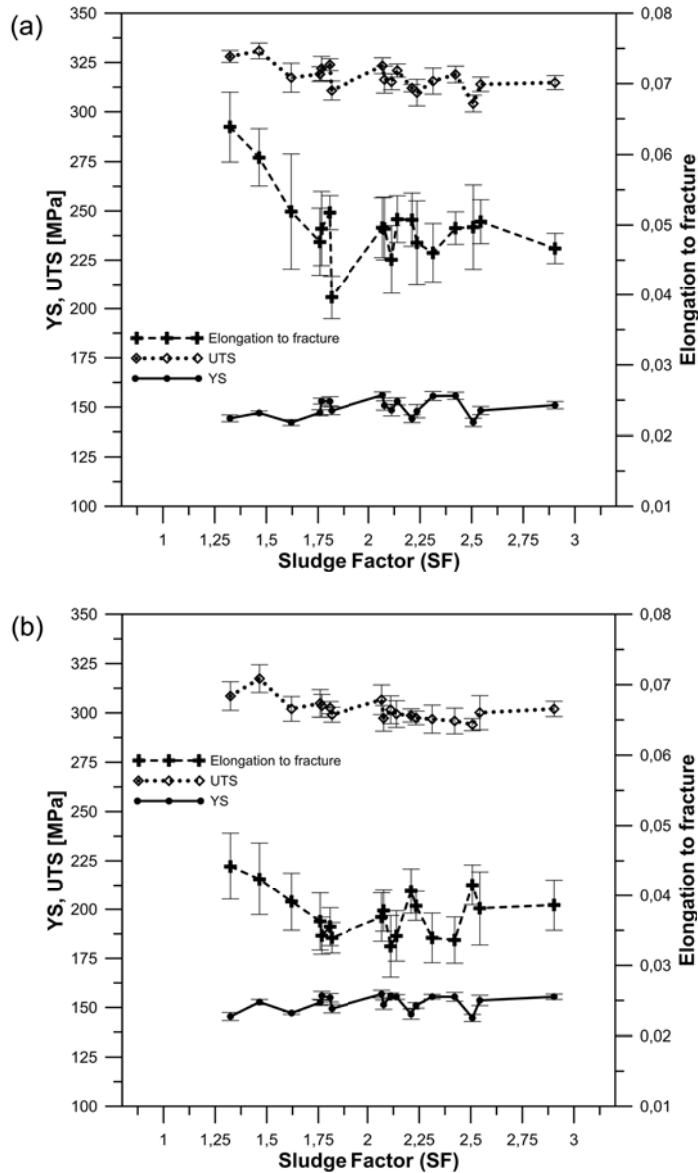


Figure 7: Average YS, UTS and El as function of the *sludge factor* in die-cast AlSi9Cu3(Fe) alloy. Graphs refer to (a) round and (b) flat tensile specimens; standard deviations are given as error bars.

The results highlight that the YS is almost steady at ~147 MPa for both the tensile specimens, showing the maximum value (155 MPa) in the Alloy 18 where there exists the highest Fe, Mn and Cr concentration. On the other hand, the

UTS shows a slight decrease by increasing the *sludge factor*, with a reduction of 8% if compared to the base alloy (Alloy 1). As evidenced from Fig. 7, the elongation to fracture seems to suffer a loss mostly by increasing the Fe, Mn and Cr contents. However, it does not decrease steadily with increasing the *sludge factor*. The minimum value of EI was obtained for the Alloy 13, which presents an industrially tolerable value of *SF* (1.82), by considering the working temperatures (see Fig. 4), but the highest Fe:Mn ratio (5.71). In this condition, the content of Mn and Cr is not enough to change completely the morphology of the Fe-rich particles, and thus a large number of β -Al₅FeSi particles coexists with the α -Fe phase, as show in Fig. 2c. This needle-like phase is generally brittle because it tends to crack easily during the deformation process and consequently it tends to lower the material's ductility [3-5,30]. In the present investigation a further increase over 1.75 of *SF* corresponds to a reduction of Fe:Mn ratio, with a morphology variation of primary Fe-rich intermetallics again into large polyhedral and star-like particles. Accordingly, the elongation to fracture of the alloys with *SF*>2 seems to be almost steady, with a reduction of 30% compared to Alloy 1. Even with the highest volume fraction of brittle sludge particles, corresponding to the highest Fe, Mn, Cr content, the alloy satisfy the minimum tensile properties' requirements indicated in the Standard EN 1706:2010 [35].

Similar trends were obtained for both round and flat tensile specimens, even if lower values were revealed for the latter. This result can be explained by considering the effect of the thickness, or shape, of the tensile specimens on the solidification time of the alloy, which is nicely accounted for by Chvorinov's rule [50]:

$$t_s = M \cdot \left(\frac{V}{S} \right)^n \quad (4)$$

where t_s is the solidification time, V is the volume of the specimen, S is the surface of the specimen that contacts the mold, n is a constant and M is the mold constant, which depends on the characteristics of the metal being cast (its density, heat capacity, and heat of fusion), the mould material (its density, thermal conductivity, and heat capacity), the mould thickness, and the amount of

superheat. The variation of the solidification modulus V/S changes the solidification time and therefore influences the microstructure and the mechanical features of the die-cast alloy. Moreover the tensile properties are also influenced by *defect bands*, which are positive macrosegregation of eutectic Al-Si [43-45]. These banded defects are typical in high-pressure die-cast alloys and follow the contour of the casting surface [23,36].

Porosity is one of the major factor that influences the mechanical properties. Besides, castings with thin section, such as those produced by HPDC, suffer even more the presence of defects because a single macro-defect can cover a significant fraction of the load bearing area. Nevertheless in the present work, the constant porosity level cannot deeply influence the mechanical properties of the experimental alloys, as highlight in Fig. 6.

The tensile properties of round and flat specimens are plotted as parametric curves in Figg. 8 and 9, respectively, in order to analyse the influence of each single element (Fe, Mn and Cr) on the final results. The Fe increase reduces the elongation and the UTS, while the YS appears to be almost steady (Figg. 8-9a and d). These data are in agreement with the results of Seifeddine et al. [3-5] and Shouxun et al. [31], where the Fe addition over 0.8 wt.% decreases significantly the UTS and elongation due to the presence of β -Al₅FeSi phase. On the contrary, a slight enhancement of the YS was revealed but in wider compositional range (0-1.6 wt.% [4] and 0-2.5 wt.% [31]).

While the variation of Mn in the AlSi9Cu3(Fe) alloy seems to produce a progressive reduction of the UTS, the elongation to fracture decreases up to 0.4 wt.% Mn and it is almost steady for greater Mn levels. The YS shows an enhancement with Mn increase (Figg. 8-9b and e). The present YS and elongation results are confirmed in literature [5,18], while the UTS shows an opposite trend.

The Cr addition does not affect the YS of the die-cast experimental alloys (Fig. 8-9c), as already described elsewhere [23]. Moreover, the UTS and EI seem to be closely related to the specific composition of the base AlSi9Cu3(Fe) alloy more than the Cr addition, which doesn't produce a significant variation of the tensile properties.

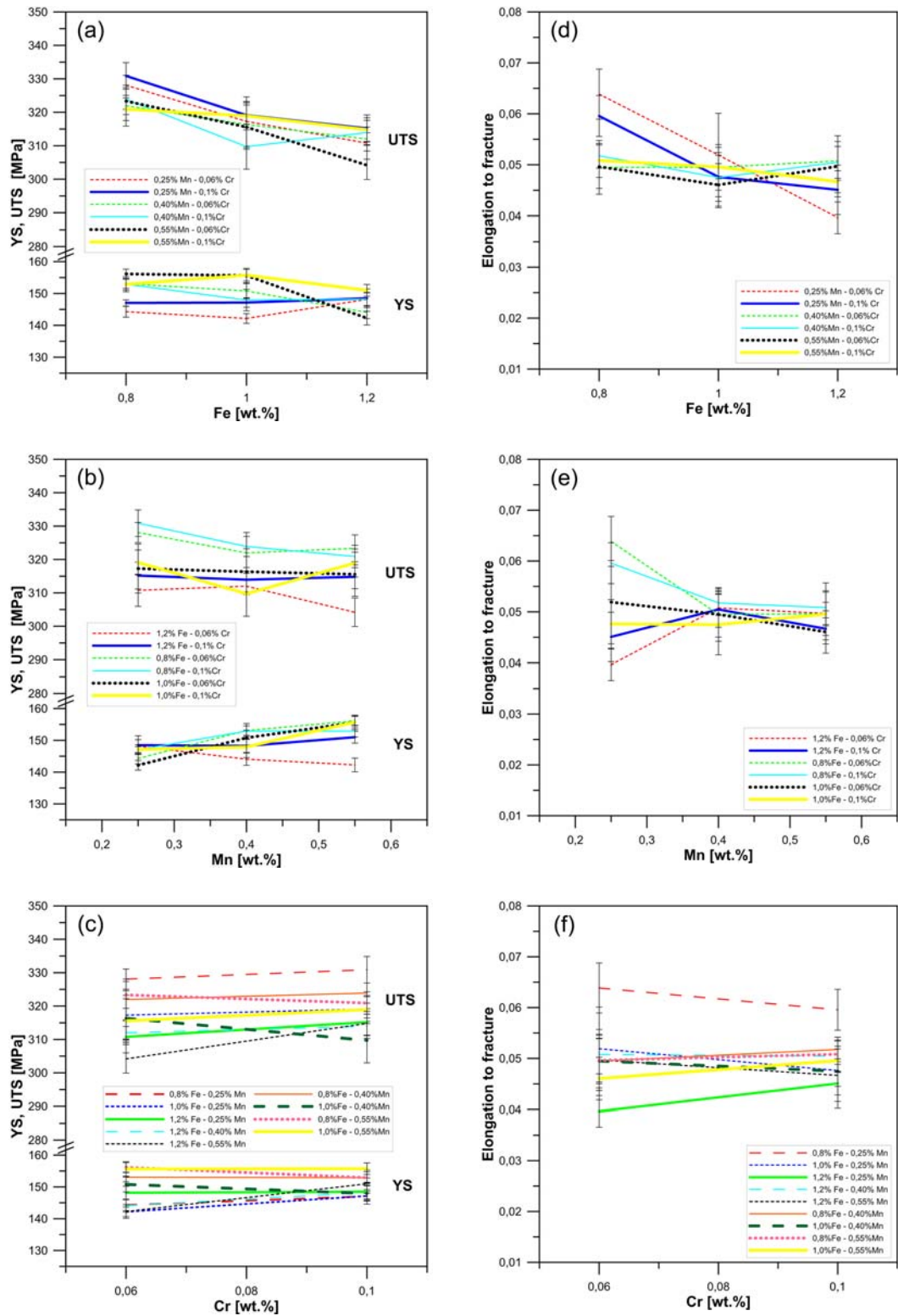


Figure 8: . Parametric curves display the influence of Fe, Mn and Cr on the tensile properties of round tensile specimens. (a), (b), (c) YS and UTS; (d), (e), (f) elongation to fracture; standard deviations are given as error bars. The chemical compositions refer to the targeted levels of Table 2.

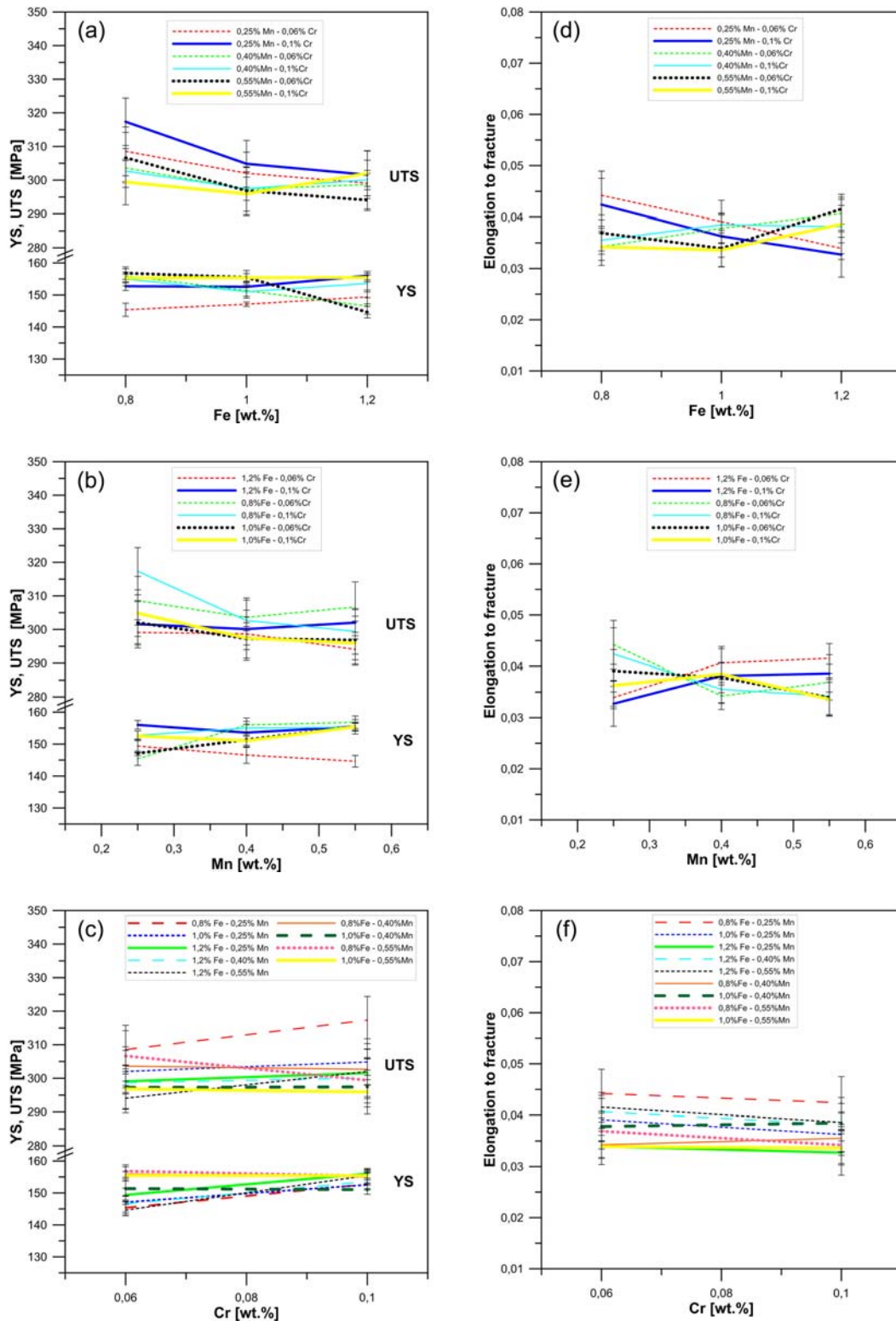


Figure 9: Parametric curves display the influence of Fe, Mn and Cr on the tensile properties of flat tensile specimens. (a), (b), (c) YS and UTS; (d), (e), (f) elongation to fracture; standard deviations are given as error bars. The chemical compositions refer to the targeted levels of Table 2.

3.4. Design of experimental matrix and ANOVA

The *design of experiments* (DOEs) is a statistical approach to the experimental investigation that allows to analyze which process input have a significant impact on the process output. An *analysis of variance* (ANOVA) should be performed by considering the independent factors (inputs) and their interaction that influence the response (output). The ANOVA is a statistical methodology, similar to a regression method, that enables to investigate and to model the relationship between the output and one or more input variables [38,39].

In this work, a factorial ANOVA approach was implemented in order to investigate the effects of Fe, Mn and Cr contents (*independent variables*) on the tensile properties (*dependent variables*).

In order to realize the DOE matrix, independent variables were analysed at two levels each. The targeted compositions of resulting eight alloys used in the statistical approach are listed in Table 3. Besides Fe, Mn and Cr contents as independent variables, four interactions were also considered, namely, Fe·Mn, Fe·Cr, Mn·Cr and Fe·Mn·Cr.

Table 3: Targeted levels (wt.%) of Fe, Mn and Cr in the eight experimental alloys used to perform the DOE. The alloy numbers refer to Table 2.

<i>Alloy No.</i>	<i>Fe</i>	<i>Mn</i>	<i>Cr</i>
1	0.80	0.25	0.06
2	0.80	0.25	0.10
5	0.80	0.55	0.06
6	0.80	0.55	0.10
13	1.20	0.25	0.06
14	1.20	0.25	0.10
17	1.20	0.55	0.06
18	1.20	0.55	0.10

The main result of the ANOVA procedure is the *interaction effect* among the variables, which occurs when the change in response from the low level to the high level of one factor is not the same as the change in response at the

same two levels of a second factor, i.e. the effect of one factor is dependent upon a second factor. In general, the interaction effects can be displayed by means of the interaction plots, such as those displayed in Fig. 10b-12b. In this type of graphs, the interaction among the factors produces effect on the response only if the connection lines are not parallel to each other. Moreover, the larger is the slope of the line and more pronounced is the effect of the independent variable on the response. A positive slope indicates that, changing the variable from the first to the second level, the tensile properties increase favourably, and vice-versa.

Generally, in the *normal probability plots* (see Fig. 10a-12a), each point represents the independent factors or their interaction on a dependent variable. The p -value is used to determine whether a factor is statistically significant; the higher the p level, the lower the probability that the observed relation between two variables in a single sample is a reliable indicator of the relation between the respective variables in the population. The straight line of Fig.10a-12a is a reference line drawn for a p -value of 0.05, which corresponds to a 5% probability that the relation between the variables is fortuitous. The *normal probability plots* allow to highlight simultaneously the magnitude and the direction of variables on response. Consequently, the input variables that produce considerable effects on the response are far from the reference line, while the negligible ones tend to have a standard effect close to zero.

The analysis of the data by means of ANOVA revealed a complete and exhaustive evaluation of the relationship between the tensile properties and the concentration of Fe, Mn and Cr in the experimental alloys (Fig. 10-12). These relationships help to better clarify the influence of chemical composition on the mechanical features if compared to the use of a single factor, i.e. SF, as previously described. Figg. 10-12 report the results for the round tensile specimens. Similar information were obtained from the flat tensile specimens.

While it is clear that Fe is the main factor that reduces the tensile properties, the effect of Mn depends on the specific characteristic. Upon increasing this element, the YS increases while the UTS and EI decrease. On the contrary, the Cr addition shows a slight improvement or a null interaction on tensile properties in the analysed range of composition. Recently, it has been

demonstrated that Cr has a negative effect on tensile properties only with concentrations higher than 0.12 wt.% [23].

In addition to the single effect of the elements, it is important to analyse the results concerning the relationships among them. The interactions between Fe and Mn (Fe·Mn, also *AB* factor in Figg. 10-12) and between Fe and Cr (Fe·Cr, also *AC* factor in Figg. 10-12) seem to have significant effects on the tensile properties. The most important among them is the interaction Fe·Mn. Although it decreases the YS, this property seems to be almost steady for the analysed alloys (Fig. 7), so it seems to not be critical. However, the Fe·Mn factor shows a considerable improvement of the elongation to fracture. This property seems to be the most sensitive to the presence of Fe-rich intermetallics that tend to crack relatively early in the deformation process. Consequently a low Fe:Mn ratio, obtained by adding Mn, increases the *SF* and the amount of sludge, but at the same time it increases the ductility of the material, balancing the detrimental effect generated by iron.

The effects of other relationships among the elements, such as the interactions of Mn and Cr (Mn·Cr factor) appear statistically insignificant, with a *p*-value higher than 0.05. Different results regarding the combined effect Mn·Cr was obtained by Kim et al. [29], where an improvement of tensile properties was evaluated in an alloy with a substantially lower content of Fe and Mn (0.20Fe-0.13Mn-0.13Cr).

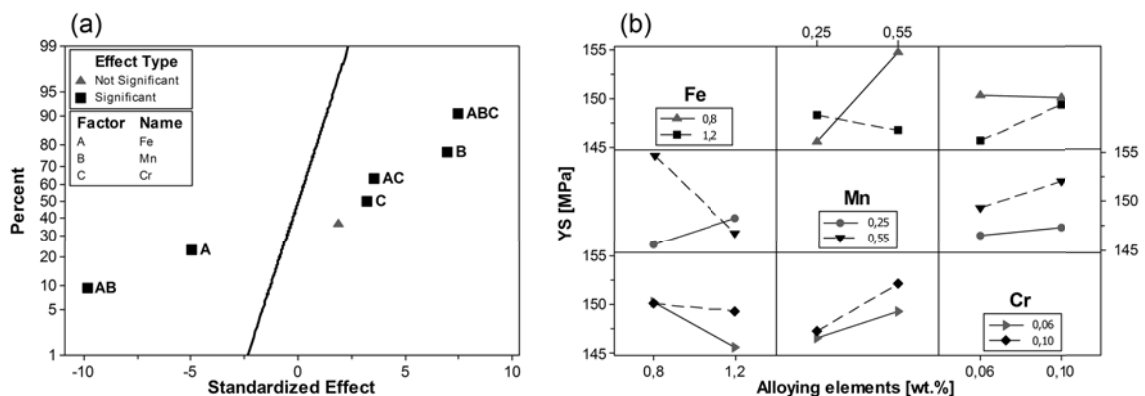


Figure 10: (a) Normal probability plot of the effects of Fe, Mn Cr, and their interaction, on the YS. The straight line point out a *p*-value of 0.05; (b) Interaction effect of Fe, Mn and Cr on the YS. Each line is draw from the mean value of YS at two levels. The data refers to round tensile specimens.

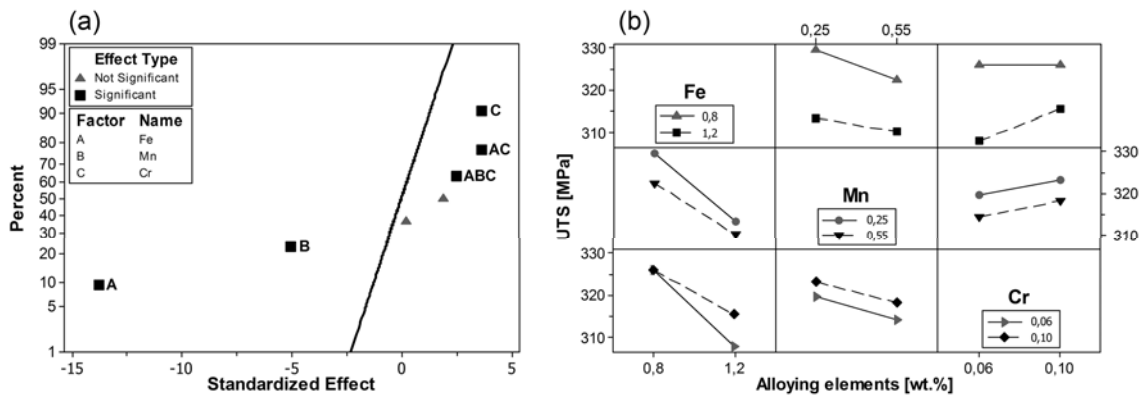


Figure 11: (a) Normal probability plot of effect of Fe, Mn Cr, and their interaction, on the UTS. The straight line point out a p-value of 0.05; (b) Interaction effect of Fe, Mn and Cr on the UTS. Each line is draw from the mean value of UTS at two levels. The data refers to round tensile specimens.

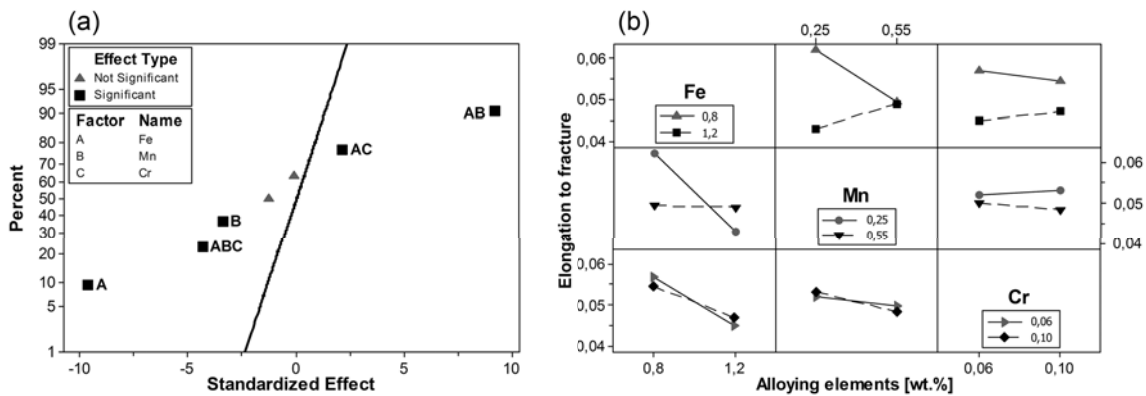


Figure 12: (a) Normal probability plot of effect of Fe, Mn Cr, and their interaction, on the elongation to fracture. The straight line point out a p-value of 0.05; (b) Interaction effect of Fe, Mn and Cr on the El. Each line is draw from the mean value of El at two levels. The data refers to round tensile specimens.

On the basis of the significance level, a regression model can be developed describing the relationship between the response and predictor variables. The reliability of the model is based on the goodness coefficient R^2 . It measures the quality of the least-squares fitting to the original full experimental alloy, described in Table 2.

In the considered range of composition, the average tensile properties, such as YS, UTS and elongation to fracture can be described by the following semi-empirical model:

$$P = k + x_1 \cdot Fe + x_2 \cdot Mn + x_3 \cdot Cr + x_4 \cdot Fe \cdot Mn + x_5 \cdot Fe \cdot Cr \quad (5)$$

where P is the selected features (YS, UTS, EI), while k is a constant and x_1 - x_5 are the regression coefficients of the selected properties, whose values as indicated in Table 4; Fe, Mn and Cr correspond to weight percent in the die-cast AlSi9Cu3(Fe) alloy. In order to verify the reliability of the regression model, the Fe, Mn and Cr content of the achieved chemical composition (Table 2) were used to predict the tensile properties. These results were compared with the real ones to describe the quality of the model by means of goodness coefficient R^2 , as reported in Table 4.

Table 4: Regression coefficients of the tensile properties analysed, used in Eq.(5). The goodness coefficient R^2 , based on achieved chemical composition of all alloys, is given for each features in order to describe the quality of the regression models.

<i>Property P</i>		<i>Sample</i>	<i>k</i>	x_1	x_2	x_3	x_4	x_5	R^2
YS	[MPa]	Round	130.7	9.44	102.9	-202.9	-90.1	247.7	0.82
UTS	[MPa]	Round	392.0	-73.8	-17.45	-379.0	0	474.9	0.88
Elongation		Round	0.14	-0.09	-0.17	0	0.16	0	0.83
YS	[MPa]	Flat	137.3	1.00	90.0	-228.5	-82.8	364.7	0.81
UTS	[MPa]	Flat	352.5	-47.0	-19.6	-226.6	0	313.5	0.74
Elongation		Flat	0.09	-0.05	-0.10	0	0.10	0	0.69

4. Conclusions

The effects of Fe, Mn and Cr content on the tensile properties of a high-pressure die-cast AlSi9Cu3(Fe) has been investigated. The following conclusions can be drawn from this work.

- The microstructure of die-cast AlSi9Cu3(Fe) alloy with different Fe, Mn and Cr content show primary α -Al_x(Fe,Mn,Cr)_ySi_z particles, with polyhedral and star-like morphologies. At the highest Fe:Mn ratio the presence of primary β -Al₅FeSi is also observed.

- The content of primary Fe-rich compounds increases as the Fe, Mn and Cr content increases and it can be accurately predicted from the sludge factor by a linear relationship.
- There exist no relationship between the concentration of Fe, Mn and Cr and the level of porosity in the die-cast material.
- In the analysed range of compositions, the YS of both round and flat tensile specimens is almost constant, while the UTS shows a steady decrease with sludge factor.
- The ductility of the alloy decrease by increasing the Fe, Mn and Cr contents. However, its value is more related to the presence of primary β -Al₅FeSi phases and to the Fe:Mn ratio than the sludge factor.
- The mechanical properties of the die-cast alloy cannot be significantly estimated from the sludge factor.
- A low Fe:Mn ratio, obtained by adding Mn, increases the sludge factor and the amount sludge, but it improves the ductility of the material, balancing the detrimental effect generated by iron.
- Mn and Cr do not interact with each other on tensile properties, and their combined effect appears as statistically insignificant.
- In the considered range of composition, the average mechanical properties can be significantly described by a regression model that considers the concentration of Fe, Mn, Cr and the interactions between Fe and Mn and between Fe and Cr.

Acknowledgements

This work was developed with the financial support of Raffineria Metalli Capra SpA (Brescia, Italy). The authors would like to acknowledge the skilful contribution of Toolcast Snc (Brugine, Italy) for high-pressure die-casting of the tensile test specimens.

References

- [1] P.N. Crepeau, AFS Trans., 103 (1995) 361-366.
- [2] L.F. Mondolfo, Aluminium alloys : structure and properties, Butterworths, 1976.
- [3] S. Seifeddine, I.L. Svensson, Mater. Design, 31 (2010) S6-S12.
- [4] S. Seifeddine, I.L. Svensson, Metall. Sci. Technol., 27 (2009) 11-20.
- [5] S. Seifeddine, S. Johansson, I.L. Svensson, Mater. Sci. Eng. A, 490 (2008) 385-390.
- [6] Z. Ma, A.M. Samuel, F.H. Samuel, H.W. Doty, S. Valtierra, Mater. Sci. Eng. A, 490 (2008) 36-51.
- [7] A.M.A. Mohamed, A.M. Samuel, F.H. Samuel, H.W. Doty, Mater. Design, 30 (2009) 3943-3957.
- [8] A.M.A. Mohamed, F.H. Samuel, A.M. Samuel, H.W. Doty, Mater. Design, 30 (2009) 4218-4229.
- [9] S.G. Shabestari, Mater. Sci. Eng. A, 383 (2004) 289-298.
- [10] L. Backerud, G. Chai, J. Tamminen, Solidification Characteristics of Aluminum Alloys, vol 2: Foundry Alloys, AFS-Skanaluminium, Stockholm, 1990.
- [11] J.A. Taylor, G.B. Schaffer, D.H. StJohn, Metall. Mater. Trans. A, 30 (1999) 1643-1650.
- [12] C.M. Dinnis, J.A. Taylor, A.K. Dahle, Mater. Sci. Eng. A, 425 (2006) 286-296.
- [13] L. Lu, A.K. Dahle, Metall. Mater. Trans. A, 36 (2005) 819-835.
- [14] S. Shankar, D. Apelian, Metall. Mater. Trans. B, 33 (2002) 465-476.
- [15] M.M. Makhlouf, D. Apelian, Work Performed Under DOE Contract No. DEFC07-99ID13716, (2002) 1-46.
- [16] G. Gustafsson, T. Thorvaldsson, G.L. Dunlop, Metall. Trans. A, 17 (1986) 45-52.
- [17] P. Ashtari, H. Tezuka, T. Sato, Scripta Mater., 53 (2005) 937-942.
- [18] J.Y. Hwang, H.W. Doty, M.J. Kaufman, Mater. Sci. Eng. A, 488 (2008) 496-504.
- [19] M. Mahta, M. Emamy, A. Daman, A. Keyvani, J. Campbell, Int. J. Cast. Met. Res., 18 (2005) 73-79.
- [20] S. Murali, K.S. Raman, K.S.S. Murthy, Mater. Charact., 33 (1994) 99-112.

- [21] S.G. Shabestari, M. Keshavarz, M.M. Hejazi, *J. Alloys Compd.*, 477 (2009) 892-899.
- [22] Y.-H. Tan, S.-L. Lee, Y.-L. Lin, *Metall. Mater. Trans. A*, 26 (1995) 1195-1205.
- [23] G. Timelli, F. Bonollo, *Mater. Sci. Eng. A*, 528 (2010) 273-282.
- [24] X. Cao, N. Saunders, J. Campbell, *J. Mater. Sci.*, 39 (2004) 2303-2314.
- [25] S.G. Shabestari, J.E. Gruzleski, *Metall. Mater. Trans. A*, 26A (1995) 999-1006.
- [26] J. Gobrecht, *Giesserei*, 62 (1975) 263-266.
- [27] J.L. Jorstad, *Die Casting Engineer*, (1986) 30-36.
- [28] X. Cao, J. Campbell, *AFS Trans.*, 108 (2000) 391-400.
- [29] H.Y. Kim, S.W. Han, H.M. Lee, *Mater. Lett.*, 60 (2006) 1880-1883.
- [30] L. Ceschini, I. Boromei, A. Morri, S. Seifeddine, I.L. Svensson, *J. Mater. Process. Technol.*, 209 (2009) 5669-5679.
- [31] J. Shouxun, Y. Wenchao, G. Feng, W. Douglas, F. Zhongyun, *Mater. Sci. Eng. A*, 564 (2012) 130-139.
- [32] E. Taghaddos, M.M. Hejazi, R. Taghiabadi, S.G. Shabestari, *J. Alloys Compd.*, 468 (2009) 539-545.
- [33] R. Dunn, *Die Casting Engineer*, (1965) 8-30.
- [34] P. Beeley, *Foundry Technology*, 2nd Edition, Butterworth-Heinemann, Oxford, United Kingdom, 2001.
- [35] Standard EN 1706:2010, Aluminium and aluminium alloys - Castings - Chemical composition and mechanical properties, (2010).
- [36] G. Timelli, S. Ferraro, F. Grosselle, F. Bonollo, F. Voltazza, L. Capra, *La Metallurgia Italiana*, 101 (2011) 5-17.
- [37] ASTM Standard B557-10, Standard Test Methods for Tension Testing Wrought and Cast Aluminum- and Magnesium-Alloy Products, ASTM International, West Conshohocken, PA, 2010.
- [38] D.C. Montgomery, *Design and Analysis of Experiments 8ed.*, John Wiley & Sons, 2012.
- [39] F. Grosselle, G. Timelli, F. Bonollo, *Mater. Sci. Eng. A*, 527 (2010) 3536-3545.
- [40] G. Berti, M. Monti, L. Salmaso, *Introduzione alla metodologia DOE nella sperimentazione meccanica. Disegno sperimentale e superfici di risposta*, Cleup, 2002.

- [41] G.F. Vander Voort, *Metallography - Principles and Practice*, 2 ed., ASM international, Materials Park, OH, 1999.
- [42] M. Warmuzek, W. Ratuszek, G. Sęk-Sas, *Mater. Charact.*, 54 (2005) 31-40.
- [43] H.I. Laukli, C.M. Gourlay, A.K. Dahle, O. Lohne, *Materials Science and Engineering: A*, 413-414 (2005) 92-97.
- [44] C.M. Gourlay, H.I. Laukli, A.K. Dahle, *Metall. Mater. Trans. A*, 38 (2007) 1833-1844.
- [45] S. Otarawanna, C.M. Gourlay, H.I. Laukli, A.K. Dahle, *Metall. Mater. Trans. A*, 40 (2009) 1645-1659.
- [46] G. Timelli, S. Ferraro, A. Fabrizi, *Int. J. Cast. Met. Res.*, 26 (2013) 239-246.
- [47] R.I. Mackay, J.E. Gruzleski, *Int. J. Cast. Met. Res.*, 10 (1997) 131-145.
- [48] A. Fabrizi, S. Ferraro, G. Timelli, *Mater. Charact.*, 85 (2013) 13-25.
- [49] G. Timelli, F. Bonollo, *Metall. Sci. Technol.*, 26 (2008) 2-8.
- [50] J. Campbell, *Complete Casting Handbook: Metal Casting Processes, Metallurgy, Techniques and Design*, Elsevier Butterworth-Heinemann, UK, 2011.